The Effect of Dispersal Heterogeneity in Bioinvasions

by

Ali Gharouni

BSc Mathematics, Shiraz University, 2005
MSc Mathematics, Isfahan University of Technology, 2008

A DISSERTATION SUBMITTED IN PARTIAL FULFILLMENT OF THE REQUIREMENTS FOR THE DEGREE OF

Doctor of Philosophy

In the Graduate Academic Unit of Mathematics and Statistics

Supervisor(s):	Lin Wang, PhD, Dept. of Math and Statistics
	James Watmough, PhD, Dept. of Math and Statistics
Examining Board:	Myriam A. Barbeau, PhD, Dept. of Biology
	Jeffrey Picka, PhD, Dept. of Math and Statistics
	Stephen B. Heard, PhD, Dept. of Biology
External Examiner:	Michael G. Neubert, PhD, Dept. of Biology,
	Woods Hole Oceanographic Institution

This dissertation is accepted by the

Dean of Graduate Studies

THE UNIVERSITY OF NEW BRUNSWICK

November, 2016

Dedication

To my parents, my niece Diba and my nephew Sam.

Preface

All chapters of this thesis except for the General Introduction (Chapter 1), and General Discussion (Chapter 5) will be submitted for publication, have been submitted for publication or have been published in peer-reviewed scientific journals.

Chapter 2 (an earlier version) has been published in the *Journal of Marine Ecology Progress Series*: A. Gharouni A, M. A. Barbeau, A. Locke, L. Wang, and J. Watmough, *Sensitivity of invasion speed on dispersal and demography: an application of spreading speed theory to the green crab invasion on the coast of the northwest Atlantic*, Marine Ecology Progress Series 541 (2015) 135-150.

Contributions of authors:

AG developed and analysed mathematical models; contributed to writing

MB/LW/JW advised and contributed to writing

AL provided data and contributed to writing

NOTE: Written permissions were obtained from publishers to incorpo-

rate these chapters in the thesis.

Chapter 3 has been submitted for publication to the Journal of *PLOS ONE*: A. Gharouni A, M.A. Barbeau, J. Chassé, L. Wang, J. Watmough, *Stochastic dispersal increases the rate of upstream spread: a case study with green crabs on the northwest Atlantic coast*, Submitted for publication to PLOS ONE, July 2016.

Contributions of authors:

AG developed and analysed mathematical models; contributed to writing

MB/LW/JW advised and contributed to writing

JC provided hydrodynamic model and contributed to writing.

Chapter 4 will be submitted for publication A. Gharouni A, M.A. Barbeau, J. Chassé, L. Wang, J. Watmough, *Estimation of larval dispersal distribution: an application of hydrodynamic models to the green crab invasion on the coast of the northwest Atlantic*

Contributions of authors:

AG developed and analysed mathematical models; contributed to writing

MB/LW/JW advised and contributed to writing

JC provided hydrodynamic model and contributed to writing.

Abstract

The spread against a dominant flow of a marine invasive species with pelagic larval stage is a complex ecological phenomenon. This upstream spread involves the interplay between a number of processes including demography and dispersal of organisms, and variability in these processes. The main objectives of this thesis are to study the connection between dispersal, demography and spread in this setting and to understand the effect of variability in dispersal on spreading speeds. As a case study, I used the invasive green crab, *Carcinus maenas*, which has maintained a relatively consistent rate of spread for over 100 years covering a wide range of temperate latitudes and local hydrological environments along the Atlantic coast of North America. I developed a stage-structured integrodifference equation modelling framework to link spreading speed to underlying demographic and dispersal processes. First, simple kernels (namely Normal and Laplace) were used to model the larval dispersal. Then, a mechanistic kernel with behaviour was incorporated into the stage-structured integrodifference equation model. The temporal variability of the kernel was parameterized by using a particle-tracking

submodel embedded into a 3-dimensional hydrodynamic model of the Gulf of St. Lawrence. Results indicated that the relationship between demography and dispersal was compensatory for all the three kernels. Sensitivity analysis indicated that larval dispersal had more effect on spreading speed than any demographic parameter. Our simulation implied that there was a spatial structure in the larval dispersal. Further, when dispersal parameters vary with time, using the time-averaged dispersal would underestimate the upstream invasion spread rates. Thus, accounting for spatial and annual variations in dispersal in population models is important to enhance understanding of spatial dynamics and population spread rates.

My research thus contributed to (i) applied science by ranking different possible strategies in the management of a marine invasive species, (ii) theoretical ecology by developing tools to incorporate biophysical and behavioural features into the dispersal component of an integrodifference equation model, and by showing that the year-to-year dispersal variability increases the upstream spreading speed.

Acknowledgements

I would like to thank the many people who helped me reach this point. Dr. Lin Wang and Dr. James Watmough, for their continuous support of my Ph.D study and research. I am indebted for their guidance and patience as my thesis supervisors. Dr. Myriam A. Barbeau, for starting the green crab project, for her frequent insights into my research and her faith in my abilities. The members of my examining committee, Professors Jeffrey Picka, Stephen B. Heard, Michael G. Neubert, for their invaluable comments and patience. Dr. Andrea Locke and Renée Bernier, for providing the green crab data. Dr. Joël Chassé, for providing the hydrodynamic model and his help. The Faculty and staff of Department of Mathematics and Statistics at university of New Brunswick, for their support during my program. To my friends: Serkan Sutlu, Fang Yu, Xi Hu, Hongying Shu, Pius Ariho, Shohreh Rahmati and Xingde Duan, for their friendship and encouragement. I would also like to thank NSERC for funding this project. Thank you to Mom, Dad, my family and Judi: no matter where I have gone, home has always been with you. Without you all, this work would not have been possible.

Table of Contents

List of Tables

List of Figures

Chapter 1

Introduction

Ecological questions regarding biological invasions in marine systems can be addressed by mathematical models. Fundamental questions include: (i) "At what rate will the population invade a new territory?" (ii) "What are underlying mechanisms of a biological invasion?" (iii) "How sensitive is the invasion spread rate to changes in the underlying mechanisms?" (iv) "What is the effect of dispersal heterogeneity on the spread rate?". Answering such questions can provide insights on and rank possible management strategies to anticipate, plan for and respond to bioinvasions. In this thesis, I investigate these questions by developing a series of spatial models to study the invasion of the green crab, *Carcinus maenas*, on the east coast of North America. Although I use the green crab invasion as a case study, the models can be modified for any species of interest.

Invasive species are those that are introduced to an area outside of their

natural environment. They are more formally known as non-native or non-indigenous invasive species. Some have the ability to spread very rapidly and cause enormous environmental and industrial damage. The green crab is a highly effective predator that has maintained a relatively consistent rate of advance for over 120 years covering a wide range of temperate latitudes and local hydrological environments along the Atlantic coast of North America [73]. Green crabs were first detected on the east coast of North America in New York and southern Massachusetts in 1817 [53]. Genetic analysis indicated that this lineage originated from southern Europe (likely from Portugal; [133]), hence the name "southern lineage". Green crabs were later introduced near Chedabucto Bay in eastern Nova Scotia in the 1980s from the northern end of the crab's native range in Europe (likely Norway; [133]), hence the name "northern lineage". It took about 120 years for the crab to expand its geographical range from south of Massachusetts to southwest of the Halifax area. Samples collected from Kouchibouguac Lagoon (eastern shore of New Brunswick) in 2013 showed the establishment of green crab in that area (Fisheries and Oceans, unpublished data). The northward expansion occurs against the dominant water flow, which is southwestward along the Scotian Shelf (Nova Scotia Current; [35]) and counterclockwise in the Gulf of St. Lawrence (surface circulation; [35]). Once introduced, the establishment and spread of this predator is readily apparent due to its impact on local communities and ecosystems, fisheries (e.g., shellfisheries and eels), and bivalve aquaculture [53, 73, 175].

This thesis consists of two models to predict and study the invasion speed of the green crabs on the east coast of North America. The first model (in Chapter 2) is an age-structured integrodifference equation (IDE) model to investigate the green crab's spreading speed and the relationship between demography and dispersal. I assumed that dispersal occurs during the pelagic larval stage and model it by using simple Normal and Laplace distributions for simplicity. Sensitivity analyses were conducted to evaluate the change in spreading speed in response to changes in demographic and dispersal parameters. The second model (in Chapter 3) is an age-structured integrodifference equation model with a stochastic dispersal component to investigate the observed upstream spread rate of the invasive green crab on the east coast of North America. This model was extended from the first model by using a mechanistic approach for the larval dispersal kernel which allows incorporating year-to-year variability into the dispersal kernel.

In the present Chapter, modelling strategies and background relevant to the work in this thesis are discussed. In Section 1.1, reaction diffusion models are reviewed as a background to integrodifference equation models. A general introduction to some of the concepts and basic analysis are discussed. In Section 1.2, integrodifference equation models are then reviewed. In Section 1.3, some recent developments in stochastic modelling are briefly discussed.

1.1 Reaction-diffusion models

There is a substantial mathematical literature dealing with modelling and analysis of the spread of invasive species. One of the most fundamental conclusions of such models is the potential for spatial expansion of a population in the form of an invasion wave. The rate of advance of such a wave (the invasion spread rate) can be calculated from such models.

The earliest studies of invasion spread rates used single-species reaction-diffusion models of the form

$$\frac{\partial u}{\partial t} = f(u)u + D\frac{\partial^2 u}{\partial x^2}, \tag{1.1}$$

where $u(x,t)$ is population density at location x and time t, $f(u)$ is the density-dependent per-capita growth rate, and D (space^2/time) is the diffusion coefficient representing the diffusive movement of the dispersers [43].

Diffusion models can be derived as the large scale limits of dispersal models based on random walks [116, 156]. They can also be derived from Fick's law which describes the flux of a diffusing substance in terms of its gradient [112, 116], or from stochastic differential equations [45].

In a pioneering work, Skellam [143] (see also [60]) combined the diffusive description of dispersal with population dynamics, effectively introducing reaction-diffusion equations into theoretical ecology, paralleling Fisher's earlier contribution to genetics [43]. Skellam analyzed the spread of muskrat in Europe by using a special case of Equation (1.1) when growth is Malthusian.

That is, the population grow or decay exponentially due to assuming that $f(u) = \epsilon$, with ϵ constant.

Analytically, Kolmogorov et al. [74] showed that single-species reaction-diffusion models like Equation (1.1) with a step function for the initial population density, $u(x, 0)$, predict an asymptotically constant spreading speed

$$c^* = 2\sqrt{RD}, \tag{1.2}$$

where R is recruitment rate and equal to $f(0)$ and D is the diffusion coefficient. Aronson and Weinberger [5, 6] proved the same result if the step function is replaced by a compact non-zero initial population density. Note that expression (1.2) relates the spreading speed of the population, c^*, with the demographic parameter, R, and the dispersal parameter, D. Specifically, for a given c^*, the recruitment rate R and the diffusion coefficient D are in a hyperbolic relationship. This relationship is often referred to as "compensatory relationship". This is due to the fact that high R can compensate for low diffusivity D, or low R can be compensated by high D to allow the population spread at a consistent speed c^*.

These models oversimplify the demography and dispersal processes by neglecting (i) demographic structure, such as age, size and developmental stage, and (ii) possible dispersal complexities other than diffusive movement (modeled by Gaussian distribution). Note that the Gaussian (Normal) distribution is a single-parameter probability density function which is rarely

supported by field measurements of dispersal [e.g., 44, 171, 172]. Instead, leptokurtic distributions, which have fatter tails compared to the Normal distribution, are more commonly observed [116, 117]. Further, the reaction-diffusion models assume that movement and reproduction are independent processes and that the population is observed on a time-scale that allows the two processes to be modelled as synchronous.

Reaction-diffusion models have been extended to incorporate features such as population structure, dispersal behaviour and species interactions. The importance of population structure for demography is well known [21, 155]. Population structure has been incorporated into reaction-diffusion models and has been applied to many systems [see 21, 116, 140, and references therein]. Reaction-diffusion models have also been extended to account for dispersal behaviour that is more complex than simple diffusion, specifically advection or taxis, and dispersal in response to densities of conspecifics, prey, or predators; see for example Kareiva and Odell [71] and Belgacem and Cosner [11] or the discussion of chemotaxis and cross-diffusion in Murray [112]. Further, species interactions, spatial heterogeneity and Allee effects (i.e., whereby per capita growth rate is diminished at low densities [1]) have been incorporated in reaction-diffusion models [see 140, and references therein].

Note that despite the various extensions mentioned above, for a structured population with a different dispersal pattern for each stage, the use of a structured reaction-diffusion framework is not appropriate. Specifically, for

aquatic species (such as the green crab) with a pelagic larval stage, the dispersal process of larvae is more complex than that of the sessile adults. The larval dispersal is influenced by factors such as water currents, turbulence and environmentally-induced variability. Thus, a single-parameter Gaussian distribution might not appropriately represent the larval dispersal features, but might be a good approximation for adult dispersal. A more general approach to incorporate different types of dispersal rather than Gaussian has been made possible by integrodifference equation (IDE) models [76], which I review in the next section.

1.2 IDE models

IDE models assume a separation between the demography and dispersal processes, and this is suitable for organisms that have distinct dispersal and reproduction stages and that reproduce during a brief interval at a specific time of the year. Importantly, a wide range of dispersal functions including leptokurtic distributions can be used in IDEs. Leptokurtic dispersal patterns can be better described by functions with additional parameters [76] or by mixtures [26, 27]. These models change the predictions of spread and allow constant, accelerating and decelerating spread rates, unlike reaction-diffusion models that only result in a constant spread rate [76].

For the sake of simplicity, I restrict my consideration to one spatial dimension and populations with non-overlapping generations. I also assume

that dispersal takes place in an infinite space to neglect boundary effects. I first briefly review unstructured IDE modelling framework. Then I describe the more general structured IDE models and provide a brief review of recent results.

1.2.1 Unstructured IDE

Assuming that the species first reproduces and then disperses, the IDE model combines a nonlinear operator for density-dependent growth with a linear operator for dispersal. The unstructured (single-staged) IDE model is

$$u_{t+1}(x) = \int_{-\infty}^{+\infty} k(x-y)b(u_t(y))u_t(y)dy. \tag{1.3}$$

The dispersal kernel, $k(x-y)$, is the probability density of finding at position x an offspring released at position y. b is the per capita growth rate function and t is discrete time. It is assumed that the environment is homogeneous, so that dispersal probability depends on the distance between positions x and y rather than on both of them separately. More generally, in a heterogeneous environment with density-dependent dispersal, both the dispersal kernel and the birth rate could depend on x, y and u independently [114].

Weinberger [166] showed that a broad class of models predict that spread rate eventually approaches a constant value, provided that the dispersal kernel is exponentially bounded. There are some cases that exponentially unbounded dispersal arise from data [116, 117, 171]. The value of the constant

spread rate depends on the shape of the kernel, more leptokurtic kernels typically yielding a larger value spread rate [76]. Fat-tailed kernels (kernels which are not bounded by any exponential function) result in a rapid expansion [107, 108].

Although density-dependence often plays a crucial role, surprisingly, when $b(u) \leq b(0)$ and under certain conditions (see next section), linearization of Equation (1.3)

$$u_{t+1}(x) = b(0) \int_{-\infty}^{+\infty} k(x-y)u_t(y)dy, \tag{1.4}$$

gives a good estimate for the invasion speed. This is known as the linear conjecture [109, 157] which is discussed in detail in the next section. The result is that, in the case that an invasive species spreads in the form of a traveling population wave, in the absence of an Allee effect [1, 149], the wave speed is determined by the population dynamics at the leading edge of the moving front [166]. At the edge of the front, the population density is small and thus $b(u) \simeq b(0)$.

A stationary wave (i.e., the traveling wave with a profile of a constant shape) traveling with a speed c is a solution which exhibits invariance translation, i.e.,

$$u_{t+1}(x) = u_t(x-c). \tag{1.5}$$

There are two key types of population waves associated with biological

invasions. "Pulled waves" are driven by growth and dispersal processes at the leading edge of the invasion where densities are low. "Pushed waves" are driven by the growth and dispersal processes further back in the wave where densities are higher. This may occur when the reproductive dynamics exhibit an Allee effect and the linear conjecture no longer holds [84]. In this case, the wave is no longer "pulled" by the leading edge of the wave, but is "pushed" by individuals reproducing at higher densities and spilling outwards (via the dispersal kernel) at densities sufficient to overcome the threshold for population growth [76]. See also [46] for a formal description of pushed and pulled waves.

Since equation 1.4 is linear, we look for a solution of the form

$$u_t(x) = C \cdot e^{-s(x-ct)}, \tag{1.6}$$

where C is a constant and s is a parameter giving the slope of the wave front. Having substituted (1.6) into (1.4) and assuming that $z = x - y$, we obtain

$$e^{-sx}e^{sc} = b(0) \int_{-\infty}^{+\infty} k\,(z)\, e^{sy}\mathrm{dy} \tag{1.7}$$

and hence

$$e^{sc} = b(0)M(s), \tag{1.8}$$

where

$$M(s) = \int_{-\infty}^{+\infty} k(z)e^{sz}\mathrm{dz}. \tag{1.9}$$

Equation (1.8) is referred to as the characteristic equation of (1.4). M is called the moment generating function corresponding to the dispersal kernel k. We immediately can obtain the equation for the speed of the population wave:

$$c(s) = \frac{1}{s}\ln\Big[b(0)M(s)\Big]. \tag{1.10}$$

It is seen that Equation (1.10) has a family of solutions parameterized by s. Here, a remarkable theorem by Weinberger [165, 166] states that the wave propagates with the minimum value of $c(s)$ defined by (1.10) for particular kinds initial data. The existence and stability of travelling wave solutions and a formula for the asymptotic spread rate c^* as

$$c^* = \min_{0<s} \frac{1}{s}\ln\Big[b(0)M(s)\Big], \tag{1.11}$$

followed from Weinberger's theorem.

1.2.2 Structured IDE

Individuals differ in their vital rates and response to the environment, and much of that difference is determined by age, size, developmental stage, or other population structure. Stage-structure may lead to a lower estimate of spreading speed [114, 155].

To add stage structure, I considered one equation for each of the n stages as follows:

$$u_{t+1}^i(x) = \int_{-\infty}^{+\infty} \sum_{j=1}^{n} k_{ij}(x-y) b_{ij}\Big(u_t^1(y), \cdots, u_t^n(y)\Big) u_t^j(y) dy, \tag{1.12}$$

for $i = 1, \cdots, n$, where $u_t^i(x)$ is the population density in the i^{th} stage at location x and time t. b_{ij} is the density-dependent per capita production rate of stage i individuals at time $t+1$ by stage j individuals at time t. $k_{ij}(x-y)$ is the probability that an individual making the transition from stage j to stage i moves from location y to location x in a homogeneous habitat. The representation of structured IDE models in simplified matrix notation reads as

$$\mathbf{u}_{t+1}(x) = \int_{-\infty}^{+\infty} [\boldsymbol{K}(x-y) \circ \mathbf{B}_{\mathbf{u}}] \mathbf{u}_t(y) dy, \tag{1.13}$$

where the symbol "$\circ$" stands for the Hadamard product, wherein multiplication is componentwise. The element in the i^{th} row and j^{th} column of $\boldsymbol{K}(x-y) \circ \mathbf{B}_{\mathbf{u}}$ is $k_{ij}(x-y) b_{ij}(u_t^1(y), \cdots, u_t^n(y))$.

I shall use boldface symbols like $\mathbf{u}$ to denote a vector in $\mathbb{R}^n$, that is $\mathbf{u} = (u_1, u_2, \ldots, u_n)$. Here n is the number of species involved in the system. A componentwise order relation is defined on the set of n-vector valued functions. Specifically, I define $\mathbf{u} \geq \mathbf{v}$ to mean that $u_i(x) \geq v_i(x)$ for all i and x. I use $\mathbf{u} \gg \mathbf{v}$ to mean that $u_i(x) > v_i(x)$ for all i and x. I use the notation $\mathbf{0}$

for the constant vector all of whose components are 0. The norm I consider here is the supremum norm, defined as

$$\|\mathbf{u}\| := \sup_x |\mathbf{u}(x)|, \tag{1.14}$$

where $|\mathbf{u}(x)|$ denotes the Euclidian norm.

Given a constant n-vector $\boldsymbol{\beta} \gg \mathbf{0}$, I define the set of functions

$$\mathscr{C}_{\boldsymbol{\beta}} = \{\mathbf{u} : \mathbf{u} \text{ is continuous and } \mathbf{0} \leq \mathbf{u}(x) \leq \boldsymbol{\beta}, x \in \mathbb{R}\}. \tag{1.15}$$

Consider an operator $\boldsymbol{Q}$ on $\mathscr{C}_{\boldsymbol{\beta}}$ in form of a discrete-time recursion

$$\mathbf{u}_{t+1} = \boldsymbol{Q}[\mathbf{u}_t] \text{ for } t = 0, 1, 2, \ldots. \tag{1.16}$$

where the vectored-valued function $\mathbf{u}_t(x) = (u_t^1(x), u_t^2(x), \ldots, u_t^n(x))$ represents the population densities of the populations of n species or classes at the point x at time t.

Definition 1.2.1. *The operator* $\boldsymbol{Q}$ *is said to be* ***order-preserving*** *if* $\mathbf{u} \geq \mathbf{v}$ *implies that* $\boldsymbol{Q}[\mathbf{u}] \geq \boldsymbol{Q}[\mathbf{v}]$ *for all* $\mathbf{u}$ *and* $\mathbf{v}$ *in* $\mathscr{C}_{\boldsymbol{\beta}}$. *A recursion system* (1.16) *in which* $\boldsymbol{Q}$ *has this property is said to be* ***cooperative****.*

Definition 1.2.2. *A function* $\mathbf{u}$ *is said to be an equilibrium of* $\boldsymbol{Q}$ *if* $\boldsymbol{Q}[\mathbf{u}] = \mathbf{u}$.

Definition 1.2.3. *Given* $x, y \in \mathbb{R}$, *the translation and reflection operators are defined by* $\boldsymbol{T}_y[\mathbf{u}(x)] = \mathbf{u}(x - y)$ *and* $\boldsymbol{R}[\mathbf{u}(x)] = \mathbf{u}(-x)$ *respectively for*

$\mathbf{u} \in \mathscr{C}_{\boldsymbol{\beta}}$. *An operator* $\boldsymbol{Q}$ *is said to be* ***translation invariant*** *if* $\boldsymbol{Q}[\boldsymbol{T}_y[\mathbf{u}]] = \boldsymbol{T}_y[\boldsymbol{Q}[\mathbf{u}]]$ *for all* y. *An operator* $\boldsymbol{Q}$ *is said to be* ***reflection invariant*** *if* $\boldsymbol{Q}[\boldsymbol{R}[\mathbf{u}]] = \boldsymbol{R}[\boldsymbol{Q}[\mathbf{u}]]$ *for all* $\mathbf{u}$.

In biological terms, a translation invariant operator represents a homogeneous habitat, so that the growth and dispersal properties are independent of location.

Definition 1.2.4. *A linear operator* $\boldsymbol{L}$ *is said to be a linearization (or Fréchet derivative) of* $\boldsymbol{Q}$ *at* $\mathbf{0}$ *if for any* $\epsilon > 0$ *there exists a* $\delta > 0$ *such that* $\|\mathbf{u}\| \leq \delta$ *implies* $\|\boldsymbol{Q}[\mathbf{u}] - \boldsymbol{L}[\mathbf{u}]\| \leq \epsilon\|\mathbf{u}\|$.

For single stage recursion, i.e., $n = 1$ in (1.16), it has been shown by Weinberger [166] that if $\boldsymbol{Q}$ has only two spatial homogeneous equilibria, namely $\mathbf{0}$ and $\boldsymbol{\beta}$, is order-preserving and is translation and reflection invariant, then under some natural conditions on $\boldsymbol{Q}$, there is a spreading speed c^* with the properties that for any positive $\epsilon > 0$,

$$\lim_{t\to\infty} \left\{ \max_{|x|\leq(c^*-\epsilon)t} |\mathbf{u}_t(x) - \boldsymbol{\beta}| \right\} = 0 \tag{1.17}$$

for any initial function $\mathbf{u}_0(x)$ which lies above $\mathbf{0}$ plus some positive constant on a sufficiently long interval. Also

$$\lim_{t\to\infty} \left\{ \max_{|x|\geq(c^*+\epsilon)t} |\mathbf{u}_t(x)| \right\} = 0. \tag{1.18}$$

for any initial function $\mathbf{u}_0(x)$ which lies between $\mathbf{0}$ and $\boldsymbol{\beta}$ and is $\mathbf{0}$ outside a

bounded set. Expressions (1.17) and (1.18) state that if an observer moves slower than c^*, then he or she will eventually see the population rise to its none-zero equilibrium state $\boldsymbol{\beta}$. On the other hand, if the observer moves faster than c^*, then he or she will eventually see the population decline to the zero equilibrium state.

Further, Weinberger [165, Theorem 3] has proven that expression (1.17) implies that the equilibrium state $\boldsymbol{\beta}$, unlike $\mathbf{0}$, is stable in the following sense. Let $\mathbf{u}_t$ be a solution of the recursion in (1.16) and $\mathbf{0} \leq \mathbf{u}_0 \leq \boldsymbol{\beta}$ is bounded away from $\mathbf{u}_0$ outside a bounded set.Then, $\mathbf{u}_t$ converges to $\boldsymbol{\beta}$ uniformly in x as $t \to \infty$.

If $\boldsymbol{Q}$ is replaced by its linearization $\boldsymbol{L}$ at $\mathbf{0}$, then

$$c^* \geq \bar{c}, \tag{1.19}$$

where $\bar{c}$ is the spreading speed for the linearized recursion. Further, if

$$\boldsymbol{Q}[\mathbf{u}] \leq \boldsymbol{L}[\mathbf{u}], \tag{1.20}$$

then

$$c^* = \bar{c}. \tag{1.21}$$

Definition 1.2.5. *The system* (1.16) *is said to be* ***linearly determinate*** *if property* (1.21) *holds.*

A statement of belief that under certain conditions a system is linearly

determinate is called a linear conjecture [109, 157]. It states that the speed of invasion for any nonlinear model is governed by its linearization at low population densities, as long as there are no Allee effects and no long-distance density dependence. The linear conjecture is supported by many numerical studies [20, 23, 114].

Lui [93, 94] obtained sufficient conditions for the linear determinacy of a certain class of multi-species cooperative models in which operator $\boldsymbol{Q}$ in recursion (1.16) has only two equilibria and satisfies relation (1.20).

Weinberger and co-authors considered (1.16) for the case where the system is allowed to have three or more equilibria [85, 87, 167, 168]. Their results show that, under certain conditions, relation (1.19) holds for recursion (1.16). Also, if there are only two equilibria, these two speeds are identical, thus (1.21). Their results have been obtained under a sharper set of conditions than Lui's.

In the case that the recursion (1.16) is not cooperative, linear determinacy has been proven for a class of reaction-diffusion systems and integrodifference equations in which $\boldsymbol{Q}$ can be bounded between two cooperative operators [e.g. see 162, 163].

Liang et al. [90] and Liang and Zhao [88] have extended the theory of spreading speeds and traveling waves for monotone autonomous semiflows to periodic semiflows in the monostable case. The linear determinacy for cooperative periodic systems has been proven in these studies.

Note that in all of the studies above, operator $\boldsymbol{Q}$ has to be compact (or

precompact) with respect to the topology of uniform convergence on bounded intervals for the existence of traveling waves. That is, every sequence $\mathbf{u}_t$ of functions in $\mathscr{C}_{\boldsymbol{\beta}}$ has a subsequence $\mathbf{u}_{ti}$, such that the sequence $\boldsymbol{Q}[\mathbf{u}_{ti}]$ converges uniformly on every bounded subset of $\mathbb{R}$. Liang and Zhao [89] relaxed this condition using a sequence of operators with compact support to approximate the given operator $\boldsymbol{Q}$.

Note that the models developed in this thesis are all cooperative. Thus, their dynamics are linearly determined (Definition 1.2.5) and the existence of travelling wave solution is the result of the theory developed by [94]. The following proposition is adapted from [101, Proposition A.1] which is a summary of the theoretical work of Lui [94].

Proposition 1.2.1. *Let $\boldsymbol{Q} : \mathscr{C}_{\boldsymbol{\beta}} \to \mathscr{C}_{\boldsymbol{\beta}}$ satisfy the following conditions:*

(1) $\boldsymbol{Q}[\mathbf{0}] = \mathbf{0}$, $\boldsymbol{Q}[\boldsymbol{\beta}] = \boldsymbol{\beta}$, $\mathbf{0}$ is unstable and $\boldsymbol{\beta}$ is stable with respect to $\boldsymbol{Q}$.

(2) $\boldsymbol{Q}$ is translation invariant and has no other fixed point besides $\mathbf{0}$ and $\boldsymbol{\beta}$ in $\mathscr{C}_{\boldsymbol{\beta}}$.

(3) $\boldsymbol{Q}$ is order-preserving in $\mathscr{C}_{\boldsymbol{\beta}}$.

(4) $\boldsymbol{Q}$ is continuous in the topology of uniform convergence on bounded subsets of $\mathbb{R}$.

(5) Let

$$(\boldsymbol{L}[\mathbf{u}](x))_i = \sum_{j=1}^{n} \int_{-\infty}^{+\infty} u_j(x-y) l_{ij}(y) dy$$

be the linearization of $\boldsymbol{Q}$ *at* $\mathbf{0}$*, where* $l_{ij} \geq 0$ *is an integrable function. I assume that*

$$\boldsymbol{Q}[\mathbf{u}] \leq \boldsymbol{L}[\mathbf{u}] \text{ forall } \mathbf{u} \in \mathscr{C}_{\boldsymbol{\beta}}. \tag{1.22}$$

(6) Given that $\hat{s} > 0$*, the matrix* $\boldsymbol{H}(s) = (h_{ij}(s))$*, where*

$$h_{ij}(s) = \int_{-\infty}^{+\infty} l_{ij}(z)\mathrm{e}^{sz}dz \tag{1.23}$$

is irreducible for $0 < s < \hat{s}$*.*

Let $\lambda_1(s)$ *be the spectral radius of* $\boldsymbol{H}(s)$ *and let*

$$c^* = \min_{0<s<\hat{s}}\Big[\frac{1}{s}\ln\lambda_1(s)\Big], \tag{1.24}$$

Then c^* *is the asymptotic spreading speeds of the operator* $\boldsymbol{Q}$ *in the positive direction in the following sense. Let* $\mathbf{u}_0 \in \mathscr{C}_{\boldsymbol{\beta}}$*,* $\mathbf{u}_0$ *is non-trivial and vanishes outside of a bounded interval in* $\mathbb{R}$*. Let* $\mathbf{u}_t$ *be a solution of recursion* (1.16)*. Then for any small* $\epsilon > 0$*,*

$$\lim_{t\to\infty}\Big\{\min_{|x|\leq(c^*-\epsilon)t}|\mathbf{u}_t(x) - \boldsymbol{\beta}|\Big\} = 0 \tag{1.25}$$

and

$$\lim_{t\to\infty}\Big\{\max_{|x|\geq(c^*+\epsilon)t}|\mathbf{u}_t(x)|\Big\} = 0. \tag{1.26}$$

Neubert and Caswell [114] developed a straightforward method to calculate the asymptotic spread rate c^* (1.24). They also developed mathemat-

ical theory to carry out sensitivity analysis for structured IDE models like (1.13). In general, it is not possible to minimize the expression in (1.24) and determine c^* analytically. Thus, the spreading speed must be determined numerically from (1.24).

1.3 Stochastic models

The dynamics of ecological populations is affected by numerous and diverse processes that are stochastic in essence. Although some processes can be approximated by deterministic models in which stochasticity is averaged out, there are cases where neglecting variability may lead to miss some important ecological features of the population dynamics.

Some notable examples that deterministic models have been successfully addressed ecological problems include: predator population response to prey density [160], algae response to sunlight intensity [40], predicting the spreading speed of invading populations and determining the basic relationship between the invasion spreading speed and the underlying demography and dispersal processes [114, 121]. Also, diffusion equation (described in Section 1.1) is a classical example that a stochastic phenomenon can be described by a deterministic model. Although application of the diffusion equation is somewhat restricted by the underlying assumption that the density of diffusing particles/individuals should be sufficiently high (in order to keep fluctuations small), it was shown by Skellam [143] that a random motion of

a single individual can be also described by the diffusion equation as soon as we treat its solution as the probability distribution function to locate the individual around a given position in space.

Despite the usefulness of deterministic models, there are many open questions about how good the deterministic approximations are and in what situation the stochastic component is essential to be incorporated into a model. An observation that makes this issue even more controversial is that sometimes mathematical models based on deterministic and stochastic approaches lead to very similar results; one example can be found in recent works by Kawasaki et al. [72] and Mimura et al. [105]. On the other hand, processes such as the patchy spread and variation in invasion spreading speeds observed in real systems cannot be captured by deterministic models [41, 83].

Studying the effect of demographic and dispersal stochasticity on invasion spreading speed has only recently received the attention of theoretical ecologists. Caswell et al. [23] provided a theoretical framework for calculating spreading speed and sensitivity analysis for stochastic, structured IDE models. Their results indicate that under certain conditions, the spreading speed eventually converges to an asymptotic speed in temporally varying environments. In a similar work, Schreiber and Ryan [138] proved analytically that in stochastic, structured IDEs, the invasion speeds are asymptotically normally distributed with a variance that decreases in time. For populations structured by a continuous state variable, Ellner and Schreiber [41] simi-

larly provided a stochastic version of an earlier autonomous (time-invariant) model for invasion speed [69]. Their main result is that, temporal variation in the dispersal may lead to accelerating spreading speed. It is notable that stochasticity in demographic processes typically reduces invasion speed [77, 83].

In the following thesis, I first developed deterministic models and established a basic compensatory relationship between demography and dispersal processes that was linked to consistent invasion spreading speeds in marine systems. Then stochastic dispersal was incorporated into the population model. My results indicated that in structured IDE models averaging the dispersal process over time would underestimate the spreading speed. Other types of stochasticity could be explored in the future build up from my work.

Chapter 2

Sensitivity of invasion speed on dispersal and demography: an application of spreading speed theory to the green crab invasion on the coast of the northwest Atlantic [1]

2.1 Introduction

In today's cosmopolitan world, invasive species are a common and serious environmental issue [123, 140]. Prediction of the spreading speed of an invasive

[1] This chapter is published in MEPS, [47]

species is important to anticipate, to plan for and to respond to bioinvasions. Accurate prediction requires a comprehensive understanding of the demography of the species, the dispersal capability of individuals, and the interaction between these two processes [58]. This also includes quantifying demographic and dispersal rates, which vary across the species' life stages. Tools that enable one to integrate all this information and track population dynamics include structured-population models. These models have been developed and applied to a number of marine and terrestrial systems [155].

The model that I used in this study combines a matrix describing population growth with an integral operator describing movement of individuals within a season. The result is a system of integrodifference equations (IDE). This class of models assumes discrete time and continuous space. The population is divided by age, and the demographic matrix incorporates age-specific survival probabilities and fecundities [21]. My model further assumes that the dispersal of individuals is modeled by a kernel; this dispersal kernel is a function governing the redistribution of individuals in continuous space [76]. Such models are typically used when reproduction is seasonal [76]. Structured IDEs were introduced by Neubert and Caswell [114] to describe dispersal behavior and demographic processes and have been applied to a number of systems [104, 114, 132]. Comparing the spreading speed predicted by these models to empirical observations provides a means to estimate demographic and dispersal variables affecting spreading speeds [58]. I used this procedure to better understand the processes affecting the spread rate of the European

green crab, *Carcinus maenas*, on the coast of the northwest Atlantic.

Biological invasions generally involve three phases: arrival of an alien species into a new locality, establishment of a viable population of this species in the locality, and spread of this species into surrounding areas [42]. In this thesis, the focus is on the spread phase of the green crab. The vast majority of introductions of invasive species, including *C. maenas*, throughout the world have been attributed to transport by human agents [73, 123]. The growth of transport networks has accelerated new introductions in recent years [62]. The successful establishment of the species is highly dependent on its demographic attributes and on the environmental conditions at the new locality [140]. Subsequent spread into surrounding areas is dependent on the species' demographic rates and dispersal mechanisms. The green crab seems to have all the appropriate attributes for establishment and spread [73], given its successful expansion onto the coasts of North America (both Atlantic and Pacific), South Africa, Australia, South America, and Asia. Once introduced, the establishment and spread of this highly effective predator is readily apparent due to its impact on local communities and ecosystems, shellfisheries and other fisheries (e.g., eels), and bivalve aquaculture [53, 73, 174].

Audet et al. [7] compiled diverse information and concisely documented green crab distribution along the Atlantic coast of Nova Scotia between 1951 and 2002. In a more recent examination using genetic analysis, Roman [133] discovered that the green crab population on the east coast of North America comprised two major genetic lineages: a southern lineage and a northern

lineage. Green crabs were first detected on the east coast of North America in New York and southern Massachusetts in 1817 [53, 137]. Genetic analysis indicated that this lineage originated from southern Europe (likely from Portugal; [133]), hence the name "southern lineage". Green crabs were later cryptically introduced near Chedabucto Bay in eastern Nova Scotia in the 1980s from the northern end of the crab's native range in Europe (likely Norway; [133]), hence the name "northern lineage". It took about 120 years for the crab to expand its geographical range from south of Massachusetts to southwest of the Halifax area. Specifically, from Newport (Rhode Island) in 1844, the invasion reached Prospect Bay, Nova Scotia, by 1966. Studies of intertidal animals between 1965 and 1973 did not detect any presence of green crabs between Halifax and St. Marys River (Guysborough County, eastern Nova Scotia). This time lag in the dispersal history of green crabs in Atlantic Canada is followed by the appearance of the northern lineage of green crabs in Guysborough County first reported in 1985 [128, 133]. The spread of the northern lineage has continued in both directions along the east coast with dispersal throughout Northumberland Strait and Prince Edward Island (Canada) since 1994 [133]. Annual monitoring and sampling have been employed systematically since 2001 by Fisheries and Oceans Canada. Samples collected from Kouchibouguac Lagoon (eastern shore of New Brunswick) in 2013 showed the establishment of green crab in that area (Fisheries and Oceans, unpublished data). The northward expansion for both lineages occurs against the dominant water flow (see Figure 2.1), which is southwestward

along the Scotian Shelf (Nova Scotia Current [35]) and counterclockwise in the Gulf of St. Lawrence (surface circulation [35]).

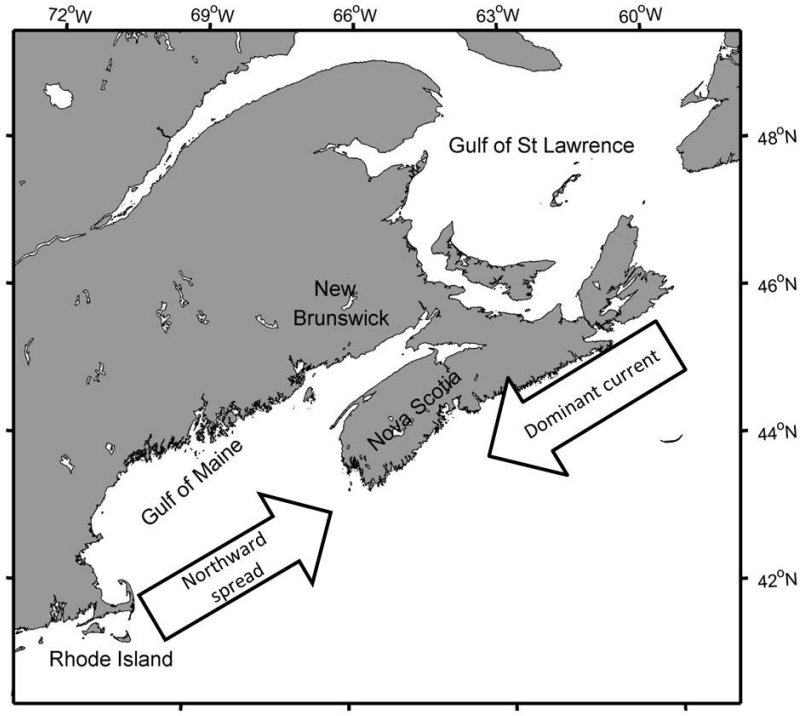

Figure 2.1: Northward spread of the green crabs on the east coast of North America.

In this thesis, I examined the surprisingly consistent northern range expansion of the green crab (*C. maenas*) on the east coast of North America, for both the southern and northern lineages. I analyzed the presence/absence data for established green crab populations along the one-dimensional coastline, and empirically estimated the spread rate using linear regression. I developed an age-structured IDE to model changes in density of three stages

of the invasive green crab (first-year juveniles, second-year juveniles, and female adults) from one generation to the next. Analysis of this model yields the relationship between spreading speed, demography (namely recruitment) and dispersal. Assuming the speed from field data as a case study, I obtained a relationship between demography and dispersal of the green crab. I investigated this relationship with and without an advective displacement downstream (southwards). I conducted sensitivity analysis to evaluate the change in spreading speed in response to changes in demographic and dispersal parameters.

2.2 Methods and mathematical model

2.2.1 Study species

The European green crab is an omnivore, native to European and North African coasts, and is invading many temperate regions around the world [73]. It has synchronous, overlapping generations. Many aspects of the life history of green crabs are conducive to a successful invasive ability: females are highly fecund, producing an average of 185000 eggs in one brood [29]; the planktonic larval period is long (50 to 90 d) and development (four zoeal stages and a megalopal stage) occurs mostly off-shore, providing larvae with the potential to naturally disperse over longer ranges than the benthic juveniles and adults. Whether the main driver of green crab spread is due to larval dispersal or adult movement is currently debated [153]. Note that an-

thropogenic vectors may also be important in the spatial dynamics of green crabs [73]. Hydrodynamically-driven dispersal, predominantly larval dispersal, has been documented for many aquatic species as a natural mechanism of dispersal through connected systems, including green crabs [73, 178], zebra mussels (*Dreissena polymorpha* [14]), and cladocerans (*Daphnia lumholtzi* [141]). Green crab larvae have some active control over their dispersal as they perform active vertical migrations in the water column between a depth of 20-25 m during the day and 30-45 m at twilight [129]. They utilize selective tidal stream transport to return to intertidal and shallow subtidal zones to settle and metamorphose into benthic juvenile crabs. The life span and seasonal timing of demographic events vary among different areas [9].In Maine and Nova Scotia, the life span of green crabs is $\sim$ 6 y, most females mature at age 2-3 y, mature females release larvae from June to August, and larval settlement occurs in late August to early October [12, 73].

2.2.2 Field data

The data considered in this chapter are a subset of a dataset of the time and location of sightings of adult green crabs from 1844 to 2013 on the west coast of the North Atlantic ([7, 73, 133]; see Canadian Aquatic Invasive Species Database[2]). In this study, I considered the spreading speed of the southern and northern lineages of green crabs separately. The range of the southern lineage extends from Newport (Rhode Island), through the Gulf of Maine,

[2]http://geoportal.gc.ca/eng/Gallery/MapProfile/3#

and up to Halifax Harbor. The northern lineage was considered partly in Nova Scotia (near the Strait of Canso) and mostly throughout Northumberland Strait up to the Kouchibouguac Lagoon (New Brunswick). Although both lineages spread northward and southward after the first introduction, and interact at some locations along the coast [70, 133], I was only interested in estimating the northward spreading rate as, excluding the areas where the 2 lineages may interact, this represents a natural (as opposed to anthropogenic) spreading rate of the green crab invasion in this region.

Empirical estimation of spreading speed was carried out in two steps. First, a coastline was defined from New York to Gaspé (Quebec) as a set of points connected by line segments. The choice of the coastline segments was based on the minimum spacing of the data. This affects the estimation of the spread rate, but to my knowledge there is no way of determining which choice of the coastline is better than another. Second, sighting locations were projected onto this coastline; the northern most point along the defined coastline was selected for each year with sightings to produce a time series of distances (Figure 2.2(a)). These were further subdivided into two datasets for the northern and southern lineages, respectively. I chose Newport, Rhode Island, as the origin of the coastline (Figure 2.2(b)). The regression analysis was carried out in R [131] by using the function $lm()$ and the function $confint()$ with a level of 0.95 to compute 95% confidence intervals of the estimated spreading speed for the two lineages.

In defining the coastline through the Bay of Fundy, I used the obser-

vation that green crabs expanded from the west coast of the bay to the opposite coast in only two years, 1951-1953. Specifically, I inferred from the data that the invasion front was near the mouth of the Magaguadavic River in Passamaquoddy Bay, New Brunswick (northwest side of the outer Bay of Fundy), in 1951 and near Sandy Cove in St. Marys Bay, Nova Scotia (southeast side of the outer Bay of Fundy), in 1953. There is a strong southeast current near between these two locations, which is part of a counterclockwise gyre in the Bay of Fundy [4]. I defined the theoretical coastline as a straight line between these two locations (rather than all the way up into and around the upper Bay of Fundy).

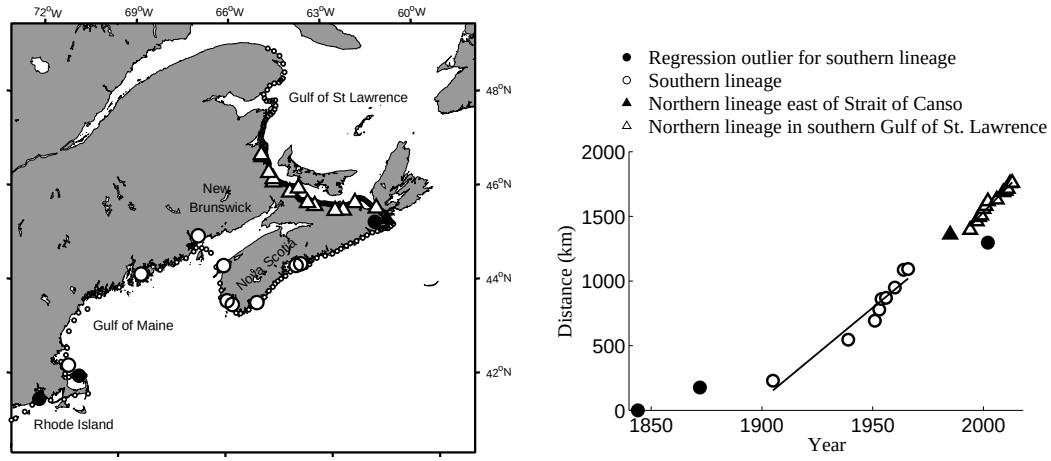

(a) (b)

Figure 2.2: (a) New England (USA) and maritime Canada with the coastline defined for this study (small white circles), and positions of first observation of establishment of green crabs *Carcinus maenas* projected onto the coastline (large symbols: circles for the southern lineage, triangles for the northern lineage; black symbols represent suspect data points). (b) Estimation of the northward spreading speed of *C. maenas* (c_S^* and c_N^* for the southern and northern lineages, respectively). Distance 0 is Newport, Rhode Island. The lines indicate the fit from a linear regression model without the suspect data points (black symbols); $c_S^* = 14.2 \pm 3$ km y^{-1} (95% CI) and $c_N^* = 17.8 \pm 3$ km y^{-1}.

2.2.3 Model formulation

My model consists of a system of IDEs describing the spatial and temporal dynamics of a stage-structured population. I considered only female green crabs, because the population dynamics are assumed to be determined by female vital rates. The model has three life stages: first-year female juveniles, second-year female juveniles, and mature female adults. Let $\mathbf{u}_t(x)$ denote the vector of abundances of each stage at discrete time (t) and continuous

space (x). Hence, the entries of $\mathbf{u}$ are for first-year crabs, second-year crabs, and third-year and older crabs. Note that time is discrete, so that t is a nonnegative integer, and space is continuous, so that x is a real number. The population at a given location at time $t+1$ is determined by summing the individuals dispersing there from the entire coastline between time t and time $t+1$. Thus, the model takes the following form:

$$\mathbf{u}_{t+1}(x) = \int_{-\infty}^{+\infty} [\mathbf{K}(x-y) \circ \mathbf{B}]\mathbf{u}_t(y)dy, \tag{2.1}$$

where $\mathbf{K}$ is the dispersal matrix, $\mathbf{B}$ is the population projection matrix. The symbol '$\circ$' represents the Hadamard product which indicates entrywise multiplication of the two matrices. The use of the Hadamard product of $\mathbf{B}$ and $\mathbf{K}$ in Equation (2.1) follows from an assumption that the population has distinct, non-overlapping reproductive and dispersal phases. The rows and columns of the matrices $\mathbf{B}$ and $\mathbf{K}$ correspond to the stages of the model.

$\mathbf{B}$ is assumed to have the form:

$$\mathbf{B} = \begin{bmatrix} 0 & 0 & \phi b_L \\ b_1 & 0 & 0 \\ 0 & b_2 & b_A \end{bmatrix}, \tag{2.2}$$

where b_A is the survival probability of adults, and b_1 and b_2 are the survival probabilities for first and second year juveniles, respectively (survival probabilities are assumed to be similar for females and males; [73]).The upper right

entry in matrix $\mathbf{B}$, ϕb_L, is the number of first-year female juveniles produced per female adult per year; specifically, it is a product of the average number of female eggs produced per mature female each year (ϕ), and the probability a given egg survives to become a settled first-year juvenile (b_L). See Table 2.1 for an overview of the demographic and dispersal parameters.

Symbol	Description	Unit
b_L	Survival probability of planktonic larvae until settlement	-
b_1	Survival probability of first-year juveniles (over 1 yr)	-
b_2	Survival probability of second-year juveniles (over 1 yr)	-
b_A	Survival probability of female adults (per year)	-
c^*	Spreading speed	km y^{-1}
μ	Net displacement downstream	km
ϕ	Average number of female eggs produced per mature female per year	Eggs $female^{-1}$ y^{-1}
r	Recruitment rate to adult females ($r = \phi b_L b_1 b_2$)	Adult female offspring $female^{-1}$ y^{-1}
σ	Standard deviation of larval dispersal	km

Table 2.1: Descriptions and units of parameters of the integrodifference equation (IDE) model used to investigate the spreading speed and its relationship between demography and dispersal of the green crab *Carcinus maenas*.

Without dispersal, Equation (2.1) is simply the linear model $\mathbf{u}_{t+1} = \mathbf{B}\mathbf{u}_t$, which is known to have exponentially growing solutions as long as the reproduction number, $R_0 = \dfrac{\phi b_L b_1 b_2}{1 - b_A}$, is larger than one [33]. Hereafter, I assume that this condition is satisfied. If instead $R_0 < 1$, the population will decay to zero.

The dispersal matrix $\mathbf{K}$ is as follows:

$$\mathbf{K} = \begin{bmatrix} 0 & 0 & k_{13} \\ \delta & 0 & 0 \\ 0 & \delta & \delta \end{bmatrix}, \tag{2.3}$$

where k_{13} is the larval dispersal kernel and δ is the Dirac delta-function.

The entries of $\mathbf{K}$ are the dispersal kernels associated with the corresponding elements of $\mathbf{B}$. For example k_{13}, the top right entry of $\mathbf{K}$, is the distribution of the settled locations of the b_L surviving first-year juveniles appearing in the top right entry of $\mathbf{B}$. In my model, I assumed that the probability of dispersal from an adult at position y to a settled juvenile at position x depends only on the relative displacement $x - y$. Thus, dispersal kernels are functions of a single variable. What I call the larval dispersal kernel is a probability distribution for the relative locations of the offspring that survive to the first-year juvenile stage. Note that k_{13} specifies the distribution of crabs recruited from the adult stage to the first-year juvenile stage; thus, k_{13} models the dispersal of crab larvae.

I did not explicitly model the population of larvae since they are present for only a few months each year only in the water column and not settled on the coastline. Instead, the larval stage appears implicitly in the model through the dispersal terms. Further, survey data are collected in a specific season (usually the end of summer) when counts of larvae are negligible and the juvenile and adult stages are dominant.

2.2.4 Dispersal kernels and model analysis

To study the effect of the form of the larval dispersal kernel on the spreading speed, I considered two exponentially bounded dispersal kernels: the Normal and Laplace distributions, denoted by k_N and k_L, respectively. The selection of these dispersal kernels was motivated by the consistency of the range

expansion of green crabs along the west coast of the North Atlantic over 120 years of recorded observations [7, 73, 133]. Fat-tailed dispersal kernels, such as the Cauchy distribution, are those lacking exponentially bounded tails; these kernels have been shown to lead to accelerating speeds of invasion [76, 107] and so were not further considered here. The kernels are symmetric, but have nonzero means to model. I incorporated a parameter to represent the net displacement "downstream" due to the dominant southwestward currents along the west coast of North Atlantic (see for example Bigelow [13] for information in the Gulf of Maine, Davis and Browne [35] for Nova Scotia and Gulf of St. Lawrence). Normal dispersal kernels are expected from simple diffusion theory [76, 156], and have been used to model random walks [118, 140]. The Normal distribution was chosen in my analysis, partly for mathematical convenience and partly owing to a lack of knowledge of larval dispersal. The Laplace distribution is a good approximation to many of the leptokurtic distributions found in nature [75]. It has a heavier tail compared to the Normal dispersal kernel [91], indicating a greater tendency for long distance dispersal. The Laplace kernel can be derived mechanistically from Gaussian diffusion by adding behavioral detail. Examples include (i) diffusion with advection towards the origin [78], as might occur in territorial individuals or central place foragers, and (ii) diffusion coupled with constant probability of settling [91, 113] possibly after finding a suitable habitat. Synchronous settling gives a Normal dispersal kernel [113].

Due to the long planktonic duration and off-shore development of green

crab larvae in open waters, it is expected that the invasion is driven mainly by larval dispersal. I therefore neglected dispersal of juveniles and adults. Specifically, I assumed a Dirac-delta dispersal function δ for all transitions except for the recruitment from adult to first-year juvenile, which involves the larval stage.

Under the previous stated assumptions that (i) $\mathbf{B}$ is nonnegative, (ii) the basic reproduction number is greater than one, and (iii) the entries of $\mathbf{K}$ are exponentially bounded, then it is known [165] that all nontrivial solutions of Equation (2.1) that start in a confined area converge to a solution with a fixed profile moving at a constant speed. The speed of this traveling wave solution can be determined as a function of the parameters in the demographic ($\mathbf{B}$) and dispersal ($\mathbf{K}$) matrices [114].

The assumption that the entries of $\mathbf{K}$ are exponentially bounded is equivalent to assuming the existence of moment generating functions for the entries of $\mathbf{K}$ [76]. The moment generating function of the dispersal matrix $\mathbf{K}(z)$ is defined as follows:

$$\mathbf{M}(s) = \int_{-\infty}^{+\infty} \mathbf{K}(z) e^{sz} dz, \tag{2.4}$$

for all s in some interval about zero [76]; where s is a parameter related to the shape of the travelling wave (a spatial decay rate). The moment generating function is well defined for the Dirac-delta function δ, and for any exponentially bounded kernel. Thus, Equation (2.1) has a finite spreading

speed and constant-speed travelling wave solutions [166].

Using the Normal and Laplace distributions (k_N and k_L, respectively), I are able to compute the corresponding moment-generating functions (m_N and m_L, respectively) as follows:

$$k_N = \frac{1}{\sqrt{2\pi}\sigma} e^{-(\frac{x-y+\mu}{\sqrt{2}\sigma})^2}, \; m_N = e^{-s\mu+(\frac{s\sigma}{\sqrt{2}})^2}, \; |s| < +\infty, \tag{2.5}$$

$$k_L = \frac{1}{\sqrt{2}\sigma} e^{\frac{-\sqrt{2}|x-y+\mu|}{\sigma}}, \; m_L = \frac{2e^{-s\mu}}{2-(s\sigma)^2}, \; |s| < \frac{\sqrt{2}}{\sigma}. \tag{2.6}$$

In both of these dispersal kernels, $\mu \geq 0$ is the net displacement downstream and σ is the standard deviation of dispersers from this mean. Note that the larval dispersal parameters μ and σ are dependent on oceanographic features, temperature, larval pelagic duration and any interaction between hydrodynamics and larval behavior.

Following the theorems of Weinberger [166] as outlined by Neubert and Caswell [114], the invasion speed c^* is given by

$$c^* = \min_{0<s<\hat{s}} \Big[\frac{1}{s} \ln \lambda_1(s)\Big], \tag{2.7}$$

where $\lambda_1(s)$ is the principal eigenvalue of the wave projection matrix $\mathbf{H}(s) = \mathbf{B} \circ \mathbf{M}(s)$ for each $0 < s < \hat{s}$. Note that $\hat{s}$ is the upper bound of the domain of $\mathbf{M}$ in Equation (2.4). The principal eigenvalue, λ_1, of $\mathbf{H}$ for a well-defined moment generating function m_{13}, corresponding to the larval dispersal kernel

k_{13}, is the leading root of the characteristic equation

$$\lambda^3 - b_A\lambda^2 - rm_{13}(s) = 0, \tag{2.8}$$

where $r = \phi b_L b_1 b_2$. Applying a technique developed by Miura [106], it follows that

$$\lambda_1 = 2\frac{b_A}{3}\cosh\psi + \frac{b_A}{3}, \tag{2.9}$$

where for the Normal distribution

$$\psi = \frac{1}{3}\cosh^{-1}\{1 + \frac{27re^{-s\mu+(\frac{s\sigma}{\sqrt{2}})^2}}{2b_A^3}\}, \tag{2.10}$$

and for the Laplace distribution

$$\psi = \frac{1}{3}\cosh^{-1}\{1 + \frac{27re^{-s\mu}}{b_A^3(2-(s\sigma)^2)}\}. \tag{2.11}$$

Note that r is a recruitment rate, i.e., the expected number of new female adults that survive to maturity per mature crab each year. Having an expression for c^*, given by Equation (2.7) with λ_1 as the leading root of (2.9), enables one to analyze the effects of demographic and dispersal parameters on the spreading speed. This dependence is illustrated by the contour plots in Figure 2.3 which were constructed as follows. Define the speed

$$c = \frac{1}{s}\ln[\lambda_1(s, r, b_A, \mu, \sigma)]. \tag{2.12}$$

Then the minimum c^* occurs when

$$\frac{\partial c(s, r, b_A, \mu, \sigma)}{\partial s} = 0. \tag{2.13}$$

Maple$^{\text{TM}}$ [98] was used to calculate Equation (2.13) symbolically and numerically compute r, σ as a function of s for a given μ. This computation gives a parametric representation of r and σ with respect to s for a given c^* and μ. The critical value for s in Equation (2.7) is denoted by s^*. The existence of s^* is guaranteed by the convexity of λ_1 with respect to s [94]. This simulation was done for both the Normal and Laplace dispersal kernels. I use Matlab® [102] to generate the contour plots in Figure 2.3.

2.2.5 Elasticity analysis

To study the effect of changes in the dispersal and demographic parameters on the invasion speed, c^*, I performed an elasticity analysis. An elasticity is a proportional measure of sensitivity and is useful when demographic and dispersal parameters are measured on different scales. It is defined here as the derivative $p\frac{\partial \ln(c^*)}{\partial p}$ where p is the parameter of interest, and it can be interpreted as the percent change in c^* with a percent change in p. The elasticity analysis of c^* with respect to the dispersal parameters μ and σ is computed by differentiation Equation (2.12), implicit differentiation of Equation (2.8) and evaluating at s^*. The elasticity analysis of c^* with respect to the demographic parameters required the technique developed by Neubert

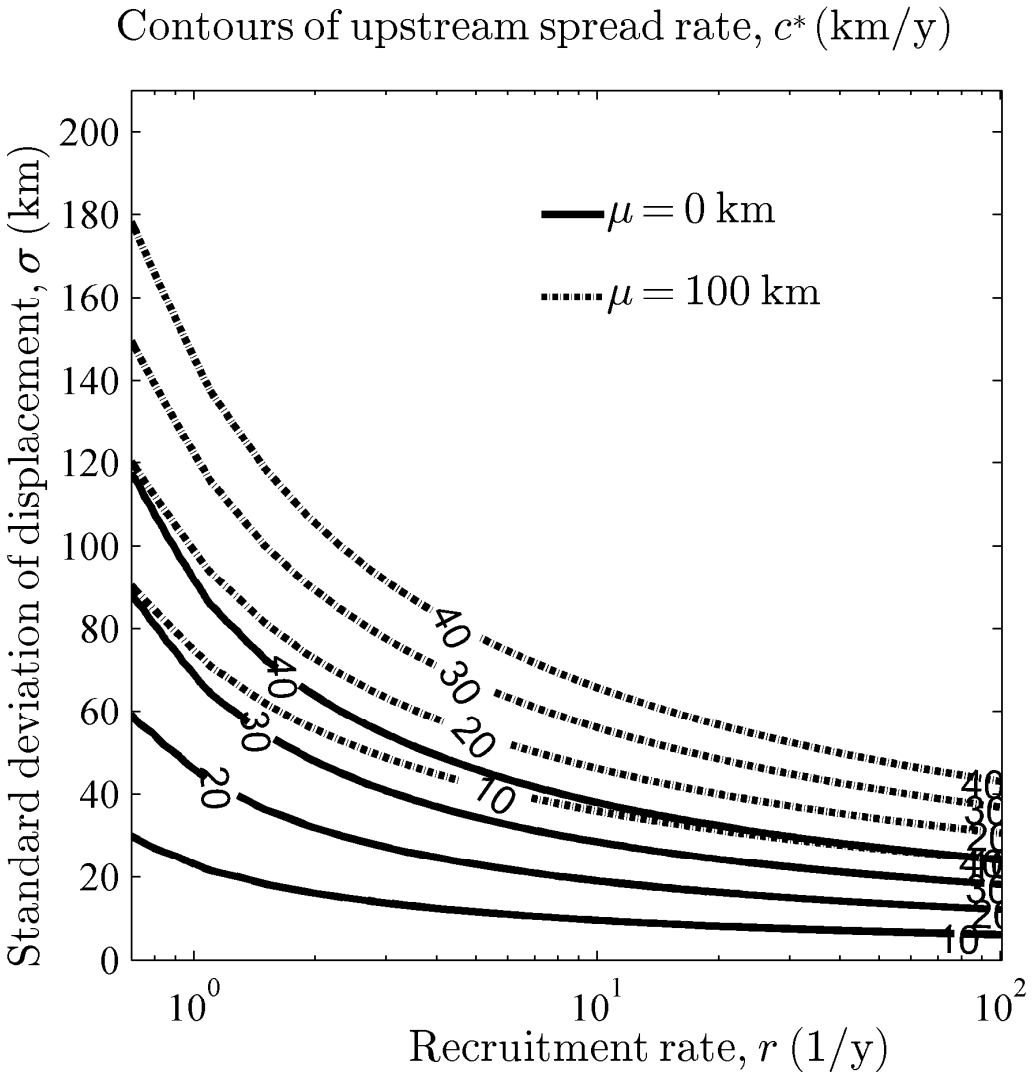

Figure 2.3: Contour plot of the spreading speed (c^*) of green crabs *Carcinus maenas* derived from the model (Equation 2.7, with Laplace dispersal kernel) versus dispersal and demographic parameters, σ and r. Four values were chosen for c^* (10, 20, 30, 40 km y^{-1}) in 2 cases: $\mu = 0$ km shown by full lines, $\mu = 100$ km shown by dash-dotted lines. I assumed $b_A = 0.75$. See Table 2.1 for definitions.

and Caswell [114] for structured IDEs.

To analyze the sensitivity of c^* to changes in demographic parameters in the matrix $\mathbf{B}$, let h_{ij} be the ijth element of $\mathbf{H}$, let $\mathbf{v}$ and $\mathbf{w}$ be the right and left eigenvectors of $\mathbf{H}(s^*)$ corresponding to $\lambda_1(s^*)$, and let $\langle , \rangle$ denote the scalar product. Following Neubert and Caswell [114], the elasticity of c^* to changes in the ijth element of the demography matrix $\mathbf{B}$, b_{ij}, is defined as follows:

$$\frac{b_{ij}}{c^*}\frac{\partial c^*}{\partial b_{ij}} = \frac{h_{ij}(s^*)}{\lambda_1(s^*)\ln(\lambda_1(s^*))}\frac{v_i w_j}{\langle \mathbf{v}, \mathbf{w}\rangle}. \tag{2.14}$$

where v_i and w_j refer to the i^{th} (j^{th}) component of $\mathbf{v}(\mathbf{w})$. Note that all quantities $m_{13}, \lambda_1, h_{ij}$, and their derivatives are functions of s; in Equations. (2.5),(2.6), (2.9) and (2.12), they are all evaluated at $s = s^*$.

Note that the adult survival probability, b_A, can be estimated according to the life expectancy of the adult crabs. Assuming the adult life expectancy to be 4 years [12], results in $b_A = 0.75$. Based on a fecundity of 185000 ± 7000 and a $1:1$ sex ratio [29], I have an estimate for ϕ on the order of $100,000$. The larval survival probability (b_L) for other marine invertebrates with similar pelagic larval stages has been estimated to be in order of 0.001 [126, 152]. To my knowledge, there is no estimate for the green crab's juvenile survival probabilities (b_1 and b_2). All I can say is that they are in the range of $(0, 1)$. Thus, I deduce r to be on the order of 100 or lower. I have an estimate for currents [13, 97, 125], which can be used to guess a range for μ of $(0, 400)$ km. In Figure 2.3-2.5, two values for μ are considered: 0 km and 100 km. To my

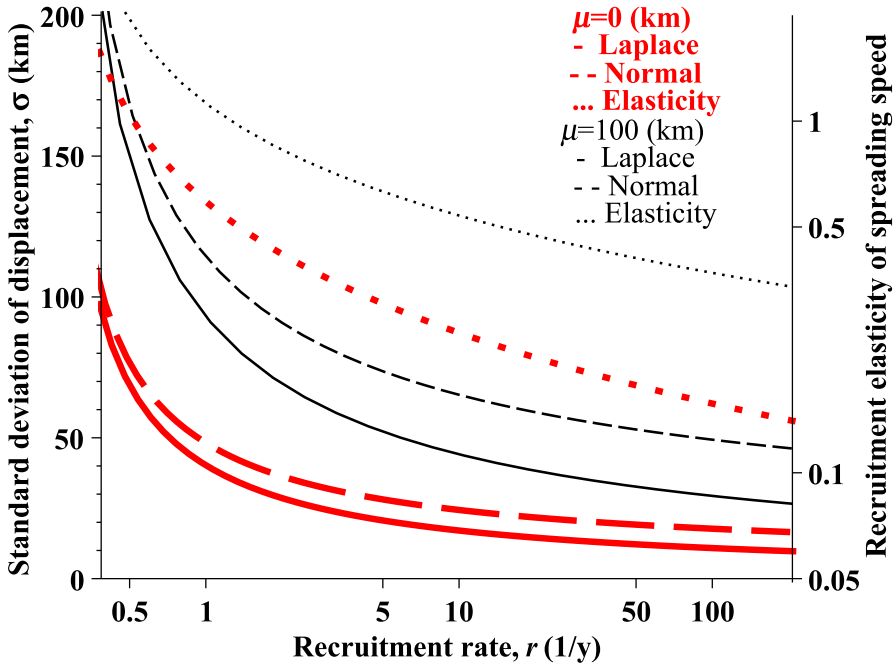

Figure 2.4: Recruitment rate, r, of green crabs *Carcinus maenas*, c^* and b_A are fixed at 17.8 km y^{-1} (see Figure 2.2) and 0.75, respectively, with Laplace and Normal dispersal kernels for larval dispersal. Elasticity of spreading speed is shown with respect to recruitment rate for different values of standard deviation of dispersal (Equation (2.6)).The curves corresponding to $\mu = 0$ km and $\mu = 100$ km are shown in bold red and fine black, respectively. See Table 2.1 for definitions.

knowledge, there is no estimate for the standard deviation of displacement (σ). To illustrate the results in Figure 2.3 and 2.4, σ varies in the range of $(0, 200)$ km. In Figure 2.5(a) and (b), I choose $b_1 = b_2 = 0.5$ and $\sigma = 30$ km.

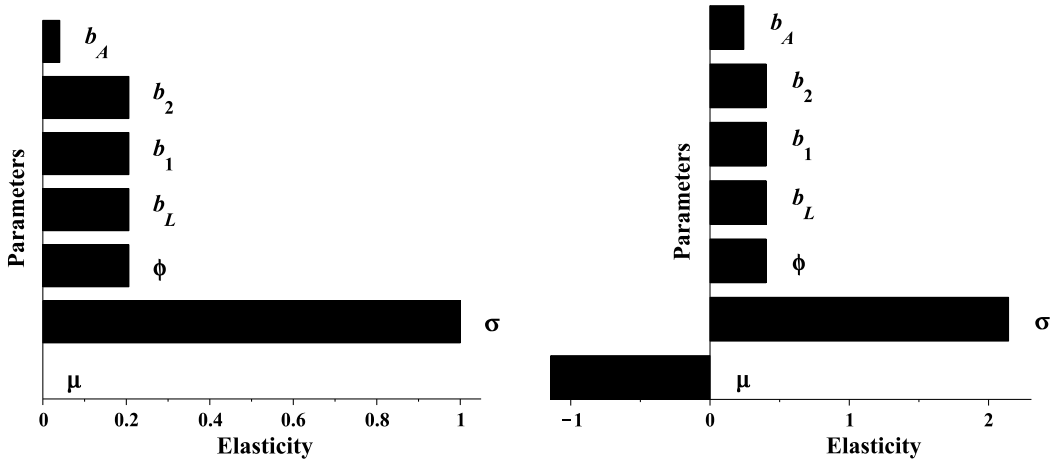

Figure 2.5: Elasticity of the spreading speed, c^*, of green crabs *Carcinus maenas* with respect to each model parameter. (a) Net displacement, $\mu = 0$ km, (b) $\mu = 100$ km (Equation 2.12). The calculations assumed a Laplace distribution for k13 (larval dispersal kernel) and the following parameter values: $b_L = 0.001$; $b_1 = b_2 = 0.5$; $b_A = 0.75$. In panel (a), $\sigma = 30$ km, and $c^* = 54$ km y^{-1}; in panel (b), $\sigma = 30$ km, and $c^* = 24$ km y^{-1}. See Table 2.1 for parameter definitions. Note that the elasticities of c^* to ϕ, b_1, b_2 and b_L are always identical and only depend on the value of the product r.

2.3 Results

2.3.1 Empirical estimates of spreading speed

A set of times (years) and locations of first appearance of adult green crabs were obtained from the larger dataset of green crab sightings. The resulting dataset for the first appearance contains several suspect points (Figure 2.2). I therefore carried out the statistical analysis with the full first appearance data and repeated the analysis with suspect points removed. The suspect points for the southern lineage are as follows: Newport (Rhode Island) in 1844, the tip of Cape Cod in 1872, and Guysborough (Nova Scotia) in 2002. The first two were suspect because the data points may not meet the criterion on sightings of recently established adult green crabs, and the third because of the likeliness of interactions with the more recently introduced northern lineage. For the northern lineage, since the spatial environment is different south and north of the Strait of Canso, I conducted the regression for the northern lineage with and without the point located before the Strait of Canso (Chedabucto Bay in 1985).

I estimated the northward spreading rate of the southern lineage as 8.8 ± 2 km y^{-1} (95% CI) with all three suspect points included, and 14.2 ± 3 km y^{-1} without them (Figure 2.2). If I just included Newport 1844 and Cape Cod 1872, and excluded Guysborough 2002, the rate was 8.7 ± 3 km y^{-1}. If the 2002 data point was included and the 1844 and 1872 were not, the rate was 12.8 ± 2 km y^{-1}. For the northern lineage, if I combined the

data points south and north of the Strait of Canso, the estimated spreading speed was 15.8 ± 3 km y^{-1}. The estimated spread rate regarding only the points north of the Strait of Canso was 17.8 ± 3 km y^{-1} (Figure 2.2). I chose the latter estimate for mathematical analysis whenever an independent estimation of the spreading speed was required. This decision was based on the higher confidence in the dataset used for the northern lineage spreading northwest of the Strait of Canso (from Aulds Cove in 1994, Nova Scotia, to Kouchibouguac, New Brunswick, in 2013).

2.3.2 Relationship between spreading speed and demographic and dispersal parameters

The analysis of my model yields a relationship between the northward spreading speed of the green crab, the demographic parameters and the parameters of the dispersal process. Assuming the observed mean spread rate, this relates the mean μ and standard deviation, σ, of larval dispersal to the recruitment rate of adult females r (Figure 2.3), and provides insight into the relative importance of these two processes during a spreading event. The results can be summarized in two parts: first, the upstream spreading speed c^* is increasing in both r and σ and decreasing in μ; and second, a given spreading speed can be achieved with various combinations of feasible values of r and σ (for example high r and low σ, or low r and high σ). More precisely, there is a concave up curve in the (r, σ) plane giving rise to the constant spread

rate observed for the green crab along the east coast of North America. If we suppose that, for example, $\mu = 0$ km (isotropic larval dispersal), the spreading speed of 17.8 km y^{-1} estimated for the northern lineage (Figure 2.2(b)) could be the result of a recruitment rate of 100 adult female offspring/female adult/y and a standard deviation of larval dispersal of 9 km, or a recruitment rate of 1 adult female offspring/female adult/y and a standard deviation of larval dispersal of 40 km. Similarly, if we suppose that $\mu = 100$ km (a net downstream dispersal), the observed spreading speed of 17.8 km y^{-1} would result from either $r = 100$ y^{-1} and $\sigma = 30$ km or $r = 1$ y^{-1} and $\sigma = 100$ km, or any combination on the contour connecting these points (Figure 2.4).

Besides the trade-off between r and σ for a given c^* value, at relatively low σ, a small decrease in σ requires a large increase in r to obtain the same spread rate, and at relatively high σ, a small decrease in σ requires a small increase in r. This trade-off is well known when modeling using IDEs population persistence in the face of advection [95, 120]. Note that in Figure 2.4 the c^* contours shift up as μ increases (i.e., as net advective displacement moves downstream) which matches with the results of Pachepsky et al. [120].

For a given spreading speed c^* (e.g., 17.8 km y^{-1}), the type of dispersal kernel (Laplace versus Normal) does not greatly affect the relationship between r and σ (Figure 2.4). However, there are differences in concavity in the c^* contours, which have implications on the sensitivity of c^* to r and σ. The sensitivity of c^* to r for low versus high values of σ is not consistent along the c^* contours for the Normal and Laplace distributions. The sensitivity

reverses as σ increases; i.e., the sensitivity of r in low values of σ is higher for the Normal than the Laplace curve, but the sensitivity of r in high values of σ is higher for the Laplace than the Normal curve.

The elasticity of c^* to r increases along c^* contours as r decreases for a given μ. That is, for a given c^*, c^* is more sensitive to changes in r at low r (Figure 2.4). Also the elasticity of c^* to r increases with μ. In a broader elasticity analysis of c^* to the underlying parameters, I considered two cases (in Equation (2.6)). First, I assumed that the net displacement downstream was small relative to σ ($\mu = 0$ km), which is equivalent to using the isotropic larval dispersal kernel in the model (Equation (2.1)); second, I assumed a large (relative to σ) net displacement downstream (specifically, $\mu = 100$ km), which leads to a shifted dispersal kernel. Spreading speed is equally sensitive to the vital rates included in the definition of r for the two cases (Figure 2.5), i.e., the elasticity to each of ϕ, b_L, b_1, b_2 (fecundity, and survival probability of larvae and juveniles) is approximately 0.2 when $\mu = 0$, and 0.4 when $\mu = 100$. The adult's survival probability b_A has a lower proportional effect (0.04 when $\mu = 0$ km, and 0.2 when $\mu = 100$ km) than the other vital rates; Figure 2.5 implies that a percent change in r is roughly 5 times in first case (2 times in second case) more effective at reducing the spreading speed c^* as a similar percent change in b_A. Contour plots of the elasticity of spreading speed c^* to recruitment rate r or adult survival b_A in the (r, b_A) plane with $\mu = 0$ (Supplementary material, Figure 2.6) indicate that c^* is less sensitive to adult survival than to recruitment rate. Note that c^* is most sensitive to

recruitment rate r when both r and adult survival b_A are low (Figure 2.6 a). Sensitivity of c^* to b_A does not seem to be similarly affected by values of r (Figure 2.6 b) . The dispersal standard deviation, σ, has the largest elasticity, and so the most effect on c^* (Figure 2.5). The elasticity is 1 when $\mu = 0$, which means that, if σ increases by 1%, then c^* would increase by 1%. It also indicates that a percent change in the dispersal parameter, σ, has 5 times more effect on c^* than a similar percent change in r when $\mu = 0$. Information on the sensitivity of c^* to variations in the parameters can be used to design sampling methods that maximize the accuracy of estimates of the most critical parameters. The elasticity information also informs us about the parameter that managers could focus on to try to control the invasion if possible. The above discussion of the elasticities is based on the specific parameter values noted in the figure captions (Figure 2.4, 2.5). I speculate that these results are valid more generally for the full range of feasible parameter values.

2.4 Discussion

2.4.1 Relationship between spreading speed and demographic and dispersal parameters

The spread of the invasive green crab (*Carcinus maenas*) along the east coast of North America has provided an opportunity to examine the relationship

between demographic and dispersal processes involved in the spread in a theoretical context. Despite many studies and much attention on the green crab problem, there is a need for new advances in both empirical and theoretical work. The results presented here illustrate that there are many combinations of the recruitment rate (a demographic parameter, r) and the standard deviation of larval dispersal (a dispersal parameter, σ) that give rise to a given spreading speed c^*. More specifically, I computed c^*-contours in the (r, σ) parameter plane and found that (i) The importance of recruitment rate on c^* is dependent on the values of the recruitment rate; (ii) the net displacement downstream, μ, has a negative impact on c^*; and (iii) the elasticity of c^* to r increases as r decreases. However, c^* is more sensitive to the dispersal parameter, σ, than the demographic parameters. Although the observation of a consistent spreading speed of the green crab on such large geographical and temporal scales triggered my study, it remains difficult to conceive that the demographic and dispersal parameters are constant along the entire coast or that they change in such a way as to keep c^* constant. It seems that the advance might be limited to extremes in annual conditions and only appear steady on the scale of decades.

The realized trade-off relationship between demography and dispersal parameters in the context of spreading speed theory has been previously observed in the Fisher equation [43, 165]. The Fisher equation is a scalar

reaction-diffusion model, and with advection it yields

$$c^* = 2\sqrt{RD} - v, \tag{2.15}$$

where c^* is the upstream spreading speed, R is the intrinsic growth rate of population (in my model, recruitment rate $r = \log R$), D is the diffusion coefficient, and v is the downstream advection speed experienced by the organisms ($v > 0$; note that here we have an advection speed, as opposed to a advective displacement after a set period of time as in my model). Thus, the relationship between demography and dispersal parameters in Fisher model is analytically expressed (Equation (2.15)) and the c^* contours in the $R - D$ plane are hyperbolic and shifted up as v increases. This is similar to the results of a stage-structured IDE model (as my model), which to my knowledge has not been presented in the literature before (see Figure 2.3 and 2.4). The relationship that we see in my model is not hyperbolic, but the contours are concave and increasing/decreasing with the parameters in the same ways as the Fisher model. From Fisher model to my model, there are two other models: (1) generalizations of Fisher's equation to advective systems and structured populations [120], and (2) non-structured IDEs [76]. Both give computational results similar to ours.

2.4.2 Mathematical simplifications in the model

A number of assumptions were made in developing the green crab model of Equation (2.1). First, the model assumes a one-dimensional coastline. While this is a common assumption in population dynamic models, adding an extra space dimension may include the effect of ocean back-eddies and turbulent flow on the kernel for larval dispersal. For example, Méndez et al. [103] applied a two-dimensional dispersal kernel to model the reaction transport of particles in diffusive media. However, assuming a one-dimensional coastline is appropriate for my model, because green crabs settle, grow and reproduce in intertidal and shallow subtidal areas [73]. Effectively, the two and three-dimensional aspects of the hydrodynamics are integrated, resulting in a dispersal along a one-dimensional coastline. Second, the model assumes an infinitely long coastline. This assumption is necessary to apply the traveling wave analysis leading to the spreading rate, and is reasonable (since the coastline is very long relative to the scale of the crab's demographic and dispersal processes) up until the population reaches the northern limit of the coastline. Applying the same modeling procedure to a more realistic coastline with finite length has been studied in the context of persistence in fragmented habitats [95, 159]. Understanding the role of spatial heterogeneity on invasion dynamics is currently a topic of much interest (reviewed in [58]). Third, the model assumes a simple shifted kernel for larval dispersal and assumes a negligible dispersal for juvenile and adult stage to simplify the analysis. Note that it is my future plan to relax this assumption and

examine the spatial population dynamics with adult dispersal. Fourth, the demographic processes are assumed to be linearly dependent on population density. Specifically, there is no density dependence in vital rates: no carrying capacity and no Allee effects. Finally, all vital rates are assumed to be independent of location. These last three assumptions are discussed in detail below, and are related back to my main question about the relationship between demography and dispersal.

2.4.3 Larval dispersal kernel

Determining a realistic kernel for larval dispersal is nontrivial. The larval stage is difficult to observe and track in the marine system. The simplest approach taken here was also that taken by Byers and Pringle [18], who assumed a Normal (Gaussian) dispersal kernel. My investigation of the Laplace distribution was motivated in part by the result that Normal dispersal coupled with a constant settling rate results in a Laplace kernel [113]. Asymmetric, shifted and bimodal dispersal kernels have all been suggested and applied to coastal population dynamics [19, 121, 128, 139]. In this work the shifted dispersal kernels were considered to account for advection. It is reasonable to assume that behavior and pelagic duration of larvae play a critical role in determining dispersal distance for marine species [139], and this can be examined theoretically using existing hydrodynamics models that incorporate vertical migration behavior and maturation times of larvae (e.g., [24]). Given that my elasticity analysis indicated that the spreading speed c^* was

most sensitive to the larval dispersal parameter σ, more work needs to be done to more thoroughly understand larval dispersal of green crabs in oceanic environments.

There are several approaches to estimating the dispersal parameters, μ and σ. The small size and fragility of larvae makes standard tagging approaches (e.g., [63]) inapplicable. Alternative methods to estimate propagule distribution include genetic studies [8, 144], use of natural phenotypic tags [3], and hydrodynamic models [24, 61, 66]. Since determining the pathways and distance of larval transport through direct means is neither logistically tractable nor currently affordable, using hydrodynamic models is a good alternative to understand larval transport processes [10]. At large spatial scales, such modeling can describe larval advection pathways, determine the relationship between spawning and nursery areas [37], and account for patterns of variation in recruitment rates [158]. At smaller spatial scales, numerical hydrodynamic models have identified settlement sites [65].

2.4.4 Linear model versus density dependence

My model (Equation (2.1)) assumes linear population growth, since recruitment and survival rates are density independent. Thus, the per capita growth rate derived from the demographic matrix, $\mathbf{B}$, was constant. In the absence of Allee effects, including a carrying capacity has no effect on the invasion speed because it does not affect the dynamics at the leading edge of an invasion [140]; I therefore did not include a carrying capacity to keep my model

as simple as possible. In the situation of species establishing themselves in a new environment, Allee effects may be important, as a critical number of individuals may be needed for successful production of offspring [140]. Including Allee effects in the demographic matrix gives rise to nonlinearities in the rates of population growth as well as spread [140]. Specifically, if the basic reproduction number R_0, defined as the spectral radius of $\mathbf{B}$, is less than one, then the initial rate of spread can be slower than predicted by Equation (2.1), but then it can increase with time [84]; if so, the constant rate of spread modeled in my study would no longer hold. Rather, the rate of spread would have a sigmoid pattern over time [140]. Allee effects may occur among invading green crabs, and I wondered if the time series for each crab lineage (Figure 2.2b) showed an indication of slower initial spread if I was to include the first two data points (Newport in 1844, and Cape Cod in 1872) for the southern lineage and the first data point (Chedabucto Bay in 1985) for the northern lineage. However, my data set is not precise enough to genuinely differentiate between a linear and curvilinear pattern, and so I opted to model the simpler (linear) pattern.

2.4.5 Spatial dependencies, and other estimates of spreading speed in green crabs

I assumed for my modeling exercise that the green crab's vital and dispersal rates were independent of geographic location. Yet, the northwest Atlantic

coast has different physical environments, with different water temperatures and fine-scale currents [39, 54, 56, 173]. Given that development rates are temperature dependent [36], one would expect population dynamics of green crabs, as of other organisms, to be spatially dependent (i.e., vary from one geographic location to another). Indeed, observation of the considerable decrease in abundance of green crabs (southern lineage) before reaching Halifax (actually, around Prospect Bay, Nova Scotia) in the 1960s was attributed to the influence of the cold Nova Scotia Current slowing and even arresting larval development [7]. Other studies dealing with the northward spread of green crabs along sections of the same coast as in my study provide different estimates of spreading speed, and may be indicative of finer-scale variation in spreading speed. For example, Grosholz and Ruiz [53] estimated (using data from Glude [49] and Welch [169], and applying linear regression) a spreading speed of 63 km y^{-1} from north of Cape Cod through Maine to just east of Cape Sable in southwestern Nova Scotia. Klassen and Locke [73] reported speeds of up to 100 km in a year in certain areas of the southern Gulf of St. Lawrence. I estimated speeds of 100 km y^{-1} (from 1994 to 1997) for the coast of Cape Breton, Nova Scotia, likely related to the very high currents associated with Cabot Strait (Gharouni et al. unpublished data). However, estimates similar to that in my study ($\sim 8 - 18$ km y^{-1}, depending on the data points I included in my analysis) have been reported too. Recently, Kanary et al. [70], using absolute distances between locations representing first observations of green crabs and linear regression, reported an average north-

ward spread rate of 14.3 km y^{-1} for the southern lineage from Massachusetts (1817) to Prospect Bay, Nova Scotia (1966). Glude [49] reported that green crabs took 79 years (1872-1951) to spread from Cape Cod to Passamaquoddy Bay, New Brunswick, a distance of about 690 km, which equates to an average rate of spread of 8.7 km y^{-1}. Glude [49] apparently expected a faster spread for the species, presumably based on its long planktonic duration, and attributed the slow spread to water temperatures that, for much of the region, were historically less than the species' minimum tolerance. The difference in estimated spread rate of *C. maenas* along the east coast of North America may be partly related to the use of different data sets, as well as different methods of projecting the data to derive the distance between two locations. In sum, my assumption of fixed vital and dispersal rates is simplistic; however, the present parameter values may represent good and useful time- and space-averaged values.

Three relevant studies have mathematically modeled the green crab invasion on the east coast of North America, and different modeling approaches were used to investigate spread dynamics. Grosholz [51] applied a single-stage partial differential equation (PDE) to model the invasion process, which assumed a Normal dispersal kernel and a non-structured population. In the following thesis, I have already shown that the exponentially-bounded kernel used (e.g., Normal versus Laplace) makes little difference to the estimate of spreading speed (see also [18]). However, having no built-in stage structure may make a large difference, and lead to modeled units (crabs) contribut-

ing (i.e., growing and reproducing) too quickly to the modeled population [155], and to a higher estimate of spreading speed [114]. Byers and Pringle [18] built population structure into their model: they used a cellular automata simulation with dispersing larvae and sessile adults, They concluded that green crabs could spread upstream, similar to the conclusion reached by Pachepsky et al. [120] for a generic aquatic organism. Pringle and coauthors [127, 128] used the same model to investigate various aspects of the mixing of the southern and northern green crab lineages. Kanary et al. [70] also developed a stage-structured IDE (one for each green crab genetic lineage) based on [120, 121]. However, they added competition between the two lineages and examined the spread rate of both lineages before and after they met. Their model estimated the northward spread rate of the southern lineage at 18.76 km y^{-1} (which is close to their empirical estimate and to my own estimates), a southward spread rate of the northern lineage at 38.17 km y^{-1} (which is in the same direction of the dominant current along coastal Nova Scotia), and a southward spread of the two interacting lineages of 18.82 km y^{-1}.

In other parts of the temperate world, there is wide variation in the estimated rate of range expansion by invasive *C. maenas*. In South Australia, the mean rate of spread was approximately 1.7 km y^{-1} from the early 1970s to 2003 (estimated by linear regression [153]). Such slow rates may be related to decreased vital rates of green crabs because of interactions with native species (possibly culminating to biotic resistance [68, 148]), and of physical

environmental conditions, and/or to decreased dispersal of the crabs because of spatial heterogeneity of invadable habitat or other phenomenon [58]. In South Africa, *C. maenas* spread was on average 16 km y^{-1} from 1983 to 1992 (estimated by linear regression; Grosholz and Ruiz [53]), which is within the same range as in my study. In contrast, *C. maenas* appear to have spread quickly along the North American Pacific coast. Following its initial detection in 1989 or 1990, the species spread throughout San Francisco Bay (maximum distance of about 80 km) in only 3 years ($\approx$ 27 km y^{-1}; Cohen et al. [30]), apparently through natural dispersal. Although there are a number of mechanisms that could have facilitated its spread around the bay (a bait industry, heavily fouled tires used as bumpers on vessels), none of these are strongly implicated as important in its spread [153]. Between 1993 and 1994, the species spread from San Francisco Bay to Bodega Harbor in northern California, a distance of about 120 km [53]. Subsequently, the species very rapidly spread to Oregon and possibly southern Washington in 1996, and to the west coast of Vancouver Island, Canada, in 1998 (i.e., 100's km y^{-1}; [175]). In many such studies, it is difficult to tease out whether spread was assisted by anthropogenic transport and/or strong currents; in the case of the west coast of North America, the rapid spread rate is correlated with strong coastal currents associated with the 1997/1998 El Niño event [176]. It is interesting that green crab spread rates similar to those observed on our coast can be found elsewhere in the world (e.g., South Africa).

2.4.6 Implications for further field research and for management

Once established at a location, management of a green crab invasion consists of finding ways of controlling the densities and limiting secondary spread. Eradication does not appear to be a viable option for established green crabs given the high biotic potential and long-dispersing larval stage of the species [38, 134]. Managing anthropogenic activities that facilitate green crab spread, such as anthropogenic transport vectors if identified, is an obvious management option [73] that is currently being implemented in various areas [151]. Managing or manipulating natural aspects of the green crab's life cycle is more difficult. My modeling exercise provides insights here, since it can assess the influence of demographic processes and dispersal on the spreading speed. Specifically, the results of elasticity analysis can be used to identify the most influential parameters involved in the spread rate, which could be targeted by managers.

Elasticity analysis indicated that the standard deviation of larval dispersal (σ), rather than vital rates (fecundity, survival probabilities) has the most effect on spreading speed. This result is partly due to my assumption that only larvae disperse and not adults. It has been shown in age-structured reaction-diffusion models that the spreading speed increases as the mobility of the immature population stages increases [e.g., 146]. For this model, the invasion is due to the larval dispersal and the wave is pushed forward by lar-

vae dispersal. I conjecture that the average age of the adult crabs decreases towards the front of the wave. This conjecture could be generalized to any spreading species where dispersal is dominated by the larval stages and the adults are sessile, and should be checked in the field. Based on the elasticity analysis, anything affecting larval dispersal distances is expected to cause relatively large changes in the spreading speed; so changes in weather that affect currents, changes in the location of currents, etc. are expected to be relatively important in affecting the crab spread rate.

However, larval dispersal is not manageable by humans. The next parameters that most affected spread speeds were fecundity (ϕ) and survival of larvae and juveniles (b_L, b_1, and b_2). Methods of lowering fecundity of or rendering infertile green crabs using parasites have been discussed in the past [50], although there may be problems with host specificity. Larval survival is likely another process (like larval dispersal) that cannot be manipulated; typical of marine species with long-lived larval stages, the probability of larvae surviving and returning to coastal areas for settlement is highly variable, being dependent on the oceanic environment [126]. One stage that may be manageable, but that we do not know much about, is the juvenile stage. Generally, juvenile crabs are cryptic, and their survival has been shown to be dependent on finding suitable shelter [64]. Density of juvenile green crab on intertidal shores can be reduced due to limited shelter availability or competition for shelters with other crab species [67]. There may be methods to limit juvenile densities that would be interesting as a management op-

tion, perhaps involving traps attractive to juveniles. The parameter that least affected spread dynamics in my model was survival of adults (b_A). It is noteworthy that green crab control options most considered by managers (fishing, trapping to reduce adult survival [161]) are focused on the life stage that least affects spread dynamics; the adult stage is the stage most easy to manipulate, but with the least effect. A fuller exploration of the interactions between spreading speed, recruitment rate and adult survival (Figure 2.6) suggests that manipulation of juvenile survival will have more impact on the dynamics if adult survival is also low. Note that the effect of manipulating adult survival does not seem to similarly depend on what happens to the juvenile stage. Taken together, reducing juvenile survival in combination with reducing adult survival may be an effective and achievable management strategy. The demographic sensitivity analysis (Figure 2.5) can provide a start for a cost-benefit analysis; my sensitivity analysis suggests that a change in adult survival (b_A) is 2 to 5 times less effective at reducing spreading speed than changes in the other vital rates (ϕ, b_L, b_1, b_2). So, if changing b_A is not 2 to 5 times cheaper than changing the other vital rates (juvenile survival probability envisioned to be most feasible), then it may be worth spending money to control younger stages. Note though that the factor of 2 and 5 probably depends on the values of b_A and r. Note also that a next step is to incorporate adult movement [153] in my model and to assess effects on spatial population dynamics and possible management strategies.

2.5 Conclusions

The green crab (*Carcinus maenas*) has had fairly consistent northward spread rate ($8 - 18$ km y^{-1}) along the east coast of North America since its first introduction in the 1800s, covering more than 50° of latitude, about 2000 km of coastline, different water bodies, and two cryptic invasions. This spread rate can be obtained with many combinations of realistic demographic and dispersal rates of green crabs. My age-structured integrodifference model for the green crab made a number of considered and appropriate simplifications, assuming a one-dimensional, continuous and long coastline, exponentially-bound dispersal of larvae, and no density dependence in the recently established green crab populations. I found that the choice of dispersal kernel (Normal or Laplace distribution) for larvae only minimally affected estimates of spreading speed. Furthermore, a mean displacement downstream does not affect the relationship between the standard deviation of the dispersers and recruitment rate. Whereas, it has an impact on the spreading speed. Sensitivity analysis of the model indicated that the dispersal parameter (specifically, the standard deviation of larval dispersal) had more effect on population dynamics than demographic parameters. Among demographic parameters, some (fecundity, and larval and juvenile survival probabilities) had more effect than others (adult survival probability), and this has implications for what managers might want to target to control the invasion. Future field research requirements, indicated by my modeling exercise, include better

understanding of the factors affecting survival of juvenile green crabs as well as testing model predictions in the field. Future modeling research directions include assessing the effect of different types of dispersal kernels beyond the symmetric, exponentially-bounded Normal and Laplace distributions, and evaluating the effect of patchy habitats on the crab's spreading speed and the possibility of adult movement contributing to dispersal rates. Obviously, further study of larval processes using hydrographic modeling, population models and field investigations would improve the quality of model inputs.

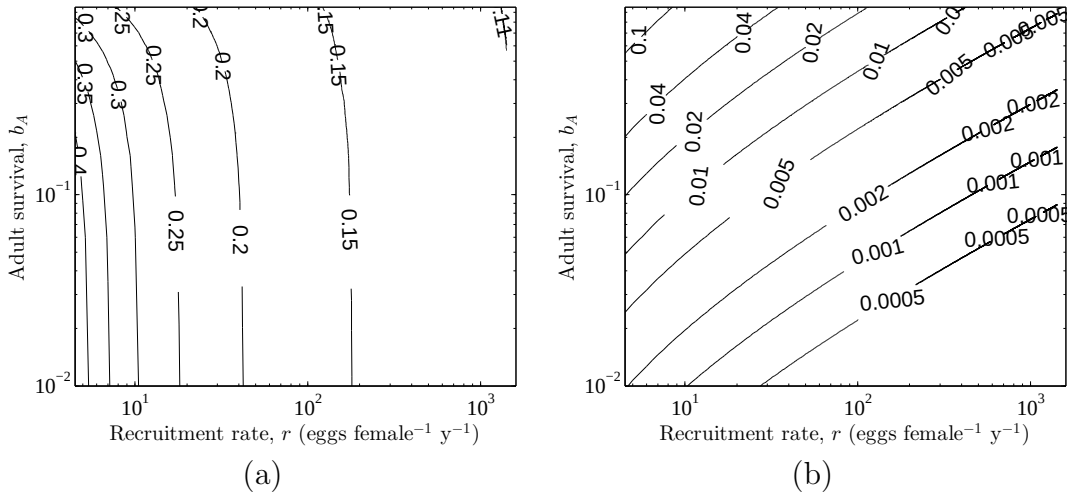

Figure 2.6: Contour plots of the elasticity of the spreading speed c^* to a) recruitment rate r and b) adult survival b_A in the (r, b_A) plane, for the stage-structured intregro-difference model Equation (2.1) of the green crab *Carcinus maenas*. The standard deviation of dispersals of crab larvae was fixed at 11 km when $\mu = 0$ km. c^* varied between realistic rates of 11 to 37 km y^{-1}, in response to changes in recruitment rate r (from 5 to 1500 adult female offspring female adult^{-1} y^{-1}) and in probability of adults surviving over one year b_A (from 0.01 to 1). The contour lines represent the elasticity of c^*. As a first example, when $r = 6$ and $b_A = 0.01$ (and so $c^* \approx 12$ km y^{-1}), elasticity of c^* to r is 0.4 (in panel a), and elasticity if c^* to b_A is 0.002 (in panel b). As a second example, when $r = 1500$ and $b_A = 0.91$ (and so $c^* \approx 37$ km y^{-1}), elasticity of c^* to r is 0.11 and elasticity of c^* to b_A is 0.005.

Chapter 3

Stochastic dispersal increases the rate of upstream spread: a case study with green crabs on the northwest Atlantic coast [1]

3.1 Introduction

Understanding the mechanisms used by invasive species to spread against a dominant current in an aquatic environment remains an interesting problem today despite more than two decades of research. Upstream spread is related to the "drift paradox", whereby populations persist even when subjected to

[1] This chapter is submitted to PLOS ONE, [48]

continuous advection [110]. One hypothesis is that variability in flow direction (e.g. due to turbulence or tides) coupled with high reproductive rates is sufficient to compensate for the downstream loss of individuals [147]. In marine systems, we see flow variability due to widely different phenomena [118]. These can be grouped broadly into two relevant time scales: (i) the dispersal period (typically the larval stage) and (ii) the adult life span. Even when variability on the shorter (within year) scale is not sufficient to resolve the drift paradox, longer-scale variability (year-to-year) may still allow persistence and upstream spread.

The green crab (*Carcinus maenas*) is a particularly interesting case study because it is a high impact invasive species and is an effective disperser [52, 73, 135]. On the coast of New England and Maritime Canada, it has shown a fairly consistent northeast spread rate over a large temporal scale ($\sim$120 y) and spatial scale (along the Gulf of Maine, the Atlantic coast of Nova Scotia and the southern Gulf of St Lawrence) [47, 73], despite spreading through water bodies with different characteristics and the occurrence of multiple introductions [133]. Further, this invasion occurred against the dominant (southwest) flow [16, 55].

There is a need for more careful study of dispersal. Not only is it challenging to obtain good estimates of dispersal distances, past modelling studies have shown that spread rates are highly sensitive to the extent and frequency of the furthest dispersal distances [22]. In my context, I am focusing on upstream dispersers (i.e., those moving against the dominant current).

In coastal marine species, the life stage with the greatest dispersal distances that occur naturally is typically the larval stage [32]. Therefore, it is important to determine the processes that influence larval dispersal. These processes can be categorized in three groups [32]: (i) biological processes including production, growth, development, and survival of larvae; (ii) physical processes such as currents and turbulence; and (iii) behaviors, such as larval vertical swimming, that link the two.

The main goal of this chapter was to study the effect of year-to-year variability in dispersal on the spread rate of an invasive species. I used an age-structured, integrodifference equation (IDE) model, extended from the model developed by Gharouni et al. [47] with the addition of a stochastic dispersal component to investigate the upstream spread rate of the green crab on the east coast of North America. my model has two components, a projection matrix describing the population stage structure (first-year juvenile, second-year juvenile and adult), and probability distributions (kernels) modelling dispersal of each stage. For the larval dispersal kernel, I used a mechanistic and flexible approach following Pachepsky et al. [121]. I first used a deterministic version of the model to examine the relationship between the spread rate and the dispersal and demographic parameters (net rate of displacement, diffusion and recruitment). Note that I used the term "net rate of displacement" rather than "advection", because behavior and various other processes in addition to passive advection influence how far a disperser is displaced. I then allowed dispersal (specifically, the net rate of displace-

ment and diffusion coefficient of larvae) to vary yearly by parameterizing the dispersal kernels using a 3-dimensional hydrodynamic model of the Gulf of St Lawrence [17, 82]. The same hydrodynamic model was used for several other biological dispersal studies [34, 99, 100, 119]. The IDE framework is well-suited to study the effect of heterogeneous dispersal on invasion spread rates. The within-year variability in dispersal distances is reflected in the shape of the larval dispersal kernel, and year-to-year variability is modelled by allowing the parameters of the kernel to vary stochastically. Although I use the green crab invasion as a case study, my model can be modified for any species of interest.

3.2 Methods

3.2.1 Model framework

my model consists of a system of IDEs describing the population dynamics of three stages of female crabs: first-year female juveniles, second-year female juveniles, and mature female adults. The general form of the model is

$$\mathbf{u}_{t+1}(x) = \int_{-\infty}^{+\infty} [\mathbf{K}(x-y,t) \circ \mathbf{B}_{\mathbf{u}}]\mathbf{u}_t(y)dy, \tag{3.1}$$

where $\mathbf{u}_t = (u_t^1, u_t^2, u_t^3)$ denotes the vector of abundances of each stage at discrete time (t) and continuous position (x). $\mathbf{B}_{\mathbf{u}}$ and $\mathbf{K}$ denote, respectively,

the population projection matrix and the dispersal matrix, and are defined as

$$\mathbf{B_u} = \begin{bmatrix} 0 & 0 & \phi\ b_L \\ b_1 & 0 & 0 \\ 0 & \dfrac{\kappa - b_A u_3}{\kappa - b_A u_3 + b_2 u_2} b_2 & b_A \end{bmatrix}, \mathbf{K} = \begin{bmatrix} 0 & 0 & k_{13} \\ \delta & 0 & 0 \\ 0 & \delta & \delta \end{bmatrix}. \qquad (3.2)$$

The projection matrix, $\mathbf{B_u}$, contains the demographic components of the model. The parameters include the average number of female eggs produced per mature female per year (ϕ), the probability that a given egg survives to become a settled first-year juvenile (b_L), the survival probabilities for first and second year juveniles (b_1 and b_2, respectively) and the survival probability of adults (b_A). The fraction of second-year female juveniles that survive to settle as adults (row 3, column 2 entry of $\mathbf{B_u}$) is assumed to be density dependent. I assumed that there are κ sites available for adults to occupy, that surviving female adults from the previous year, $b_A u_3$, continue to occupy their sites, and that second-year female juveniles then compete for the remaining spaces. Thus, a fraction, $\frac{\kappa - b_A u_3}{\kappa - b_A u_3 + b_2 u_2}$, of the $b_2 u_2$ maturing year-two juveniles obtain sites. Note that if u_2 is small relative to the number of remaining sites, then the number surviving approaches $b_2 u_2$ and if u_2 is large, the number of survivors approaches the number of remaining sites.

Although my main interest is the effect of annual variations in dispersal distances, I first considered the case where the dispersal matrix has no year-to-year variations. The larval dispersal kernel, k_{13} , models the dispersal of the current year's offspring that survive to become first-year juvenile

recruits. It is assumed that spread is driven by larval dispersal, so dispersal in other stages is modelled by the Dirac delta function, δ. A mechanistic larval dispersal kernel is used for k_{13} following Pachepsky et al. [121]:

$$k_{13}(x-y) = \int_0^{+\infty} p(T)\omega(T, x-y)dT, \tag{3.3}$$

where $p(T)dT$ is the probability a given larva settles in the time interval $(T, T+dT)$, conditional on its having survived the dispersal process, and $\omega(T, x-y)$ is the probability distribution of dispersing larvae at time T following release. This approach enabled us to describe the dispersal process more mechanistically than can be done using a simple Normal or Laplace distribution for k_{13}. For this chapter, I assumed a uniform distribution of settling rates

$$p(T) = \begin{cases} \frac{1}{T_2 - T_1} & T_1 \leq T \leq T_2, \\ 0 & \text{otherwise}, \end{cases}. \tag{3.4}$$

That is, the duration of the larval pelagic period ranges from T_1 (earliest settlement) to T_2 (latest settlement). I model larval drift as a normal distribution:

$$\omega(T, x-y) = \frac{e^{-\frac{((x-y)-vT)^2}{4DT}}}{2\sqrt{\pi DT}}. \tag{3.5}$$

This is a common assumption for marine species with a pelagic larval stage (see e.g. [80, 142]). More specifically, I assumed larvae drift with mean displacement $\mu = vT$ and standard deviation $\sigma = \sqrt{2DT}$, where v is the net rate of displacement and D is the diffusion coefficient. I refer to Equations

(3.1)-(3.5) as my deterministic model. I then introduce a time dependence into $\mathbf{K}$ by allowing v and D to vary with year and refer to Equations (3.1)-(3.5) with year-to-year varying v and D as my stochastic model.

To illustrate the shape of kernel k_{13} and its dependence on v and D, I numerically computed Equations (3.3)-(3.5) (Figure 3.1). Note that for our choice of p and ω, k_{13} does not have an explicit representation in terms of simple functions. For illustration, I used several pairs of v (net rate of displacement) and D (diffusion coefficient). Note that a small fraction of individuals move upstream even with a downstream net rate of displacement (negative v) [121]. The shape of the kernel changes with different values of v and D, because of the interplay between the modifying effect of the settling rate function and smoothing effect of the integration. Unlike the shifted Normal, which is a rigid shift (no change in shape), this kernel shifts, flattens and appears to approach a uniform distribution as v increases.

For deterministic models like Equation (3.1), it is conjectured that solutions converge to a travelling wave solution with speed c^* provided certain conditions are met [114], where c^* is the speed of the stable travelling wave solution of the linearization of the model near $\mathbf{u} = \mathbf{0}$. The conditions of the conjecture are that (1) the initial conditions are bounded, positive and zero outside a closed interval, (2) the leading eigenvalue of $\mathbf{B_0}$ is larger than one, (3) $\mathbf{0} \leq \mathbf{B_u u} \leq \mathbf{B_0 u}$, and (4) the entries of $\mathbf{K}$ have moment generating functions. I have verified that these conditions hold for my deterministic model in Appendix A. The computations of c^* follow the procedures detailed in [47],

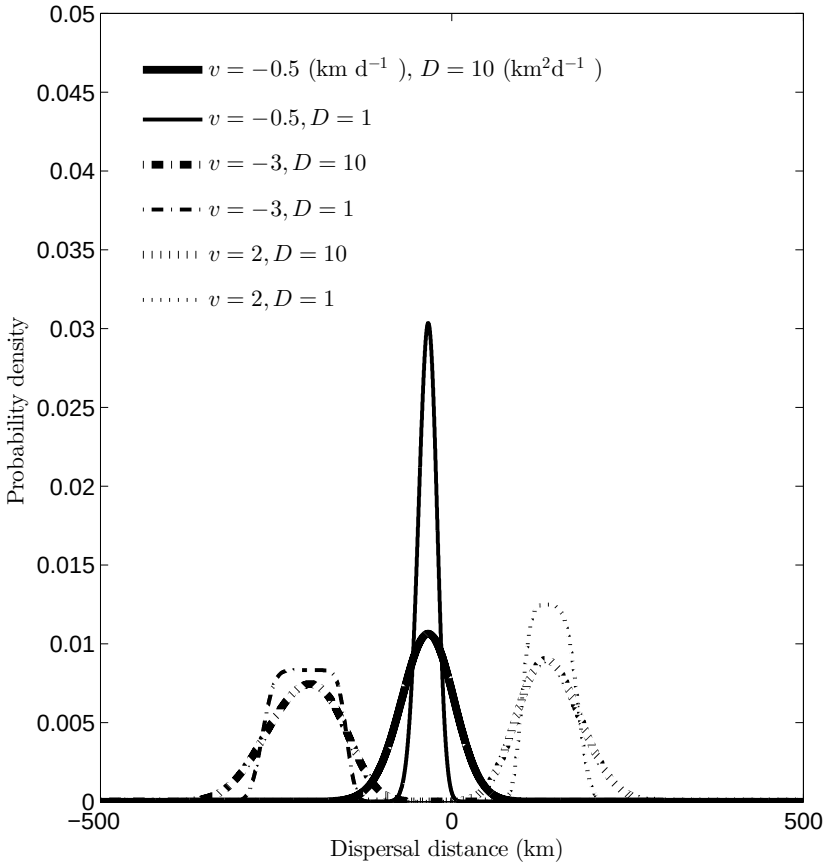

Figure 3.1: Representations of the larval dispersal kernel k_{13} (Equations (3.3)-(3.5)) with different values for the net rate of displacement v (km d^{-1}) and diffusion coefficient D (km^2 d^{-1}). For this graph, $T_1 = 50$ d and $T_2 = 90$ d. Note how the kernel shifts, flattens, and appears to approach uniform distribution as the absolute value of v increases.

with the addition that the moment generating function for k_{13} is computed numerically. Similar to the results found in [47], there is a threshold in the v-D parameter plane such that if v and D lie below this threshold, there is no upstream travelling wave solution ($c^* < 0$; see Figure 3.2) . If v and D

are above this threshold, $c^* \geq 0$ and there is an upstream travelling wave solution. Thus, following the terminology introduced by Caswell et al. [23], I refer to a pair of v and D as a "good-year" pair if they lie above the threshold and a "bad-year" pair otherwise.

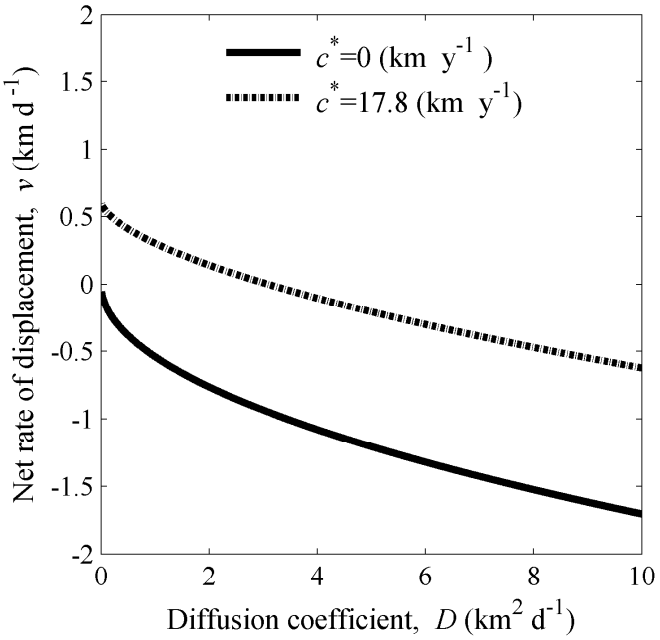

Figure 3.2: Contours for upstream spread rate c^*. The solid line shows the threshold for upstream spread, i.e., the relationship between net rate of displacement v and diffusion coefficient D suggested by my model (Equations (3.1)-(3.5)) beyond which upstream (northeastward) spread can occur ($c^* = 0$ km y^{-1}). A pair of v and D is referred as a "good-year" pair if it lies above this threshold, otherwise the pair is referred as a "bad-year" pair. The dash-dot line is the contour for $c^* = 17.8$ km y^{-1}, which is the estimated spread rate of the northern lineage of the green crab in the Northumberland Strait, Canada [47]. The other model parameters were fixed as adult survival probability $b_A = 0.75$, recruitment rate $r = 23$, and the start and end of the larval settlement period $T_1 = 50$ and $T_2 = 90$.

3.2.2 Parameter estimation

The annual survival rate of female adults is estimated as $b_A = 0.75$ based on a life span of 4 years [12]. Following [47], I define the adult recruitment rate as $r = \phi\, b_L\, b_1\, b_2$ and estimate it as $r = 23$ adult female offspring/female adult/year. Without loss of generality, I assumed $\kappa = 1$ in my simulations; this is equivalent to measuring populations as fractions of the available sites per km. Green crab larvae spend between 50 and 90 days in coastal waters and then return inshore to settle [73], thus I use $T_1 = 50$ d, $T_2 = 90$ d for all calculations and simulations.

To estimate the temporal variability of the dispersal parameters (v and D in k_{13} in Equations 3.3-3.5), I conducted particle tracking simulations using a version of an ocean circulation model based on the Nucleus for European Modelling of the Ocean (NEMO) system described in detail in [17] and [82]. The modelling system is based on the ocean code OPA version 9.0 [96]. The model domain includes the Gulf of St. Lawrence, the Scotian Shelf and the Gulf of Maine. The horizontal resolution is $1/12^\circ$ in latitude and longitude and 46 layers of variable thickness (6 m to 250 m) are used for the discretization in the vertical. It is a prognostic model allowing for advection-diffusion of the temperature and salinity fields which are only constrained through open boundary conditions, freshwater runoff and surface forcing. Tidal forcing is also included in the model. The hydrodynamic model is driving a bio-physical model that can simulate advective dispersal of "particles" representing green crab larvae in nearshore flow and hydrodynamic fields. The

particle-tracking, individual-based model enables us to virtually release and follow larvae that have behaviours (such as vertical swimming) under variable environmental conditions. Because of data storage constraints, the physical velocity fields are output as daily averages but they are interpolated to hourly values to drive the biological model offline. The small scale diffusion coefficient in the particle tracking model is set at 25 m^2s^{-1} following the work of Chassé and Miller [24] and Hrycik et al. [61] to represent within-day variation such as tidal stirring, wind waves, tides, etc. The depth within which the larvae are virtually swimming is set as 20-30 m in the Northumberland Strait, representing larvae swimming up to 20 m at nighttime and down to 30 m in daytime [130, 151].

In the particle tracking simulation, I selected 8 release locations of larvae along the mainland coast of the Northumberland Strait for each year from 2007 through to 2012 inclusive (i.e., 48 simulated dispersal kernels). The related details of this computation and the results are to be found in Chapter 4. The 48 estimated pairs of (v, D) are presented in Table 4.1 (the highlighted and bolded pairs) in Section 4.2. These estimates were used in the following section to study the effect of year-to-year larval dispersal variability on the spread rate.

3.2.3 Stochastic model spread rates

The linear conjecture and accompanying spread rate formulae cannot be applied to my stochastic model. Hence, I use numerical simulations to deter-

mine the mean spread rates with year-to-year variations in dispersal. Simulations were carried out in Matlab® (Matlab [102]; Math Works): for each simulation, the model was run over 30 time-steps with initial conditions symmetric about the point $x = 0$ on the domain -3000 km $\leq x \leq 3000$ km. The integral in Equation (3.1) was approximated by using the trapezoidal method (via the Matlab function *trapz*). The spatial domain was chosen sufficiently large so that a travelling wave developed before reaching the boundary. The location of the forward wave front (rightward in the 1-D spatial domain) was defined to be the right-most point for which the adult population density was above $\kappa/2$. The spread rate for a simulated solution to the stochastic model was then taken to be the slope of a linear regression of the wave-front locations.

To evaluate the effect of stochastic dispersal on upstream spread rate, c^*, I did the following analysis.

(i) I chose 100 sample time-sequences of size 30 by randomly sampling with replacement from the 48 estimated pairs of (v, D) (Table 4.1, highlighted part).

(ii) For each sample, I ran the model using the sequence of pairs of (v, D). This resulted in a sample-specific "stochastic spread rate" which is denoted by c_s.

(iii) I computed an "averaged (v, D)" for each sample by calculating the arithmetic mean of the 30 kernels corresponding to each time-sequence

of pairs of (v, D) obtained in step (i), and fitting the theoretical dispersal kernel (Equation (3.3)-(3.5)) to the result using the *nlinfit()* function in Matlab®. The spread rate resulting from this averaged (v, D) is referred to as the "averaged spread rate" and denoted by c_a.

(iv) I computed a "grand-averaged" estimate of (v, D) from the 48 estimated pairs of (v, D) (Table 4.1, highlighted part) by the same method of step (iii). The spread rate resulting from the grand-averaged (v, D) is referred to as the "grand-averaged spread rate" and denoted by c_g.

The same initial conditions were used for all model runs. I used a developed travelling wave, because my focus is on the asymptotic spread rate and not the transient dynamics. To obtain the developed travelling wave I ran the model for 20 time steps using the grand-averaged estimate of (v, D) with an initial population density of zero for first-year and second-year juveniles, $u_0^1(x) = u_0^2(x) = 0$, and of one for the adults, $u_0^3(x) = 1$ for x in $[-2, 2]$ and zero otherwise. 20 time-steps was observed to be sufficiently long for travelling wave to develop.

All 48 pairs obtained from the hydrodynamics model were "good-year" pairs. Since I were interested in scenarios where upstream spread did not occur every year, I obtained a second set of 100 samples by simply subtracting 3 km d^{-1} from v in each of the 100 samples obtained in step (i) above. This resulted in a mixture of good and bad years in each time-sequence. Then, I repeated steps (ii), (iii), and (iv) with the shifted (v, D) pairs. Spread

rates resulting from the shifted pairs are denoted by c_s^s, c_a^s and c_g^s for shifted stochastic, shifted averaged, and shifted grand-averaged spread rates.

Finally, I compared the stochastic, averaged and grand-averaged spread rates by computing the differences $c_s - c_g$, $c_s - c_a$, and $c_a - c_g$, as well as $c_s^s - c_g^s$, $c_s^s - c_a^s$, and $c_a^s - c_g^s$.

3.3 Results

Observations collected from various field studies over many years lead to an estimated mean spread rate $c^* = 17.8$ km y^{-1} for the upstream (northwestward) invasion of green crabs in the Northumberland Strait [47]. Using this value for spread rate in the relationship derived from my deterministic model, Equation (3.1)-(3.5), gives a set of feasible net rates of displacement, v, and diffusion coefficients, D, for a given recruitment rate, $r = \phi\, b_L\, b_1\, b_2$ (Figures 3.2 and 3.3). Moreover, setting $c^* = 0$ kmy^{-1} (termed the critical spread rate) provides a threshold for dispersal parameters above which the advancing wave spreads upstream (northwest, positive spread) and below which the wave retreats downstream (southeast, negative spread) (Figure 3.2). When setting the recruitment rate to a reasonable estimate from field data for the green crab ($r = 23$ adult female offspring per female per year; [47]) for these two situations (the observed and the critical spread rates), the curve representing the feasible set of v and D is concave and decreasing in the (D, v) plane (Figure 3.2). This indicates a compensatory relationship between the

diffusion coefficient and the net rate of displacement. Specifically, when a cohort of larvae experiences a downstream net rate of displacement ($v < 0$, mostly due to downstream current), increased diffusion can compensate, leading to spread against the current [120]. In contrast, when the dominant flow is upstream and results in an upstream net rate of displacement ($v > 0$), the diffusion coefficient can be very low. When the recruitment rate, r, is increased, the feasible values of v and D can be reduced for a given spread rate (Figure 3.3). Thus, high downstream currents can be compensated for by either increased D, increased r, or a combination of the two.

Environmental stochasticity can also lead to upstream spread. The set of simulations seeded with both good years and bad years resulted in upstream spread even when the averaged dispersal kernels did not support upstream spread (Figure 3.4 c). In these simulations, almost all spread rates using averaged kernels were smaller than spread rates using stochastic kernels (99 out of the 100 samples; middle boxplot in Figure 3.4 d). In addition, spread rates using averaged kernels were negative for all 100 samples, while spread rates using stochastic kernels were positive for 89 out of the 100 samples (Figure 3.4 c). Similarly, in simulations run with only good years, the spread rates from the model using stochastic kernels were all higher than those from the model using the averaged kernels (Figure 3.4 a and b). As expected, the comparison of the model using the sample-averaged kernel to that using the grand-averaged kernel (right boxplots in Figure 3.4 b and d) did not differ much, which is an indication that sampling (with replacement)

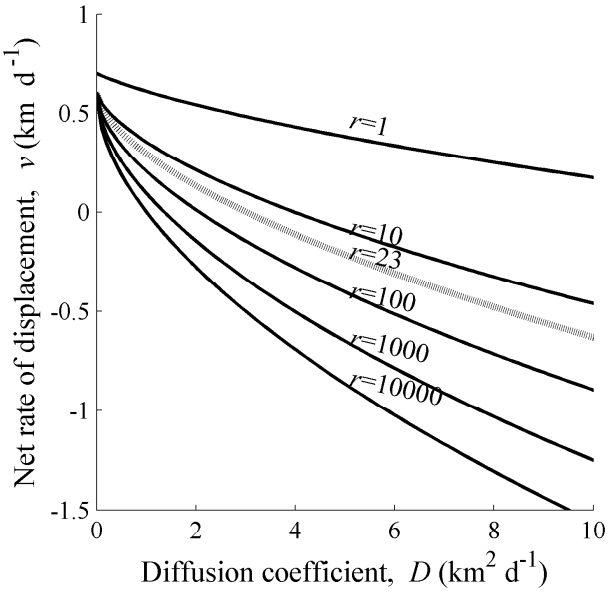

Figure 3.3: Level curves at upstream spread rate $c^* = 17.8$ km y^{-1} for different values of recruitment rate r. The dotted curve is $r = 23$ and is the estimate for recruitment rate for the green crab [47]. If the values of v and D lie below one of these curves, then the deterministic model predicts slower or no upstream spread for that particular value of r. The other model parameters were fixed as $b_A = 0.75$, $T_1 = 50$ and $T_2 = 90$.

30 out of the 48 kernels is sufficient to adequately capture the variability among kernels.

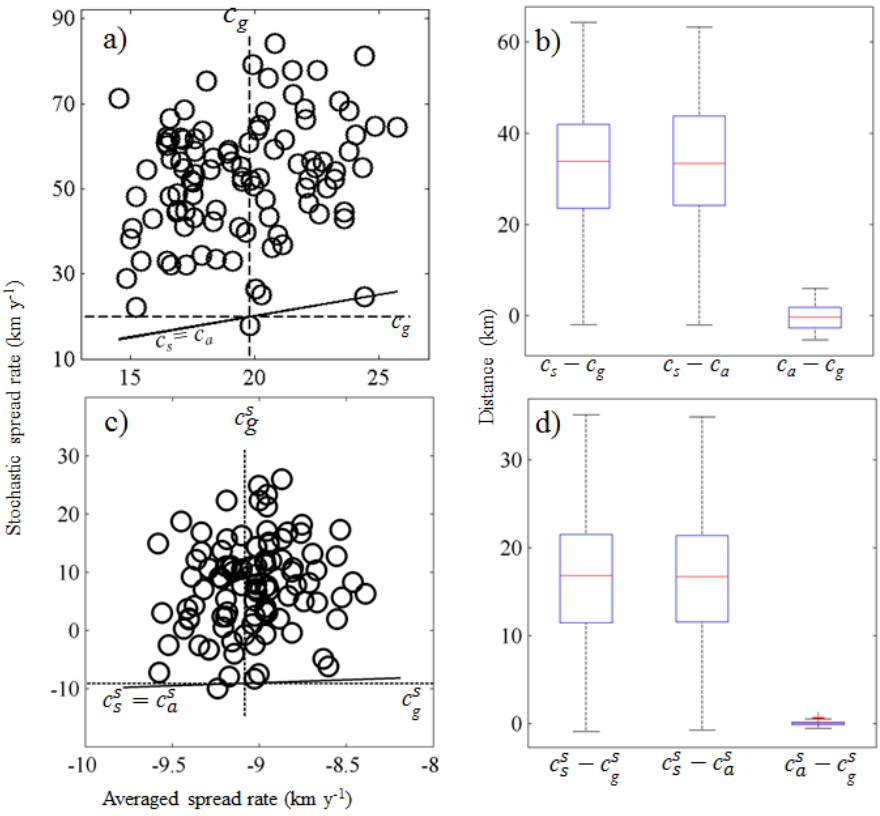

Figure 3.4: Comparison of the upstream spread rate for stochastic, sample-averaged, and grand-averaged dispersal kernels. Panels (a) and (b) are a scenario with only good years (featured by some upstream dispersal), and panels (c) and (d) are a scenario with a mixture of good and bad years (the latter featured by no upstream dispersal). See text for explanation of the symbols associated with the spread rate c. Each point in the scatterplots in panels (a) and (c) represents a pair of simulated spread rates, averaged and stochastic, for a given random sample (a 30-year sequence of dispersal kernels or parameters; see Figure 4.2 and table 4.1). If a point is above the solid line, then the stochastic spread rate is greater than the corresponding averaged rate. The dashed line represents the grand-averaged of my dispersal kernels (Figure 4.2), which has the value $c_g = 21.5$ km y^{-1} in panel (a) and $c_g^s = -8.2$ km y^{-1} in panel (c). The box plots in panels (b) and (d) present the differences between the different types of modelled spread rates (stochastic, sample-averaged and grand-averaged). The other model parameters were fixed as $b_A = 0.75$, $r = 23$, $T_1 = 50$ and $T_2 = 90$ for all simulations.

3.4 Discussion

Analysis of my deterministic model (Equations (3.1)-(3.5)) showed that upstream spread and range expansion of marine organisms (such as aquatic invasive species) can occur, because of the compensatory relationship between the demographic parameter (recruitment rate, $r = \phi\, b_L\, b_1\, b_2$) and the two dispersal parameters (larval net rate of displacement, v, and larval diffusion coefficient, D). Upstream spread and range expansion can also be aided by stochastic dispersal. As a second step in and for the main objective of my modelling exercise, time-varying larval dispersal (using a hydrodynamic model) was estimated and incorporated in the population model, thereby converting it to a stochastic model. my results indicated that when dispersal parameters vary with time, knowledge of the time-averaged dispersal process is insufficient for determining the upstream spread rate of the population. Specifically, and as an example, I showed that for the green crab invasion along the east coast of North America, an upstream invasion spread is possible over a number of years, even when there are only a few "good years" featured by upstream dispersal among many "bad years" featured by downstream dispersal. In the following discussion, I compared my results to previous studies investigating effects of environmental stochasticity on population dynamics. I included an examination of the different ways that dispersal heterogeneity can be incorporated into a spatial model.

3.4.1 Comparison with existing theory

The compensatory relationship I observed between the dispersal parameters v and D is similar to that predicted by Fisher's equation with advection [43, 165]. The latter gives a hyperbolic relationship between advection, diffusion and the intrinsic growth rate of the population. Fisher's equation is a single-stage partial differential equation. Petrovskii and Li [124] argued that Fisher's relationship also holds for the single-stage IDE when the dispersal kernel is exponentially bounded. Here, I present an example to support the generalization of this theory to structured IDEs (with multiple stages) with exponentially bounded dispersal kernels (see also [47]). The compensatory relationship means that a higher recruitment rate or a higher diffusion can compensate for the negative effect of downstream larval advection.

Organisms can effectively increase D and decrease v through behavioral adaptations exploiting variations in currents. Thus, more caution should be taken when estimating dispersal parameters from oceanographic studies. For example, Bonardelli et al. [15] estimated downstream advection in the Northumberland Strait between 2 and 8 km d^{-1} (these estimates are similar to [81] and [136] for general region (Gulf of St. Lawrence)). If this range of advection is used as an upper bound for the net rate of downstream displacement of larvae, v, then my model suggests that for diffusion coefficients in the range of 10 to 100 $km^2 d^{-1}$, the recruitment rate, r, should range from 10,000 to 100,000 female recruits per female adult per year to maintain an upstream spread. This range of recruitment is not realistic for green crabs

(literature suggests $r = 23$ female recruits per female adult per year; [47]). Note that the estimate of $2 - 8\,\mathrm{km\,d^{-1}}$ is for passive particles drifting in surface current. However, larvae can swim vertically to take advantage of different currents [59, 122], which may result in a higher diffusion coefficient and/or lower net rate of displacement [57].

3.4.2 Time-varying dispersal in structured population IDEs

In addition to exploiting the vertical structure in currents, organisms may also take advantage of temporal variability in currents and turbulence. Studying the effect of time-varying dispersal on invasion spread rates in structured models has only recently received attention of theoretical ecologists. Caswell et al. [23] provided a stochastic version of an earlier time-invariant model of invasion speed for stage-structured populations [114]. For populations structured by a continuous state variable, Ellner and Schreiber [41] similarly provided a stochastic version of an earlier autonomous (time-invariant) model for invasion speed [69]. Both Caswell et al. [23] and Ellner and Schreiber [41] found that year-to-year variability in dispersal accelerated population spread. my work with stochastic dispersal kernels supports this, as it resulted in higher upstream spread rates than using the corresponding time-averaged dispersal kernels.

Dispersal heterogeneity can be incorporated in population models in

various ways. In my work, the dispersal heterogeneity includes both individual-based and year-to-year variability. Specifically, the hydrodynamic model [17, 82] that I used to simulate daily flow fields for a given year and coastal location included an individual-based particle tracking submodel [24] to obtain daily settler displacements within the larval settlement period. This is analogous to Stover et al. [150]'s "heterogeneity", where the diffusivity of individuals is sampled from a probability distribution. They showed that intra-annual dispersal variations leads to leptokurtic dispersal kernels, increases the population's spread rate, and lowers the critical reproductive rate required for persistence in the face of advection. In my work, the hydrodynamic model also provided us with a set of realistic dispersal kernels that I sampled from to represent year-to- year variability. This is somewhat analogous to Ellner and Schreiber [41]'s approach, which included an annual, random change in the importance (or weight) of two modes of dispersal, namely short-distance dispersal and long-distance dispersal. Other means of incorporating dispersal heterogeneity that I could explore include heterogeneity in larval behavior and development (for an example of a within year process) or randomly changing the order of "good" and "bad" years (for an example of a between year process).

Population persistence in an advective environment is theoretically related to the ability to invade upstream: aspects such as dispersal heterogeneities which affect spread rates also affect persistence in similar ways [120]. For example, Williams and Hastings [170] consider metapopulation

persistence in a patchy marine coastal environment, where the unidirectional dispersal by larvae between patches is governed by a binomial random variable. This year-to-year stochasticity in ocean flow patterns increases the long-run growth rate of the metapopulation and predicts persistence, compared to using a long-term average of ocean flow. Note that an opposite result has been observed in other modelling studies on persistence in metapopulations [145, 164]. For example, Watson et al. [164] showed that growth rates calculated from a constant, averaged connectivity between populations rather than the time series (connectivity versus year) were typically higher and so overestimated the likelihood of persistence. Obviously, more modelling studies are needed to better understand when heterogeneities in dispersal lead to persistence and when they do not.

3.4.3 Other considerations and future work

Geometric versus arithmetic averaging of dispersal kernels has an effect on the spread rate of IDE models. Indeed, if the growth rate of a population varies over time, the total population size is described by the geometric average of annual growth rates [154]. Using the same logic, this geometric averaging also appears in the computation of asymptotic spread rates for stochastic IDE models [23]. In my paper, I compared spread rates arising from arithmetic averages, which is a common averaging approach. Stover et al. [150] noted that the asymptotic spread rate resulting from arithmetic averaging is always higher than that from geometric averaging. Thus, had I

used geometric averaging, the difference between the stochastic spread rate and that calculated from the averaged dispersal kernels would have been even larger (box plots in Figure 3.4, panels b and d). Therefore, the type of averaging done in modelling or experimental studies needs to be considered carefully.

The simplification of a uniform settling rate of larvae in my model has also recently been used in modelling green crab population dynamics [101]. Other forms of probability distributions for settlement rate include Gaussian when it is normally distributed during the settlement period (i.e., with a main event in the middle of the period; Siegel et al. [142]), peaked when there is a one-time particularly strong settlement event at some point during the settlement period [31], decay when initially settlement is high and decreases over time [25], and, more generally, gamma when there is one main settlement event which could be modelled any time during the settlement period [177]. Such settlement probability distributions are useful approximations for various settlement temporal patterns. However, beyond this consideration on shape of the probability distribution for settlement rate, it is likely that dispersal and settlement should not be separated into two functions (as is typically done, including in my study). The dispersal and settlement components of the kernel incorporate all sorts of physiological, behavioral and hydrodynamic processes, including larval developmental rates and behaviors (e.g., responding to differential currents, water temperatures and/or other cues) [126]. The interconnectedness among dispersal, development and

settlement processes needs to be better understood and formally modelled.

Schreiber and Ryan [138] emphasized the importance of stochastic models to address predictions of increased interannual variability as a result of climate change. My model can be used to assess the effect of environmental stochasticity on rates of spread and range expansion of marine organisms. More specifically, rising sea temperatures across the globe could lead to the appearance of anomalous flow patterns, with incidental effects on dispersal and population dynamics in many marine species [111]. Further, it has been documented that the increase in water temperature causes pelagic larval durations to be shortened and results in lower dispersal distances for marine organisms [115]. Decreased larval development times in warmer water could influence the dispersal kernel and spread rates. Thus, my modelling framework can be applied to develop and provide tools that predict spread rates under various conditions and climate change scenarios (e.g. [92] for recent climate change scenarios). Such tools are essential to inform maps of range expansions and risk maps of areas prone to habitat degradation due to aquatic invasive species activities.

3.5 Conclusions

Population spread is a complex ecological phenomenon involving the interplay between a number of processes, including demography and dispersal of organisms, and variability in these processes. My results showed that

incorporating time-varying dispersal in population models is important to enhance understanding of spatial dynamics and population spread rates. I showed that upstream invasion spread is possible even when there are only a few "good" years (featured by upstream dispersal) among many "bad"years (featured by downstream dispersal). This enhanced understanding of dispersal patterns helps guide quantification of connectivity among populations, explain measurements of genetic structure of populations, and untangle the past history of population and community dynamics that may not correspond to observed averaged current patterns. Furthermore, improved estimation of spread rates is key to developing effective responses to biological invasions in marine systems.

Chapter 4

Variability in larval dispersal of aquatic invasive species: a case study with green crabs on the northwest Atlantic coast

Estimating the parameters of the dispersal kernel is important to better understand invasion spread rates in the IDE framework. In this chapter, I review the procedure of estimating the larval dispersal kernel used in my models in the previous chapter. Having dispersal data simulated using the particle tracking and the hydrodynamic model discussed in Section 3.2.2, two dispersal kernels are fitted to the dispersal data and results are compared. Specifically, the two-parameter mechanistic dispersal kernel given by Equa-

tions (3.3)-(3.5) is compared with the Normal dispersal kernel of Equation (2.5). Both of these kernels are exponentially bounded. However, the mechanistic kernel takes into account the bahavioural component of larval settlement. Also, this kernel cannot be represented in terms of simple functions (see Appendix A). This makes the computation of the invasion spreading speed, c^*, expressed in Equation (1.24), difficult compared to the case that the Normal dispersal kernel is used. The objectives are (i) to identify any spatial structure in larval dispersal, and (ii) to determine which kernel better captures long distance dispersal.

4.1 Method

Estimates of the parameters of the dispersal kernels were computed using a nonlinear regression to the output of a behavioural, particle-tracking submodel [24] embedded into a hydrodynamic model [17, 82] of the Gulf of St Lawrence and the Gulf of Maine.

As mentioned in the previous chapter (Section 3.2.2), I selected 8 locations in the southwest of the Northumberland Strait as release locations of green crab larvae along the mainland coast of the Northumberland Strait for each year from 2007 through 2012 inclusive (6 years). The release locations were approximately 20 to 40 km apart and extended in a sequence from southeast to northwest of the Northumberland Strait (see Figure 4.1). The release dates within each year were daily from July 1^{st} to 31^{st}, and the

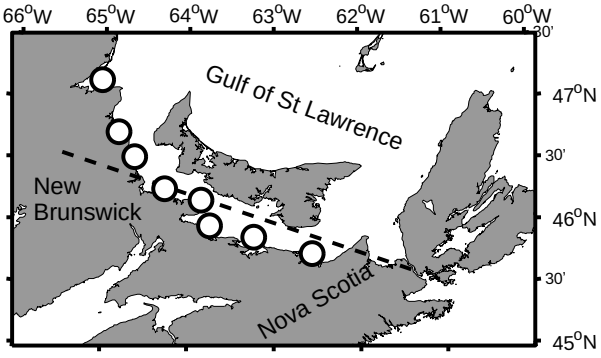

Figure 4.1: Release locations of particles (representing green crab larvae) in the Northumberland Strait, Canada. The locations are numbered from 1 to 8, from the southeast to the northwest. The dashed line is the modelled coastline used for calculating dispersal displacement of projected particles.

release period was every hour during each day (to approximate the spawning period of green crabs in this region; [73]). This procedure of virtually releasing and tracking larvae was repeated 5 times for a given location and year. The trajectories of the particles were tracked for 90 days from the date of release. Particle locations were recorded every day between day 50 and 90 to mimic the settling behaviour of the green crab [73]. The output locations (latitude and longitude) resulting from the hydrodynamic model were projected onto a straight 1-dimensional coastline (dashed line in Figure 4.1). The dispersal displacement from a source for a given particle is defined as the distance between its projected locations at the release time and settling time. Thus, for each year, each location and over the 40 days of recording the trajectories' locations, 148800 dispersal displacements were obtained.

I used the Matlab® [102] package M_{Map} to do all map-related computa-

tions such as projection of a point on map and on a specified straight line (see Figure 4.1), or the calculation of the distance between two points. The two points in degrees (longitude, latitude) representing the straight coastline are $A = (-61.41, 45.61)$ and $B = (-65.49, 46.54)$. I used point A as a reference point from which the upstream (northwestward dispersal, positive dispersal displacement) or downstream (southeastward dispersal, negative dispersal displacement) dispersal was measured. For each trajectory, projection of the initial release and end locations was taken to be the closest point on the line. Then, two distances were calculated: (i) the distance from the projected release point to the reference point A and (ii) the distance from projected endpoint to A. The displacement is positive if the resulting distance in (ii) is greater than the distance in (i) and the displacement is negative otherwise. Note that for the choice of the 8 release locations, no particle trajectory left the Gulf of St. Lawrence and thus point A was the most eastward point in the whole calculation.

Further, for each year, the dispersal displacement data of the 8 locations were pooled together to estimate the "pooled over locations" dispersal kernel. Similarly, for each location, the dispersal displacement data of the 6 years were pooled together to estimate the "pooled over years" dispersal kernel. Finally, all 48 dispersal displacement data were pooled together to estimate the "grand pooled" dispersal kernel. Note that the term "pool" has been used whenever dispersal data are put together as opposed to the term "average" which was used in Chapter 3 when we are referring to the arithmetic average

of a set of probability density functions.

The general statistical procedure to estimate the dispersal parameters and to verify the goodness of fit is as follows.

Step 1. A frequency distribution of dispersal displacement data was obtained for a given set of data output from the hydrodynamic model.

Step 2. A probability density function representing the modelled larval dispersal kernel was fitted to the frequency distribution and the dispersal-specific parameters were estimated.

Step 3. Two samples of size 1000 from each of the previous steps were drawn randomly, standardized, sorted and the coefficient of determination between the two samples was calculated.

In Step 1, a probability density from the output (frequency distribution) was produced.

In Step 2, the maximum likelihood estimation [2] method was used for the parameter estimation. The likelihood function based on a data set of size N, $X = \{x_1, \cdots, x_N\}$, is

$$L(X|\theta) = \prod_{i=1}^{N} k(x_i, \theta), \tag{4.1}$$

which is the probability of the data X given a set of parameter values $\theta \in \Theta$, where Θ represents a feasible parameter space. k is the probability density function which represents the larval dispersal kernel here. The *maximum like-*

lihood estimator is the value $\theta^* \in \Theta$ that maximizes the likelihood function. $fminsearch()$ which uses the simplex search method of Lagarias et al. [79] was used in Matlab® [102] to estimate θ^*. Note that two modelled dispersal kernels were involved in step 2: (i) the mechanistic kernel, k_{13} Equations (3.3)-(3.5) in Chapter 3, with two parameters v (net rate of displacement) and D (diffusion coefficient), and (ii) Normal kernel, k_N in Equation (2.5) in Chapter 2, with two parameters μ (net displacement downstream) and σ (standard deviation).

In Step 3, through a graphical approach, if the two samples used in this step are from similar distributions, then the scatter plot of the standardized and sorted samples would appear as the 1:1 straight line. In addition, the deviation of this plot from the straight line and the magnitude of the coefficient of determination, r^2, give information about how different the two distributions are.

The fitted mechanistic dispersal kernel, k_{13} (Equations 3.3-3.5), is plotted for the 8 release locations and 6 release years in Figure 4.2 following the statistical method in Step 2 of this section. In addition, for the purpose of illustration, the fitted mechanistic dispersal kernel is plotted for "pooled over locations" (the top row in Figure 4.2) and "pooled over years" (the most right column in Figure 4.2). Note that the top right panel in Figure 4.2 represents the "grand pooled" dispersal. The values of estimated pairs of the dispersal parameters, (v, D), are presented in Table 4.1 in the order corresponding to the order of panels in Figure 4.2.

4.2 Results

It seems that there is a spatial structure in dispersal in Figure 4.2. Patterns such as bimodal and leptokurtic dispersal are more apparent for some locations (such as location 2 and 8) than the others despite the fact that these patterns does not seem to be consistent or repeatable. Also, it appears that pooling the dispersal kernels over the release locations makes the dispersal look more like a Normal distribution while pooling over years does not seem to have this effect. This would imply that there are geological features in each release location which are not independent from year to year and pooling over time does not resolve these features. While by pooling over release locations, much of those spatial structures which are independent of one another, would be averaged out and this makes the pooled-over-locations' kernel looks more like a Normal distribution.

The comparison results of the mechanistic kernel and the Normal kernel suggest that neither of the two modelled kernels could capture the dispersal in the tail, which is likely due to the high variability in ocean currents from location to location and year to year. For the purpose of illustration, results of using the mechanistic and the Normal kernels are presented in Figures 4.3 and 4.4, respectively, for two selected locations and years. For example, both kernels underestimate the positive dispersal displacement in location 1 through the 6 years, although it seems that Normal kernel is slightly a better choice here than the mechanistic kernel (by comparing the r^2). In contrast,

the positive dispersal displacement is overestimated by the two kernels in location 4 year 2010.

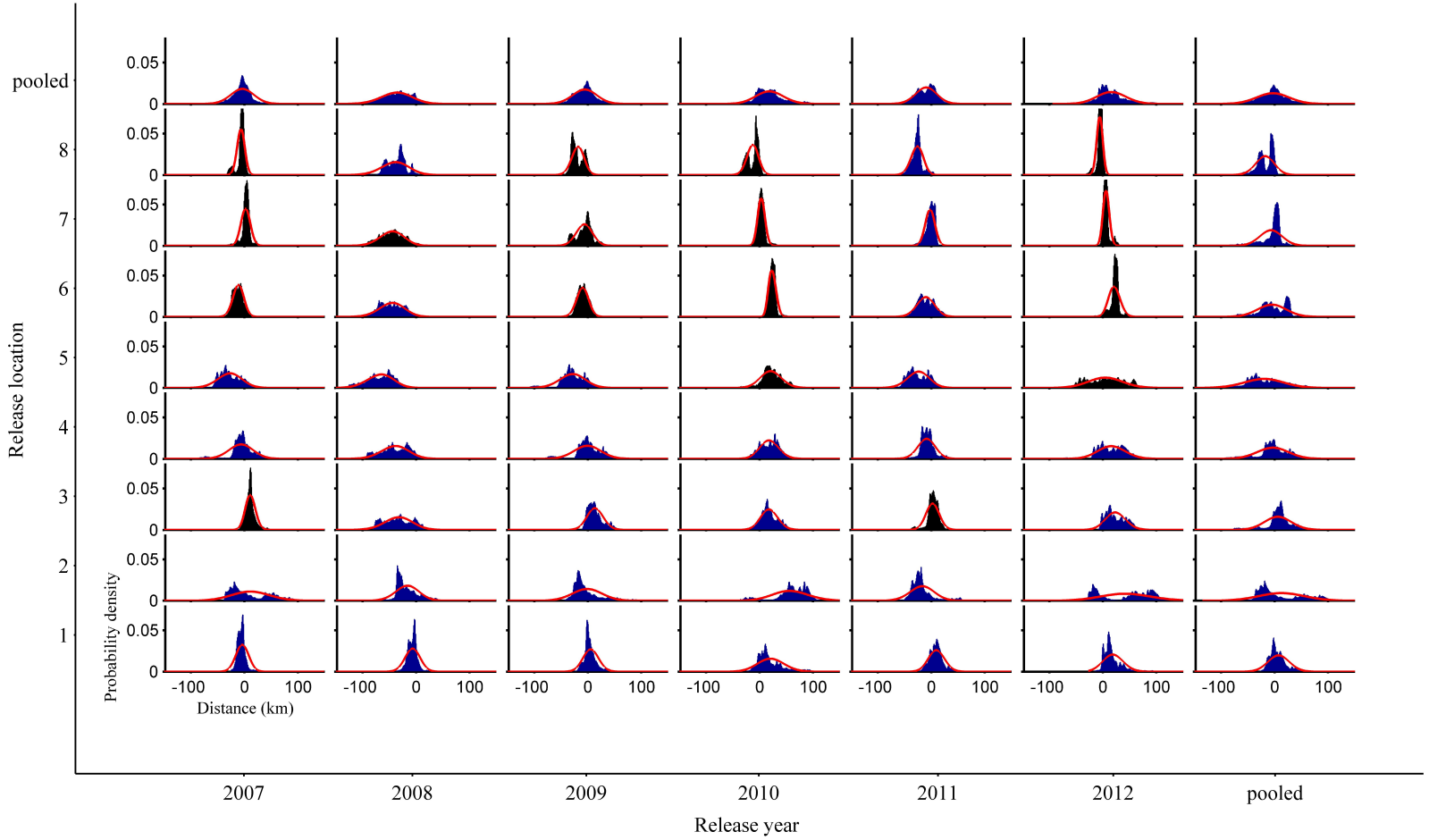

Figure 4.2: Larval dispersal kernels obtained from simulations of the hydrodynamic model of the Gulf of St. Lawrence for different locations in the Northumberland Strait (see Figure 4.1) and different years. For a given panel, the frequency distribution of the displacements of dispersing particles (representing green crab larvae) is in blue, and the fitted theoretical dispersal kernel (Equations (3.3)-(3.5)) is in red. See Table 4.1 for the estimated values of the pairs of v (net rate of displacement) and D (diffusion coefficient) corresponding to each simulated kernel.

Release location	2007	2008	2009	2010	2011	2012	pooled
pooled	(-0.057,3.49)	(-0.53,5.84)	(-0.085,3.8)	(0.269,4.95)	(-0.14,2.9)	(0.225,5.52)	(-0.05,6.89)
8	**(-0.095, 0.368)**	**(-0.565, 4.53)**	**(-0.271,0.923)**	**(-0.188,0.844)**	**(-0.383,0.824)**	**(-0.09,0.225)**	(-0.27,2.19)
7	**(0.032, 0.574)**	**(-0.652, 3.35)**	**(-0.0959, 1.7)**	**(0.0448,0.34)**	**(-0.033,0.602)**	**(0.083, 0.252)**	(-0.10,3.25)
6	**(-0.165, 0.753)**	**(-0.654, 3.64)**	**(-0.144,0.913)**	**(0.339, 0.239)**	**(-0.151, 2.02)**	**(0.304, 0.779)**	(-0.08,5.32)
5	**(-0.398, 3.62)**	**(-0.965, 3.46)**	**(-0.419, 3.97)**	**(0.303, 2.76)**	**(-0.351, 2.89)**	**(0.0624, 7.55)**	(-0.29,9.85)
4	**(-0.0926, 3.81)**	**(-0.569, 4.51)**	**(-0.012, 4.64)**	**(0.26, 2.29)**	**(-0.129, 1.96)**	**(0.227, 4.92)**	(-0.05,6.39)
3	**(0.159, 0.63)**	**(-0.475, 4.77)**	**(0.195, 1.66)**	**(0.258, 1.84)**	**(0.0357, 1.15)**	**(0.337, 2.51)**	(0.08,4.63)
2	**(0.163, 9.42)**	**(-0.239, 3.44)**	**(-0.018, 5.72)**	**(0.833, 7.48)**	**(-0.249, 3.7)**	**(0.614, 15.8)**	(0.18,13.49)
1	**(-0.06, 1.09)**	**(-0.096, 1.48)**	**(0.0784, 1.57)**	**(0.302, 4.58)**	**(0.138, 1.7)**	**(0.27, 2.63)**	(0.11,2.95)

Release year

Table 4.1: Pairs of (v, D) for larval dispersal kernels simulated from the hydrodynamic model for the Gulf of St. Lawrence and then estimated using the fitted Equation (3.3)-(3.5) (see also Figure 4.1 and 4.2). Units of the net rate of displacement v and diffusion coefficient D are km d^{-1} and km^2 d^{-1}, respectively.

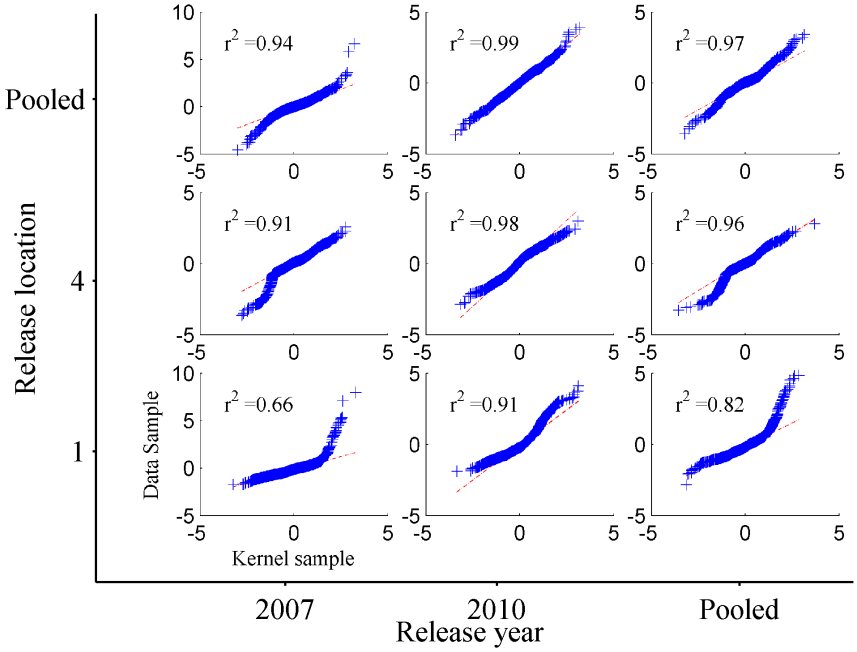

Figure 4.3: Comparison of the mechanistic dispersal kernel k_{13} (Equations (3.3)-(3.5)) and the hydrodynamic model data for various year and locations. The sample size is 1000 in each panel.

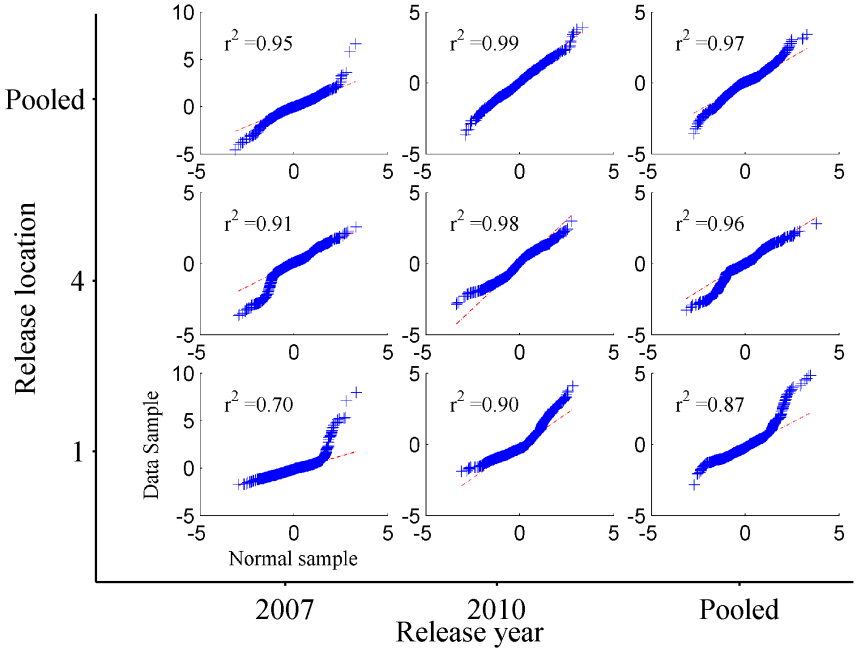

Figure 4.4: Comparison of Normal dispersal kernel k_N (Equation (2.5)) and the hydrodynamic model data for various year and locations. The sample size is 1000 in each panel.

4.3 Discussion

Determining the larval dispersal kernel in the IDE models is important to capture spatial dynamics of aquatic invasive species. The underlying biophysical processes that influence larval dispersal can be grouped into (i) biological (such as development and survival), (ii) physical (such as currents and turbulence), and (iii) behavioural (such as vertical swimming and settlement) [32]. Although the dispersal component is assumed to be independent of the demographic component in a general IDE model in Equation (1.13), this assumption can be improved. Specifically, some of the biophysical processes can be taken into account in the dispersal component and particularly in the larval dispersal kernel.

The tool that I used in Chapter 3 to capture some of these biophysical processes was the mechanistic dispersal kernel (Equations 3.3-3.5) parameterized by the hydrodynamic model output. Specifically, the settling component, p, the movement component, ω, and the settling period, $T_2 - T_1$, have been included in the mechanistic kernel k_{13} in Equation (3.3). Although, for the sake of simplicity, I used uniform settling in Equation (3.4) and Normal distribution in Equation (3.5) for p and ω respectively, other functions can be used as discussed in Section 3.4.3. In addition, the hydrodynamic model [96] equipped with the particle-tracking, behavioural submodel [17, 82] approximates currents and turbulence. Further, the structure of this model, as explained in Section 3.2.2, allows us to simulate and track some

behavioural processes such as larval vertical swimming through the particle-tracking model. Certainly, incorporating the biophysical processes into the particle-tracking model will change the tail of the larval dispersal kernel, k_{13} (3.2), and consequently will influence the results of the invasion spreading speed (see Chapter 1). Further work is required in the development of the theory and testing different hypotheses.

On the other hand, the lack of data is a challenge to study the effect of the biophysical processes on the larval dispersal. Further study needs to be done on the type of the required data in this field as well. Incorporating the biophysical processes into the hydrodynamic model enables one to capture some of these biophysical processes that may help researchers to test some important hypotheses such as:

(i) If the larvae spend shorter period in warmer water (e.g., caused by climate change), they quite likely disperse less because they develop and settle sooner and more of them survive to settlement relative to the situation that they spend longer duration in water;

(ii) Some of the larval dispersal variability might be due to the fact that they disperse longer or those that do not go close enough to the coast survive less.

There are also open questions in our understanding of the biological invasion process that have management implications. Some of these questions are as follows.

(i) What are the behaviours that allow larvae to return to the coast?

(ii) How is larval survival influenced by currents and turbulence?

(iii) How far offshore must a larva reach to be able to successfully settle?

As a methodological example, in the approach used in this thesis, all released particles (representing larvae) were assumed to be settled and involved in the statistical analysis. This can be improved by filtering out those larvae that did not fall close to the coastline after certain developmental duration and would not presumably survive.

Note that a nonparametric approach, as opposed to my approach in this thesis, can also be followed to estimate the larval dispersal kernel and to estimate the spreading speeds. Specifically, a nonparametric estimator for the moment generating function (1.9) which makes no assumption about the form of the underlying kernel was developed by Clark et al. [28] (see also [86]).

Chapter 5

Conclusions

5.1 Summary

Developing and analyzing mathematical models are helpful to enhance understanding of processes and provide insight on possible practices to manage the spread of an aquatic invasive species. The spread of the invasive green crab (*Carcinus maenas*) along the east coast of North America has provided an opportunity to examine the relationship between demographic and dispersal processes involved in the spread in a theoretical context. In summary, the aim of this work was to provide insight on

- the consistent spread rates against dominant flow,
- the relationship between invasion spread rate, demography and dispersal,

- the elasticity of the spread rate to changes in underlying parameters and insights on and rank possible management strategies,
- the effect of year-to-year variability in dispersal on the spread rate of an invasive species, and
- larval dispersal estimation.

Empirical estimation of spreading speed of southern (c_S^*) and northern (c_N^*) green crab was carried out in Chapter 2 for the presence/absence data for established populations along the one-dimensional east coast of North America. For the southern lineage, $c_S^* = 14.2 \pm 3$ km y^{-1} and for the northern lineage $c_N^* = 17.8 \pm 3$ km y^{-1}. While there are different reports of the green crab spread rate in this zone [73], I estimated the invasion spread rates of each lineage as accurately as possible by identifying and excluding suspect data points from the regression analysis. The difference in estimated spread rate of *C. maenas* along the east coast of North America may be partly related to the use of different data sets, as well as different methods of projecting the data to derive the distance between two locations. Also, it seems that the advance might be limited to extremes in annual conditions and only appear steady on the scale of decades (see the discussion in Section 2.4.5).

Examining the trade-off between demographic and dispersal parameters in the context of spreading speed theory for structured IDE models was central to my work. This relationship is hyperbolic in the Fisher equation [43] and in unstructured IDEs [124]. Here, I present an example to support the

generalization of this theory to structured IDEs. This relationship enhances our understanding of how effectively organisms can exploit variations and spread consistently in an extremely variable aquatic environment.

Elasticity analysis for the model with Normal and Laplace distributions, representing the larval dispersal kernel in Chapter 2, indicated that the standard deviation of larval dispersal (σ), rather than vital rates (fecundity, survival probabilities) has the most effect on spreading speed. However, managing larval dispersal in coastal waters would be difficult to impossible. The next parameters that most affected spread speeds were fecundity (ϕ) and survival of larvae and juveniles (b_L, b_1, and b_2). The parameter that least affected spread dynamics in our model was survival of adults (b_A), which is currently and has been in the past the most considered parameter to manipulate by managers. Our analysis suggested that reducing juvenile survival in combination with reducing adult survival may be an effective and achievable management strategy.

Dispersal heterogeneity occurs at two temporal scales: within the larval period and among years. The kernel models variation within the larval period. To model the variation among years, I allow the kernel parameters to vary by year. Results indicated that when dispersal parameters vary with time, knowledge of the time-averaged dispersal process is insufficient for determining the upstream spread rate of the population. Rather upstream spread is possible over a number of years when incorporating the yearly variation, even when there are only a few "good years" featured by some upstream

dispersal among many "bad years" featured by only downstream dispersal. Accounting for annual variations in dispersal in population models is important to enhance understanding of spatial dynamics and population spread rates.

The mechanistic approach to model the larval dispersal, as in Chapter 3, allows the incorporation of different types of motions integrated with settling behaviour. This approach is more flexible as opposed to using simple Normal or Laplace dispersal kernels in Chapter 2. Despite the flexibility of the mechanistic dispersal modelling, our simulation shows that none of these kernels is a good representative of larval displacement data in the tail.

5.2 Future Work

The structured IDE models studied in this thesis include three stages of a population with demographic and dispersal features formulated. In all studied models, it was assumed that the juvenile and adult stages are sessile compared to the larval stage. The spread of the green crab has shown a fairly consistent northeast (upstream) speed in the east coast of North America, despite much environmental variability. Note that it is not obvious that the larvae are the longest distance dispersers upstream. This is because there is a dominant drift downstream, discussed in Chapter 2, that has a negative impact on the upstream dispersal of larvae. In addition to the dispersal upstream, there is also survival process to the juvenile stage, settlement pro-

cess and variability of these processes that influence the larval dispersal. This makes it plausible to think that this consistency of the upstream invasion might be due to a consistent natural dispersal of other stages such as juvenile and adult stages. Obviously, further study of (i) larval dispersal processes using hydrographic modelling, (ii) field investigations of juvenile and adult movement and incorporating these stages' dispersal into the developed models, (iii) assessing the effect of different types of dispersal kernels beyond the exponentially-bounded Normal and Laplace distributions, and (iv) evaluating the effect of patchy habitats on the crab's spreading speed would improve the quality of model outputs.

The elasticity analysis carried out in Chapter 2 indicated that the standard deviation of larval dispersal (σ), rather than vital rates (fecundity, survival probabilities) has the most effect on spreading speed. This result is partly due to our assumption that only larvae disperse and not juveniles and adults. It has been shown in age-structured reaction-diffusion models that the spreading speed increases as the mobility of the immature population stages increases [146]. For the models developed in this thesis, the invasion is due to larvae dispersal and the wave is pulled forward by growth and larval dispersal at the leading edge of the invasion. This means that the average age of the adult crabs decreases towards the front of the wave. This conjecture could be generalized to any spreading species where dispersal is dominated by the larval stages and the adults are sessile, and should be checked in the field.

In Chapter 3, further study is required to compare the effect of using geometric versus arithmetic averaging of dispersal kernels on the spread rate of IDE models. Specifically, in Chapter 3 the simulated averaged spread rates arise from arithmetic averages, which is a common averaging approach in ecology. However, Stover et al. [150] noted that the asymptotic spread rate resulting from arithmetic averaging is always higher than that from geometric averaging. Thus, had I used geometric averaging, the difference between the stochastic spread rate and that calculated from the averaged dispersal kernels would have been even larger (box plots in Figure 3.4, panels b and d). The comparison of spread rates arising from these two types of averaging in modelling or experimental studies needs to be studied.

The decomposition of demography and dispersal processes in the IDE models can be improved. This is due to the fact that larval dispersal is influenced by all sorts of physiological, behavioural and hydrodynamic processes, including larval developmental rates and behaviours (e.g., responding to differential currents, water temperatures and/or other cues) [126]. One way to improve my model, is to incorporate some processes such as survival and development into the settlement of larvae. Specifically, the mechanistic dispersal kernel, k_{13} in Equation (3.3), includes two processes of settlement and dispersal through p and ω respectively. For the sake of simplicity, settling rate was assumed to be uniform, Equation (3.4), in my model which can be changed. It would be interesting to examine the impact of this change on the spatial dynamics of population and the invasion spread rate. This needs

to be better understood and formally modelled.

The model developed in Chapter 3 can be used to assess the effect of environmental stochasticity and climate change on rates of spread and range expansion of marine organisms. More specifically, rising sea temperatures across the globe could lead to the appearance of anomalous flow patterns, with incidental effects on dispersal and population dynamics in many marine species [111]. Further, it has been documented that the increase in water temperature causes pelagic larval durations to be shortened and results in lower dispersal distances for marine organisms [115]. Decreased larval development times in warmer water could influence the dispersal kernel and spread rates. Thus, our modelling framework can be applied to develop and provide tools that predict spread rates under various conditions and climate change scenarios (e.g. Long et al. [92] for recent climate change scenarios). Such tools are essential to inform maps of range expansions and risk maps of areas prone to habitat degradation due to aquatic invasive species activities.

This thesis was motivated by some ecological questions regarding the spread of aquatic invasive species in general and regarding the spread of the green crab in particular. For the green crab, our data analysis showed that the green crab has had a fairly consistent northward spread rate along the east coast of North America since its first introduction in the 1800s, covering more than 5° of latitude, about 2000 km of coastline, different water bodies, and two cryptic invasions. The underlying factors involved in any invasion process can be grouped into demographic and dispersal. Using the integro-

difference modelling approach enabled us to incorporate these processes into a theoretical model and examine the sensitivity of the spread rate to the underlying parameters. I found that changes in dispersal had more effect on the spread rate than changes in demographic parameters. Lastly, I incorporated and examined the effect of dispersal heterogeneity in an invasion process. I concluded that environmental stochasticity can lead to upstream spread in aquatic systems and year-to-year variability in dispersal accelerated population spread.

Bibliography

[1] W. C. Allee, O. Park, A. E. Emerson, T. Park, and K. P. Schmidt. *Principles of animal ecology.* WB Saunders Co. Ltd., Philadelphia, PA, 1st edition, 1949.

[2] E. B. Andersen. Asymptotic properties of conditional maximum-likelihood estimators. *Journal of the Royal Statistical Society. Series B (Methodological)*, 32(2):283–301, 1970.

[3] T. Antal, H. Ohtsuki, J. Wakeley, P. D. Taylor, and M. A. Nowak. Evolution of cooperation by phenotypic similarity. *Proceedings of the National Academy of Sciences*, 106(21):8597–8600, 2009.

[4] A. L. Aretxabaleta, D. J. McGillicuddy, K. W. Smith, and D. R. Lynch. Model simulations of the Bay of Fundy Gyre: 1. Climatological results. *Journal of Geophysical Research: Oceans*, 113(C10):1978–2012, 2008.

[5] D. G. Aronson and H. F. Weinberger. Nonlinear diffusion in population genetics, combustion, and nerve pulse propagation. In *Partial*

differential equations and related topics, pages 5–49. Springer-Verlag, Berlin, Germany, 1975.

[6] D. G. Aronson and H. F. Weinberger. Multidimensional nonlinear diffusion arising in population genetics. *Advances in Mathematics*, 30(1): 33–76, 1978.

[7] D. Audet, D. S. Davis, G. Miron, M. Moriyasu, K. Benhalima, and R. Campbell. Geographical expansion of a nonindigenous crab, *Carcinus maenas* (L.), along the Nova Scotian shore into the southeastern Gulf of St. Lawrence, Canada. *Journal of Shellfish Research*, 22(1): 255–262, 2003.

[8] J. C. Avise, C. A. Reeb, and N. C. Saunders. Geographic population structure and species differences in mitochondrial DNA of mouthbrooding marine catfishes (Ariidae) and demersal spawning toadfishes (Batrachoididae). *Evolution.*, 41(5):991–1002, 1987.

[9] A. Baeta, H. N. Cabral, J. M. Neto, J. C. Marques, and M. A. Pardal. Biology, population dynamics and secondary production of the green crab *Carcinus maenas* (L.) in a temperate estuary. *Estuarine, Coastal and Shelf Science*, 65(1):43–52, 2005.

[10] J. Bartsch and S. Coombs. A numerical model of the dispersion of blue whiting larvae, *Micromesistius poutassou* (Risso), in the eastern North Atlantic. *Fisheries Oceanography*, 6(3):141–154, 1997.

[11] F. Belgacem and C. Cosner. The effects of dispersal along environmental gradients on the dynamics of populations in heterogeneous environment. *Canad. Appl. Math. Quart*, 3(4):379–397, 1995.

[12] M. Berrill. The life cycle of the green crab *Carcinus maenas* at the northern end of its range. *Journal of Crustacean Biology*, 2:31–39, 1982.

[13] H. B. Bigelow. *Physical oceanography of the Gulf of Maine*, volume 40. 1927.

[14] A. M. Bobeldyk, J. M. Bossenbroek, M. A. Evans-White, D. M. Lodge, and G. A. Lamberti. Secondary spread of zebra mussels (*Dreissena polymorpha*) in coupled lake-stream systems. *Ecoscience*, 12(3):339–346, 2005.

[15] J. C. Bonardelli, J. H. Himmelman, and K. Drinkwater. Current variability and upwelling along the north shore of Baie des Chaleurs. *Atmosphere-Ocean*, 31(4):541–565, 1993.

[16] D. Brickman. Could ocean currents be responsible for the west to east spread of aquatic invasive species in Maritime Canadian waters? *Marine Pollution Bulletin*, 85(1):235–243, 2014.

[17] D. Brickman and A. Drozdowski. Development and validation of a regional shelf model for Maritime Canada based on the NEMO-OPA cir-

culation model. *Canadian Technical Report of Hydrography and Ocean Sciences*, 278:vii+57, 2012.

[18] J. E. Byers and J. M. Pringle. Going against the flow: retention, range limits and invasions in advective environments. *Marine Ecology Progress Series*, 313:27–41, 2006.

[19] J. E. Byers and J. M. Pringle. Going against the flow: How marine invasions spread and persist in the face of advection. *ICES Journal of Marine Science*, 65:723–724, 2008.

[20] C. Castillo-Chavez, B. Li, and H. Wang. Some recent developments on linear determinacy. *Mathematical Biosciences and Engineering*, 10(5): 1419–1436, 2013.

[21] H. Caswell. *Matrix Population Models: Construction, Analysis, and Interpretation*. Sinauer Associates, Inc, Sunderland, MA, USA, 2nd edition, 2001.

[22] H. Caswell, R. Lensink, and M. G. Neubert. Demography and dispersal: Life table response experiments for invasion speed. *Ecology*, 84(8):1968–1978, 2003.

[23] H. Caswell, M. G. Neubert, and C. M. Hunter. Demography and dispersal: invasion speeds and sensitivity analysis in periodic and stochastic environments. *Theoretical Ecology*, 4(4):407–421, 2011.

[24] J. Chassé and R. J. Miller. Lobster larval transport in the southern Gulf of St. Lawrence. *Fisheries Oceanography*, 19(5):319–338, 2010.

[25] S. Chiswell. Non-Gaussian larval dispersal kernels in Gaussian ocean flows. *Aquatic Biology*, 16(3):203–208, sep 2012.

[26] J. S. Clark, E. Macklin, and L. Wood. Stages and spatial scales of recruitment limitation in southern Appalachian forests. *Ecological Monographs*, 68(2):213–235, 1998.

[27] J. S. Clark, M. Silman, R. Kern, E. Macklin, and J. HilleRisLambers. Seed dispersal near and far: patterns across temperate and tropical forests. *Ecology*, 80(5):1475–1494, 1999.

[28] J. Clark, L. Horváth, and M. Lewis. On the estimation of spread rate for a biological population. *Statistics & probability letters*, 51(3):225–234, 2001.

[29] A. N. Cohen and J. T. Carlton. Nonindigenous aquatic species in a United States estuary: a case study of the biological invasions of the San Francisco Bay and Delta. Technical report, US Fish and Wildlife Service, Washington, DC, and the National Sea Grant College Program Connecticut Sea Grant, 1995.

[30] A. N. Cohen, J. T. Carlton, and M. C. Fountain. Introduction, dispersal and potential impacts of the green crab *Carcinus maenas* in San Francisco Bay, California. *Marine Biology*, 122(2):225–237, 1995.

[31] J. H. Connell. Effects of Competition, Predation by *Thais lapillus*, and Other Factors on Natural Populations of the Barnacle *Balanus balanoides*. *Ecological Monographs*, 31(1):61–104, 1961.

[32] R. K. Cowen and S. Sponaugle. Larval dispersal and marine population connectivity. *Annual review of marine science*, 1:443–66, 2009.

[33] J. M. Cushing and Z. Yicang. The net reproductive value and stability in matrix population models. *Natural Resources Modeling*, 8(4):297–333, 1994.

[34] R. M. Daigle, J. Chassé, and A. Metaxas. The relative effect of behaviour in larval dispersal in a low energy embayment. *Progress in Oceanography*, 144:93–117, may 2016.

[35] D. S. Davis and S. Browne. *Natural History of Nova Scotia. Volume 1: Topics and Habitats*, volume 1. The Nova Scotia Museum, Halifax, NS, Canada, 1996.

[36] C. E. DeRivera, N. G. Hitchcock, S. J. Teck, B. P. Steves, A. H. Hines, and G. M. Ruiz. Larval development rate predicts range expansion of an introduced crab. *Marine Biology*, 150:1275–1288, 2007.

[37] I. J. Dight, M. K. James, and L. Bode. Models of larval dispersal within the central Great Barrier Reef: patterns of connectivity and their implications for species distributions. In *Proceedings of the 6th International Coral Reef Symposium*, volume 3, pages 217–224, 1988.

[38] D. Drolet, A. Locke, M. A. Lewis, and J. Davidson. User-friendly and evidence-based tool to evaluate probability of eradication of aquatic non-indigenous species. *Journal of Applied Ecology*, 51(4):1050–1056, 2014.

[39] R. Dufour and P. Quellet. Estuary and Gulf of St. Lawrence marine ecosystem overview and assessment report. Technical report, Fisheries and Oceans Canada, Maurice-Lamontagne Institut, 2007.

[40] P. Eilers and J. Peeters. A model for the relationship between light intensity and the rate of photosynthesis in phytoplankton. *Ecological modelling*, 42(3):199–215, 1988.

[41] S. P. Ellner and S. J. Schreiber. Temporally variable dispersal and demography can accelerate the spread of invading species. *Theoretical Population Biology*, 82(4):283–298, dec 2012.

[42] C. S. Elton. *The Ecology of Invasions by Animals and Plants*. University of Chicago Press, Chicago, IL, USA, 1958.

[43] R. A. Fisher. The Wave of Advance of Advantageous Genes. *Annals of Human Genetics*, 7(4):355–369, 1937.

[44] B. D. L. Fitt, A. D. Todd, H. A. McCartney, and O. C. Macdonald. Spore dispersal and plant disease gradients; a comparison between two empirical models. *Journal of Phytopathology*, 118(3):227–242, 1987.

[45] C. W. Gardiner. *Handbook of stochastic methods*, volume 3. Springer-Verlag, New York, NY, USA, 2nd edition, 1985.

[46] J. Garnier, T. Giletti, F. Hamel, and L. Roques. Inside dynamics of pulled and pushed fronts. *Journal des Mathematiques Pures et Appliquees*, 98(4):428–449, 2012.

[47] A. Gharouni, M. A. Barbeau, A. Locke, L. Wang, and J. Watmough. Sensitivity of invasion speed on dispersal and demography: an application of spreading speed theory to the green crab invasion on the coast of the northwest Atlantic. *Marine Ecology Progress Series*, 541:135–150, 2015.

[48] A. Gharouni, M. A. Barbeau, J. Chassé, L. Wang, and J. Watmough. Stochastic dispersal increases the rate of upstream spread: a case study with green crabs on the northwest atlantic coast. *PLOS ONE*, Submitted 2016.

[49] J. B. Glude. The effects of temperature and predators on the abundance of the soft-shell clam, *Mya arenaria*, in New England. *Transactions of the American Fisheries Society*, 84(1):13–26, 1955.

[50] J. H. R. Goddard, M. E. Torchin, A. M. Kuris, and K. D. Lafferty. Host specificity of *Sacculina carcini*, a potential biological control agent of the introduced European green crab *Carcinus maenas* in California. *Biological Invasions*, 7(6):895–912, 2005.

[51] E. D. Grosholz. Contrasting rates of spread for introduced species in terrestrial and marine systems. *Ecology*, 77(6):1680–1686, 1996.

[52] E. D. Grosholz. Recent biological invasion may hasten invasional meltdown by accelerating historical introductions. *Proceedings of the National Academy of Sciences of the United States of America*, 102(4): 1088–1091, 2005.

[53] E. D. Grosholz and G. M. Ruiz. Predicting the impact of introduced marine species: lessons from the multiple invasions of the European green crab *Carcinus maenas*. *Biological Conservation*, 78(1):59–66, 1996.

[54] G. Han and J. W. Loder. Three-dimensional seasonal-mean circulation and hydrography on the eastern Scotian Shelf. *Journal of Geophysical Research: Oceans*, 108(C5), 2003.

[55] G. Han, J. W. Loder, and P. C. Smith. Seasonal-Mean Hydrography and Circulation in the Gulf of St. Lawrence and on the Eastern Scotian and Southern Newfoundland Shelves. *Journal of Physical Oceanography*, 29(6):1279–1301, jun 1999.

[56] C. G. Hannah, J. A. Shore, J. W. Loder, and C. E. Naimie. Seasonal circulation on the western and central Scotian Shelf. *Journal of Physical Oceanography*, 31(2):591–615, 2001.

[57] A. C. Hardy. The plankton community, the whale fisheries and the hypothesis of animal exclusion. *Discovery Rep*, 11:273–360, 1935.

[58] A. Hastings, K. Cuddington, K. F. Davies, C. J. Dugaw, S. Elmendorf, A. Freestone, S. Harrison, M. Holland, J. Lambrinos, and U. Malvadkar. The spatial spread of invasions: new developments in theory and evidence. *Ecology Letters*, 8(1):91–101, 2005.

[59] R. C. Hobbs and L. W. Botsford. Diel vertical migration and timing of metamorphosis of larvae of the Dungeness crab *Cancer magister*. *Marine Biology*, 112(3):417–428, mar 1992.

[60] H. Hotelling. *A Mathematical Theory of Migration.* MA Thesis, University of Washington, 1921.

[61] J. M. Hrycik, J. Chassé, B. R. Ruddick, and C. T. Taggart. Dispersal kernel estimation: a comparison of empirical and modelled particle dispersion in a coastal marine system. *Estuarine, Coastal and Shelf Science*, 133:11–22, 2013.

[62] P. E. Hulme. Trade, transport and trouble: managing invasive species pathways in an era of globalization. *Journal of Applied Ecology*, 46(1): 10–18, 2009.

[63] A. Hurford. GPS measurement error gives rise to spurious 180 turning angles and strong directional biases in animal movement data. *PLoS One*, 4(5):1–12, 2009.

[64] O. Iribarne, M. Fernandez, and D. Armstrong. Does space competition regulate density of juvenile dungeness crab *Cancer magister* Dana in sheltered habitats? *Journal of experimental marine biology and ecology*, 183(2):259–271, 1994.

[65] G. P. Jenkins, K. P. Black, M. J. Wheatley, and D. N. Hatton. Temporal and spatial variability in recruitment of a temperate, seagrass-associated fish is largely determined by physical processes in the pre- and post-settlement phases. *Marine ecology progress series*, 148(1): 23–35, 1997.

[66] G. P. Jenkins, K. P. Black, P. A. Hamer, and A. J. Fowler. Determination of spawning areas and larval advection pathways for King George whiting in southeastern Australia using otolith microstructure and hydrodynamic modelling. I. Victoria. *Marine Ecology Progress Series*, 199:231–242, 2000.

[67] G. C. Jensen, P. S. McDonald, and D. A. Armstrong. East meets west: competitive interactions between green crab *Carcinus maenas*, and native and introduced shore crab *Hemigrapsus spp. Marine ecology. Progress series*, 225:251–262, 2002.

[68] G. C. Jensen, P. S. McDonald, and D. A. Armstrong. Biotic resistance to green crab, *Carcinus maenas*, in California bays. *Marine Biology*, 151(6):2231–2243, 2007.

[69] E. Jongejans, K. Shea, O. Skarpaas, D. Kelly, and S. P. Ellner. Importance of individual and environmental variation for invasive species spread: a spatial integral projection model. *Ecology*, 92(1):86–97, jan 2011.

[70] L. Kanary, J. Musgrave, R. C. Tyson, A. Locke, and F. Lutscher. Modelling the dynamics of invasion and control of competing green crab genotypes. *Theoretical Ecology*, 7(4):391–406, 2014.

[71] P. Kareiva and G. Odell. Swarms of predators exhibit "preytaxis" if individual predators use area-restricted search. *American Naturalist*, 130:233–270, 1987.

[72] K. Kawasaki, A. Mochizuki, M. Matsushita, T. Umeda, and N. Shigesada. Modeling spatio-temporal patterns generated by *bacillus subtilis*. *Journal of Theoretical Biology*, 188(2):177–185, 1997.

[73] G. J. Klassen and A. Locke. A biological synopsis of the European green crab, *Carcinus maenas*. *Canadian Manuscript Report of Fisheries and Aquatic Sciences*, 2818:1–75, 2007.

[74] A. N. Kolmogorov, I. G. Petrovsky, and N. S. Piskunov. Etude dele-quation de la diffusion avec croissance de la quantité de matiere et son application aun probleme biologique. *Mosc. Univ. Bull. Math*, 1:1–25, 1937.

[75] M. Kot and W. M. Schaffer. Discrete-time growth-dispersal models. *Mathematical Biosciences*, 80(1):109–136, 1986.

[76] M. Kot, M. A. Lewis, and P. van den Driessche. Dispersal data and the spread of invading organisms. *Ecology*, 77(7):2027–2042, 1996.

[77] M. Kot, J. Medlock, T. Reluga, and D. Brian Walton. Stochasticity, invasions, and branching random walks. *Theoretical Population Biology*, 66(3):175–184, 2004.

[78] S. Kotz, T. Kozubowski, and K. Podgorski. *The Laplace Distribution and Generalizations: A Revisit With Applications to Communications, Exonomics, Engineering, and Finance*. Number 183. Springer, 2001.

[79] J. C. Lagarias, J. A. Reeds, M. H. Wright, and P. E. Wright. Convergence properties of the Nelder-Mead simplex method in low dimensions. *SIAM Journal on optimization*, 9(1):112–147, 1998.

[80] J. L. Largier. Consideration in estimating larval dispersal distances. *Ecological Applications*, 13(1):71–89, 2003.

[81] L. M. Lauzier. Drift bottle observations in Northumberland Strait, Gulf of St. Lawrence. *Journal of the Fisheries Board of Canada*, 22(2): 353–368, 1965.

[82] D. Lavoie, J. Chassé, Y. Simard, N. Lambert, P. S. Galbraith, N. Roy, and D. Brickman. Large-Scale Atmospheric and Oceanic Control on

Krill Transport into the St. Lawrence Estuary Evidenced with Three-Dimensional Numerical Modelling. *Atmosphere-Ocean*, 54(3):299–325, may 2016.

[83] M. Lewis and S. Pacala. Modeling and analysis of stochastic invasion processes. *Journal of Mathematical Biology*, 41(5):387–429, 2000.

[84] M. A. Lewis and P. Kareiva. Allee dynamics and the spread of invading organisms. *Theoretical Population Biology*, 43(2):141–158, 1993.

[85] M. A. Lewis, B. Li, and H. F. Weinberger. Spreading speed and linear determinacy for two-species competition models. *Journal of Mathematical Biology*, 45(3):219–233, 2002.

[86] M. A. Lewis, M. G. Neubert, H. Caswell, J. S. Clark, and K. Shea. A guide to calculating discrete-time invasion rates from data. In *Conceptual ecology and invasion biology: reciprocal approaches to nature*, pages 169–192. Springer, Netherlands, 2006.

[87] B. Li, H. F. Weinberger, and M. A. Lewis. Spreading speeds as slowest wave speeds for cooperative systems. *Mathematical Biosciences*, 196 (1):82–98, 2005.

[88] X. Liang and X. Q. Zhao. Asymptotic speeds of spread and traveling waves for monotone semiflows with applications. *Communications on Pure and Applied Mathematics*, 60(1):1–40, 2007.

[89] X. Liang and X. Q. Zhao. Spreading speeds and traveling waves for abstract monostable evolution systems. *Journal of Functional Analysis*, 259(4):857–903, 2010.

[90] X. Liang, Y. Yi, and X.-Q. Zhao. Spreading speeds and traveling waves for periodic evolution systems. *Journal of Differential Equations*, 231 (1):57–77, 2006.

[91] D. R. Lockwood, A. Hastings, and L. W. Botsford. The effects of dispersal patterns on marine reserves: does the tail wag the dog? *Theoretical population biology*, 61(3):297–309, 2002.

[92] Z. Long, W. Perrie, J. Chassé, D. Brickman, L. Guo, A. Drozdowski, and H. Hu. Impacts of Climate Change in the Gulf of St. Lawrence. *Atmosphere-Ocean*, 54(3):337–351, may 2016.

[93] R. Lui. Biological growth and spread modeled by systems of recursions. II. biological theory. *Mathematical Biosciences*, 93(2):297–312, 1989.

[94] R. Lui. Biological growth and spread modeled by systems of recursions. I. mathematical theory. *Mathematical Biosciences*, 93(2):269–295, 1989.

[95] F. Lutscher, R. M. Nisbet, and E. Pachepsky. Population persistence in the face of advection. *Theoretical Ecology*, 3(4):271–284, 2010.

[96] G. Madec. NEMO ocean engine. *Note du Pole de Modelisation Institut Pierre-Simon Laplace (NO. 27)*, 27, 2012.

[97] J. P. Manning, D. J. McGillicuddy, N. R. Pettigrew, J. H. Churchill, and L. S. Incze. Drifter observations of the Gulf of Maine coastal current. *Continental Shelf Research*, 29(7):835–845, 2009.

[98] Maple. Maplesoft (ver 14:00), 2010.

[99] F. Maps, S. Plourde, D. Lavoie, I. McQuinn, and J. Chassé. Modelling the influence of daytime distribution on the transport of two sympatric krill species (Thysanoessa raschii and Meganyctiphanes norvegica) in the Gulf of St Lawrence, eastern Canada. *ICES Journal of Marine Science*, 71(2):282–292, jan 2014.

[100] F. Maps, S. Plourde, I. H. McQuinn, S. St-Onge-Drouin, D. Lavoie, J. Chassé, and V. Lesage. Linking acoustics and finite-time Lyapunov exponents reveals areas and mechanisms of krill aggregation within the Gulf of St. Lawrence, eastern Canada. *Limnology and Oceanography*, 60(6):1965–1975, 2015.

[101] N. G. Marculis and R. Lui. Modelling the biological invasion of *Carcinus maenas* (the European green crab). *Journal of Biological Dynamics*, 10(1):140–163, jan 2016.

[102] Matlab. Matlab (ver: R2012 7.14.0.739), 2012.

[103] V. Méndez, D. Campos, and J. Fort. Speed of travelling fronts: two-dimensional and ballistic dispersal probability distributions. *Europhysics Letters*, 66(6):902–908, 2004.

[104] T. E. X. Miller and B. Tenhumberg. Contributions of demography and dispersal parameters to the spatial spread of a stage-structured insect invasion. *Ecological Applications*, 20(3):620–633, 2010.

[105] M. Mimura, H. Sakaguchi, and M. Matsushita. Reaction–diffusion modelling of bacterial colony patterns. *Physica A: Statistical Mechanics and its Applications*, 282(1):283–303, 2000.

[106] R. M. Miura. Explicit roots of the cubic polynomial and applications. *Appl. Math. Notes*, 4:22–40, 1980.

[107] D. Mollison. The rate of spatial propagation of simple epidemics. In L. LeCam, J. Neyman, and E. Scott, editors, *Proceedings of the Sixth Berkeley Symposium on Mathematical Statistics and Probability*, volume 3, pages 579–614, Berkeley, CA, 1972. The Regents of the University of California, University of California Press.

[108] D. Mollison. Spatial contact models for ecological and epidemic spread. *Journal of the Royal Statistical Society. Series B (Methodological)*, pages 283–326, 1977.

[109] D. Mollison. Dependence of epidemic and population velocities on basic parameters. *Mathematical biosciences*, 107(2):255–287, 1991.

[110] K. Müller. The colonization cycle of freshwater insects. *Oecologia*, 52 (2):202–207, 1982.

[111] P. L. Munday, J. M. Leis, J. M. Lough, C. B. Paris, M. J. Kingsford, M. L. Berumen, and J. Lambrechts. Climate change and coral reef connectivity. *Coral Reefs*, 28(2):379–395, jun 2009.

[112] J. D. Murray. *Mathematical Biology I: An Introduction, vol. 17 of Interdisciplinary Applied Mathematics*. Springer, New York, NY, USA, 2002.

[113] M. M. G. Neubert, M. Kot, and M. M. A. Lewis. Dispersal and Pattern Formation in a Discrete-Time Predator-Prey Model. *Theoretical Population Biology*, 48(1):7–43, 1995.

[114] M. G. Neubert and H. Caswell. Demography and dispersal: calculation and sensitivity analysis of invasion speed for structured populations. *Ecology*, 81(6):1613–1628, 2000.

[115] M. I. O'Connor, J. F. Bruno, S. D. Gaines, B. S. Halpern, S. E. Lester, B. P. Kinlan, and J. M. Weiss. Temperature control of larval dispersal and the implications for marine ecology, evolution, and conservation. *Proceedings of the National Academy of Sciences*, 104(4):1266–1271, jan 2007.

[116] A. Okubo. *Diffusion and ecological problems; Mathematical models*. Springer-Verlag, Berlin, Germany, 1980.

[117] A. Okubo and S. A. Levin. A theoretical framework for data analysis of wind dispersal of seeds and pollen. *Ecology*, 70(2):329–338, 1989.

[118] A. Okubo and S. A. Levin. *Diffusion and Ecological Problems: Modern Perspectives*, volume 14. Springer-Verlag, New York, USA, 2nd edition, 2001.

[119] P. Ouellet, A. Olga, V. Bui, D. Lavoie, J. Chassé, N. Lambert, N. Ménard, and P. Sirois. Seasonal distribution, abundance, and growth of larval capelin (*Mallotus villosus*) and the role of the Lower Estuary (Gulf of St. Lawrence, Canada) as a nursery area. *Canadian Journal of Fisheries and Aquatic Sciences*, 70(July):1508–1530, 2013.

[120] E. Pachepsky, F. Lutscher, R. M. Nisbet, and M. A. Lewis. Persistence, spread and the drift paradox. *Theoretical Population Biology*, 67:61–73, 2005.

[121] E. Pachepsky, F. Lutscher, and M. A. Lewis. The effect of dispersal patterns on stream populations. *Siam Review*, 47(4):749–772, 2005.

[122] C. B. Paris and R. K. Cowen. Direct evidence of a biophysical retention mechanism for coral reef fish larvae. *Limnology and Oceanography*, 49 (6):1964–1979, nov 2004.

[123] C. Perrings, H. Mooney, and M. Williamson. *Bioinvasions and Globalization*. Oxford University Press, Oxford, UK, 2010.

[124] S. V. Petrovskii and B.-L. Li. *Exactly solvable models of biological invasion*. CRC Press, Boca Raton, FL, USA, 2006.

[125] N. R. Pettigrew, J. H. Churchill, C. D. Janzen, L. J. Mangum, R. P. Signell, A. C. Thomas, D. W. Townsend, J. P. Wallinga, and H. Xue. The kinematic and hydrographic structure of the Gulf of Maine Coastal Current. *Deep Sea Research Part II: Topical Studies in Oceanography*, 52(19):2369–2391, 2005.

[126] J. Pineda. Linking larval settlement to larval transport: assumptions, potentials, and pitfalls. *Oceanography of the Eastern Pacific*, 1(2000): 84–105, 2000.

[127] J. M. Pringle and J. P. Wares. Going against the flow: Maintenance of alongshore variation in allele frequency in a coastal ocean. *Marine Ecology Progress Series*, 335:69–84, 2007.

[128] J. M. Pringle, A. M. H. Blakeslee, J. E. Byers, and J. Roman. Asymmetric dispersal allows an upstream region to control population structure throughout a species range. *Proceedings of the National Academy of Sciences*, 108(37):15288–15293, 2011.

[129] H. Queiroga. Distribution and drift of the crab *Carcinus maenas* (L.) (Decapoda, Portunidae) larvae over the continental shelf off northern Portugal in April 1991. *Journal of Plankton Research*, 18(11):1981–2000, 1996.

[130] H. Queiroga, J. Costlow, and M. Moreira. Vertical migration of the

crab *Carcinus maenas* first zoea in an estuary: implications for tidal stream transport. *Marine Ecology Progress Series*, 149:121–132, 1997.

[131] R Core Team. R: A Language and Environment for Statistical Computing. (ver 3.0.1). *R Foundation for Statistical Computing, Vienna, Austria*, 2009.

[132] S. L. Robertson and J. M. Cushing. Spatial segregation in stage-structured populations with an application to *Tribolium*. *Journal of Biological Dynamics*, 5(5):398–409, 2011.

[133] J. Roman. Diluting the founder effect: cryptic invasions expand a marine invader's range. *Proceedings of the Royal Society B: Biological Sciences*, 273(1600):2453–2459, 2006.

[134] G. M. Ruiz, A. W. Miller, and W. C. Walton. The bi-coastal invasion of North America by the European green crab: impacts and management strategies. *Aquatic Nuisance Species Task Force, Smithsonian Environmental Research Centre, USA*, page 45 p, 1998.

[135] G. M. Ruiz, J. T. Carlton, E. D. Grosholz, and A. H. Hines. Global invasions of marine and estuarine habitats by non-indigenous species: mechanisms, extent, and consequences. *American Zoologist*, 37(6):621–632, 1997.

[136] F. J. Saucier. Modeling the formation and circulation processes of

water masses and sea ice in the Gulf of St. Lawrence, Canada. *Journal of Geophysical Research*, 108(C8):3269, 2003.

[137] T. Say. *An account of the Crustacea of the United States*, volume 73. Reprinted in 1969 by Verlag Von J. Cramer, New York, NY, USA, 1817.

[138] S. J. Schreiber and M. E. Ryan. Invasion speeds for structured populations in fluctuating environments. *Theoretical Ecology*, 4(4):423–434, nov 2011.

[139] A. L. Shanks. Pelagic larval duration and dispersal distance revisited. *The Biological Bulletin*, 216(3):373–385, 2009.

[140] N. Shigesada and K. Kawasaki. *Biological Invasions: Theory and Practice*. Oxford University Press, London, UK, 1997.

[141] J. B. Shurin and J. E. Havel. Hydrologic connections and overland dispersal in an exotic freshwater crustacean. *Biological Invasions*, 4(4): 431–439, 2002.

[142] D. A. Siegel, B. P. Kinlan, B. Gaylord, and S. D. Gaines. Lagrangian descriptions of marine larval dispersion. *Marine Ecology Progress Series*, 260:83–96, 2003.

[143] J. G. Skellam. Random Dispersal in Theoretical Populations. *Biometrika*, 38(1):196–218, 1951.

[144] P. J. Smith, A. Jamieson, and A. J. Birley. Electrophoretic studies and the stock concept in marine teleosts. *ICES Journal of Marine Science*, 47(2):231–245, 1990.

[145] R. E. Snyder, C. B. Paris, and A. C. Vaz. How Much Do Marine Connectivity Fluctuations Matter? *The American Naturalist*, 184(4): 523–530, oct 2014.

[146] J. W.-H. So, J. Wu, and X. Zou. A reaction–diffusion model for a single species with age structure. I Travelling wavefronts on unbounded domains. In *Proceedings of the Royal Society of London A: Mathematical, Physical and Engineering Sciences*, volume 457, pages 1841–1853. The Royal Society, 2001.

[147] D. C. Speirs and W. S. C. Gurney. Population persistence in rivers and estuaries. *Ecology*, 82(5):1219–1237, 2001.

[148] J. J. Stachowicz, R. B. Whitlatch, and R. W. Osman. Species diversity and invasion resistance in a marine ecosystem. *Science*, 286(5444): 1577–1579, 1999.

[149] P. A. Stephens, W. J. Sutherland, and R. P. Freckleton. What is the Allee effect? *Oikos*, pages 185–190, 1999.

[150] J. P. Stover, B. E. Kendall, and R. M. Nisbet. Consequences of Dispersal Heterogeneity for Population Spread and Persistence. *Bulletin of Mathematical Biology*, 76(11):2681–2710, 2014.

[151] T. W. Therriault, L. M. Herborg, A. Locke, and C. W. McKindsey. Risk assessment for European green crab (*Carcinus maenas*) in Canadian waters. Technical report, DFO Canada, Canadian Science Advisory Secretariat, 2008.

[152] G. Thorson. Reproductive and larval ecology of marine bottom invertebrates. *Biological Reviews*, 25(1):1–45, 1950.

[153] R. Thresher, C. Proctor, G. Ruiz, R. Gurney, C. MacKinnon, W. Walton, L. Rodriguez, and N. Bax. Invasion dynamics of the European shore crab, *Carcinus maenas*, in Australia. *Marine Biology*, 142(5): 867–876, 2003.

[154] S. Tuljapurkar. *Population dynamics in variable environments*. Springer, New York, NY, USA, 1990.

[155] S. Tuljapurkar and H. Caswell. *Structured-Population Models in Marine, Terrestrial, and Freshwater Systems*, volume 18. Chapman & Hall, New York, NY, USA, 1996.

[156] P. Turchin. *Quantitative Analysis of Movement: Measuring and Modeling Population Redistribution in Animals and Plants*, volume 1. Sinauer Associates, Sunderland, MA, USA, 1998.

[157] F. van den Bosch, J. A. J. Metz, and O. Diekmann. The velocity of spatial population expansion. *Journal of Mathematical Biology*, 28(5): 529–565, 1990.

[158] H. W. Van der Veer, P. Ruardij, A. J. Van den Berg, and H. Ridderinkhof. Impact of interannual variability in hydrodynamic circulation on egg and larval transport of plaice *Pleuronectes platessa* L. in the southern North Sea. *Journal of Sea Research*, 39(1):29–40, 1998.

[159] R. W. Van Kirk and M. A. Lewis. Integrodifference models for persistence in fragmented habitats. *Bulletin of Mathematical Biology*, 59(1): 107–137, 1997.

[160] V. Volterra. Variazioni e fluttuazioni del numero d'individui in specie animali conviventi. *Accademia nazionale dei Lincei*, 2:31–13, 1926.

[161] W. C. Walton. Mitigating effects of nonindigenous marine species: evaluation of selective harvest of the European green crab, *Carcinus maenas*. *Journal of Shellfish Research*, 19(1):634–639, 2000.

[162] H. Wang. Spreading speeds and traveling waves for non-cooperative reaction-diffusion systems. *Journal of Nonlinear Science*, 21(5):747–783, 2011.

[163] H. Wang and C. Castillo-Chavez. Spreading speeds and traveling waves for non-cooperative integro-difference systems. *Discrete and continuous dynamical systems. Series B*, 17(6):2243, 2012.

[164] J. R. Watson, B. E. Kendall, D. A. Siegel, and S. Mitarai. Changing Seascapes, Stochastic Connectivity, and Marine Metapopulation Dynamics. *The American Naturalist*, 180(1):99–112, jul 2012.

[165] H. F. Weinberger. Asymptotic behavior of model in population genetics. In *Nonlinear Partial Differential Equations and Applications*, volume 648, pages 47–96. Springer, 1978.

[166] H. F. Weinberger. Long-Time Behavior of a Class of Biological Models. *SIAM Journal on Mathematical Analysis*, 13(3):353–396, 1982.

[167] H. F. Weinberger, M. A. Lewis, and B. Li. Analysis of linear determinacy for spread in cooperative models. *Journal of Mathematical Biology*, 45(3):183–218, 2002.

[168] H. F. Weinberger, M. A. Lewis, and B. Li. Anomalous spreading speeds of cooperative recursion systems. *Journal of Mathematical Biology*, 55 (2):207–222, 2007.

[169] W. R. Welch. Changes in abundance of the green crab, *Carcinus maenas* (L.), in relation to recent temperature changes. *Fishery Bulletin*, 67(2):337–345, 1968.

[170] P. D. Williams and A. Hastings. Stochastic Dispersal and Population Persistence in Marine Organisms. *The American Naturalist*, 182(2): 271–282, 2013.

[171] D. O. Wolfenbarger. Dispersion of small organisms. Distance dispersion rates of bacteria, spores, seeds, pollen, and insects; incidence rates of diseases and injuries. *The American Midland Naturalist*, 35(1):1–152, 1946.

[172] D. O. Wolfenbarger. Factors affecting dispersal distances of small organisms. In *Exposition Press*. Exposition Press, 1975.

[173] H. Xue, F. Chai, and N. R. Pettigrew. A model study of the seasonal circulation in the Gulf of Maine. *Journal of Physical Oceanography*, 30 (5):1111–1135, 2000.

[174] S. B. Yamada. *Global Invader: The European Green Crab*. Oregon Sea Grant, Corvalis Oregon, USA, 2001.

[175] S. B. Yamada, C. Hunt, and N. Richmond. The arrival of the European green crab, *Carcinus maenas*, in Oregon Estuaries. In J. Pederson, editor, *Marine Bioinvasions: Proceedings of the First National Conference. January 24, 1999, Massachusetts Institute of Technology, Sea Grant College Program*, pages 94–99, 1999.

[176] S. B. Yamada, B. R. Dumbauld, A. Kalin, C. E. Hunt, R. Figlar-Barnes, and A. Randall. Growth and persistence of a recent invader *Carcinus maenas* in estuaries of the northeastern Pacific. *Biological Invasions*, 7(2):309–321, 2005.

[177] K. Yamamura. Dispersal distance of heterogeneous populations. *Population Ecology*, 44(2):93–101, aug 2002.

[178] C. Zeng and E. Naylor. Occurrence in coastal waters and endogenous tidal swimming rhythms of late megalopae of *Carcinus maenas*: impli-

cations for onshore recruitment. *Marine Ecology Progress Series*, 136: 69–79, 1996.

Appendix A

Existence of Travelling Wave Solution for the IDE Model 3.3-3.5

Here we check the conditions of Proposition 1.2.1 for the IDE model equations 3.3-3.5 developed in Chapter 3.

Condition (1) of Proposition 1.2.1 is easily verified for our model (equations 3.3-3.5). Specifically, the unique interior equilibrium $\boldsymbol{\beta} = (\phi b_L u_3^*, \phi b_L b_1 u_3^*, u_3^*)$, where $u_3^* = \frac{\kappa(1-\alpha)}{r\alpha - b_A\alpha + b_A}$ given that $r = \phi b_L b_1 b_2$ and $\alpha = \frac{1-b_A}{r}$.

Our model satisfies condition (2) since we assumed that habitat is spatially homogeneous.

It is easy to verify that the equations for each stage are continuous and nondecreasing with respect to $\mathbf{u}$, thus our model is order-preserving, thus

conditions (3) and (4) are satisfied.

Linearization of our model (equations 3.1-3.5) in the vicinity of $\mathbf{u} = \mathbf{0}$ leads to using matrix $\boldsymbol{B}_0$ in (3.1) in the analysis. Note that $\boldsymbol{B}_0$ here is identical to the demographic matrix, $\boldsymbol{B}$, used in the linear and density independent model developed by [47]. For our model, $\mathbf{B_u} \leq \mathbf{B_0}$, thus condition (5) is met.

To prove condition (6), it is sufficient to show that the moment generating functions exist for all the kernels in dispersal matrix $\boldsymbol{K}$ in (3.2). The moment generating function for the Dirac delta function is 1. Here, we showed that the kernel k_{13} (for the stage with dispersal, i.e.,larvae) with the choices of $p(t)$ and $\omega(t, x-y)$ as in equation (3.4) and (3.5), representing settlement rate and larval dispersal kernel respectively, is exponentially bounded following the method of asymptotic expansion. The integral form of larval dispersal kernel in equations 3.3-3.5 can be expanded and represented as a summation of the error function

$$erf(x) = \frac{2}{\sqrt{\pi}} \int_0^x \exp(-t^2) dt$$

, as follows:

$$k_{13}(z) = -\tfrac{1}{80v}\, \mathrm{e}^{\frac{zv}{2D}} (\mathrm{e}^{\frac{zv}{2D}} \mathrm{erf}(\tfrac{\sqrt{2}(50v+z)}{20\sqrt{D}}) + \mathrm{e}^{-\frac{zv}{2D}} \mathrm{erf}(\tfrac{\sqrt{2}(50v-z)}{20\sqrt{D}}) -$$
$$-\mathrm{e}^{\frac{zv}{2D}} \mathrm{erf}(\tfrac{1}{60}\tfrac{\sqrt{2}\sqrt{5}(90v+z)}{\sqrt{D}}) - \mathrm{e}^{-\frac{zv}{2D}} \mathrm{erf}(\tfrac{1}{60}\tfrac{\sqrt{2}\sqrt{5}(90v-z)}{\sqrt{D}})).$$

The asymptotic expansion of $k_{13}(z)$ for $z \gg 1$ reveals the behavior of the kernel's tail. To calculate the asymptotic expansion, we used the *series*()

function in Maple [98] with z set as infinity. The following expression has been calculated

$$\left(\frac{27\sqrt{10D}}{2\sqrt{\pi}z^2}\mathrm{e}^{-\frac{45}{2}\frac{v^2}{D}} - \frac{7290\sqrt{10D}(D-15v^2)}{\sqrt{\pi}z^4}\mathrm{e}^{-\frac{45}{2}\frac{v^2}{D}} + O(z^{-6})\right)\mathrm{e}^{\frac{-zv}{2D}}\mathrm{e}^{\frac{-z^2}{360D}},$$

which is dominated by $C(z)^{-2}\mathrm{e}^{-z^2}$ for a positive constant C.

This asymptotic expansion of $k_{13}(z)$ implies that the dispersal kernel defined in equations 3.3-3.5 is bounded by the Normal distribution. Thus, all entries of the dispersal matrix $\boldsymbol{K}$ (3.2) have a moment generating function. This matrix is irreducible, due to the fact that corresponding graph of is strongly connected. Note that in the present work and following [47], $\boldsymbol{H}(s) = \boldsymbol{B_0} \circ \boldsymbol{M}(s)$, in which moment generating function is denoted by $(\boldsymbol{M}(s))_{ij} = \int_{-\infty}^{+\infty} \mathrm{e}^{sz} k_{ij}(z)\mathrm{d}z$.

Vita

Candidate's full name: Ali Gharouni
University attended:

- BSc Mathematics, Shiraz University, 2000-2005

- MSc Mathematics, Isfahan University of Technology, 2005-2008

Publications (submitted/to be submitted):

1. A. Gharouni*, M.A. Barbeau, A. Locke, L. Wang, J. Watmough, Sensitivity of invasion speed on dispersal and demography: an application of spreading speed theory to the green crab invasion on the coast of the northwest Atlantic, *Marine Ecology Progress Series*, 541 (2015).

2. L. Wang*, A. Gharouni, Modeling the spread of bed bug infestation and optimal resource allocation for disinfestation, Mathematical Biosciences and Engineering, *Mathematical Bioscience and Engineering*, 13 (2016).

3. A. Gharouni*, M.A. Barbeau, J. Chassé, L. Wang, J. Watmough, Stochastic dispersal increases the rate of upstream spread: a case study with green crabs on the northwest Atlantic coast, (submitted to PLOS ONE in 2016).

4. A. Gharouni*, M.A. Barbeau, J. Chassé, L. Wang, J. Watmough, Estimation of larval dispersal distribution: an application of hydrodynamic models to the green crab invasion on the coast of the northwest Atlantic, (to be submitted).

5. A. Gharouni*, L. Wang, Dynamics of intraguild predator-prey with specialist prey, (to be submitted).

Awards:

- International Differential Scholarship, 2009-2013, University of New Brunswick
- Mathematics and statistics graduate award, University of New Brunswick, 2015, University of New Brunswick

Conference Presentations:

- Recent application of spreading speed theory to the green crab invasion in Atlantic Canada, CMS 2015, University of Prince Edwards Island, PEI, Canada, June 5-8, 2015.
- Recent application of spreading speed theory to the green crab invasion in Atlantic Canada, ACCESS 2015, Huntsman Marine Science Centre, St. Andrews, NB Canada, May 10-12, 2015.
- Estimating the spread rate of the European Green Crab in Atlantic Canada, AARMS-CRM Workshop on Sustainability of Aquatic Ecosystem Networks, University of New Brunswick, Fredericton Canada, October 22-25, 2013.
- An Integrodifference Model for Biological Invasion of European Green Crab (*Carcinus maenas*), Special Session on Mathematical Models in Biology and Physiology I, Fall Southeastern Sectional Meeting University of Louisville, Louisville, KY, October 5-6, 2013.
- Integrodifference Model for Biological Invasion of European Green Crab (*Carcinus maenas*) :Calculation and Sensitivity Analysis of Invasion Speed, AARMS Mathematical Biology Workshop, Memorial University, NL Canada, July 27-29, 2013.
- Recent extensions of Fisher's travelling wave model and their application to the spread of invading species, ACCESS 2013, Centre of Geographic Sciences Halifax, NS Canada, May 9-11, 2013.
- SIS Patch Model for the common Bed Bug Cimex lectularius Transmission (poster session), 7 th International Congress on Industrial and Applied Mathematics, Vancouver, BC Canada, July, 2011.